2014

Analytical solutions to nonlinear differential equations arising in physical problems

Mathew Baxter
University of Central Florida

ANALYTICAL SOLUTIONS TO NONLINEAR DIFFERENTIAL EQUATIONS ARISING IN PHYSICAL PROBLEMS

by

MATHEW JOHN BAXTER
B.S. Florida Gulf Coast University, 2009
M.S. University of Central Florida, 2012

A dissertation submitted in partial fulfillment of the requirements
for the degree of Doctor of Philosophy
in the Department of Mathematics
in the College of Sciences
at the University of Central Florida
Orlando, Florida

Summer Term
2014

Major Professor:
Kuppalapalle Vajravelu

ABSTRACT

Nonlinear partial differential equations are difficult to solve, with many of the approximate solutions in the literature being numerical in nature. In this work, we apply the Homotopy Analysis Method to give approximate analytical solutions to nonlinear ordinary and partial differential equations. The main goal is to apply different linear operators, which can be chosen, to solve nonlinear problems. In the first three chapters, we study ordinary differential equations (ODEs) with one or two linear operators. As we progress, we apply the method to partial differential equations (PDEs) and use several linear operators. The results are all purely analytical, meaning these are approximate solutions that we can evaluate at points and take their derivatives.

Another main focus is error analysis, where we test how good our approximations are. The method will always produce approximations, but we use residual errors on the domain of the problem to find a measure of error.

In the last two chapters, we apply similarity transforms to PDEs to transform them into ODEs. We then use the Homotopy Analysis Method on one, but are able to find exact solutions to both equations.

ACKNOWLEDGMENTS

The author would like to thank K. Vajravelu for being the chair of the committee. The semester I began at UCF, I took his Special Functions course. This was the spark that helped me return to applied math after a few detours. His help and constant encouragement, especially in times of need, was greatly appreciated.

I would also like to thank the committee: R. Mohapatra, X. Li, D. Rollins, Z. Shuai, and A. Kassab, for their valuable input. I am very grateful for their assistance throughout my years at UCF, not just the time spent being on my committee.

I am forever indebted to R. A. Van Gorder for his motivation, training, and guidance.

TABLE OF CONTENTS

LIST OF FIGURES

CHAPTER 1

INTRODUCTION

Perturbation theory is a strong tool used to solve differential equations. These equations have a small parameter that is perturbed, meaning the solution is expanded around. However, most nonlinear DEs do not have a small parameter to perturb. In this thesis we use the Homotopy Analysis Method to introduce a parameter to any differential equation using a homotopy, a topic from algebraic topology. Even though it is not a "small" parameter, we are able to perturb this homotopy parameter and use the theory to break a nonlinear differential equation down to an infinite number of linear differential equations.

The Homotopy Analysis Method was introduced by Liao in his doctoral thesis in 1992 [14]. Since then, there have been several articles ([23] - [45], for a start) and even texts written on the subject (see [15], [20], [1]). The purpose of this dissertation is to apply this method to highly nonlinear partial differential equations, studying in particular the choice of the linear operator associated with each problem.

For most nonlinear differential equations, the approximate solutions are numerical, due to the difficulty of the problems. One of the most innovative features about the Homotopy Analysis Method is that the approximation is a function. In this thesis we use the

method to find analytical solutions that you can hold on to: evaluate at points, take their derivatives, etc.

Suppose we are trying to solve a nonlinear differential equation $N[u] = 0$, where N is a nonlinear differential operator and u is the solution to the differential equation. We introduce a parameter using a straight-line homotopy. We use

$$\mathcal{H}(u, q) = (1 - q)L[u] - qhN[u], \tag{1.1}$$

where $\mathcal{H}$ is the homotopy function, $q \in [0, 1]$ is the homotopy parameter, L is the auxiliary linear operator, and h is the convergence control parameter. We will discuss L and h below. For now, we will set the homotopy $\mathcal{H} \equiv 0$. Note that when $q = 0$ we are on the linear operator, and when $q = 1$ we are on the nonlinear operator. It is in this way we think of the homotopy continuously deforming the linear operator into the nonlinear operator.

So now, in the vein of perturbation, assume an expansion of the solution around the parameter. That is, we assume

$$u = \sum_{j=0}^{\infty} u_j q^j, \tag{1.2}$$

where we expand u around the homotopy parameter q. Then, we will use this in our equation $\mathcal{H} \equiv 0$ and equate powers of q. So we have

$$0 = (1 - q)L\left[\sum_{j=0}^{\infty} u_j q^j\right] - qhN\left[\sum_{j=0}^{\infty} u_j q^j\right], \tag{1.3}$$

which leads to

$$\sum_{j=0}^{\infty} L[u_j]q^j - \sum_{j=0}^{\infty} L[u_j]q^{j+1} = qhN\left[\sum_{j=0}^{\infty} u_j q^j\right], \tag{1.4}$$

after moving the linear operator through the sum. Now we re-index the left-hand side so we can combine summations for

$$L[u_0] + \sum_{j=1}^{\infty} \Big(L[u_j] - L[u_{j-1}] \Big) q^j = qhN \left[\sum_{j=0}^{\infty} u_j q^j \right]. \tag{1.5}$$

Matching powers of q on each side is the next step. On the right-hand side, we will expand as a Taylor Series around $q = 0$. The zeroth order equation is

$$L[u_0] = 0. \tag{1.6}$$

This is the equation that will take initial and boundary conditions. The $O(q)$ equation is

$$L[u_1] = hN[u_0]. \tag{1.7}$$

For $m > 1$, the $O(q^m)$ equation is

$$L[u_m] = L[u_{m-1}] + \frac{h}{(m-1)!} \left(\frac{\partial^{m-1}}{\partial q^{m-1}} N \left[\sum_{j=0}^{\infty} u_j q^j \right] \right) \Big|_{q=0}. \tag{1.8}$$

What we have done is take the nonlinear problem and make it infinitely many linear problems. And since we can solve for the terms of the expansion sequentially, we are able to get as many terms as we would like.

The auxiliary linear operator L in the homotopy (1.1) is chosen for the problem. This can be a benefit and a drawback. The benefit is that we get to choose the type of linear problem we can be solving. The drawback is that if we pick a linear operator that is too trivial, our solution may not be appropriate for the problem (see below for error analysis). On the other hand, if the linear operator is more sophisticated, the size of the terms greatly increases. This leads to an inability to perform error analysis. See Chapter 6, for example.

The convergence control parameter h is another part of the brilliance of the method. This parameter, while being added to the homotopy function, propagates through the solution terms (starting with the $O(q)$ term). This adds a degree of freedom in every homotopy analysis problem, and allows us to choose the value of h to minimize the residual error (see below).

How good are the approximate solutions? In previous papers in the literature, the terms of the expansion are found. What we would like to be able to do is have a measure of how good they are. Recall $u = \sum_{j=0}^{\infty} u_j q^j$, so we have a way to construct the solution to our differential equation when $q = 1$. The convergence of u can be discussed; however, we usually don't need (and can't calculate) the whole series. Once we have the first three terms of our series, call the three-term approximation $\hat{u} = u_0 + u_1 + u_2$. We do not have the entire solution u to compare it to. But, a solution is exact if it solves the differential equation, i.e., if $N[u] = 0$. If $N[\hat{u}] = 0$, then the three-term approximation is an exact solution. If not, then evaluating $N[\hat{u}](\mathbf{x})$ for $\mathbf{x}$ in the domain D of the problem gives the residual error at $\mathbf{x}$. To avoid cancellations if the error is negative, we square it. Then, if we can integrate on the domain of interest, we will have the combined area of our approximation's squared residual error:

$$E(h) = \int_D \left(N[\hat{u}]\right)^2 (\mathbf{x}) d\mathbf{x}. \tag{1.9}$$

Oftentimes, there are several issues with integration. Small residuals can add up to large amounts or error. Or, the integral over an infinite domain may not converge. In this case,

we will take a sum

$$\hat{E}(h) = \frac{1}{M} \sum_{j=1}^{M} \left(N[\hat{u}]\right)^2 (\mathbf{x}_j), \tag{1.10}$$

where M is the number of points we wish to use. This allows us to find an average that weights each point evenly.

Once we have either $E(h)$ or $\hat{E}(h)$, it will be a polynomial in h that we can minimize. The error function exists when $N[\hat{u}]$ is L^2-integrable, and a minimum exists since the function is nonnegative and continuous.

In the following Chapters, we apply the homotopy analysis method to several different ordinary and partial differential equations, most of which only have numerical results in the literature. Later on, we are also able to find exact solutions to some PDEs using self-similar transforms.

The goal of this dissertation is to discover ways in which different choices of the linear operator affect the residual error produced by the resulting analytical approximations. There is a natural progression to the work, where more and more varied operators are used until a strong candidate is found. Then, we find exact solutions to other PDEs through the use of similarity transforms.

Chapter 2 covers the Ernst equation, which is used to solve the Einstein field equations and is used as a model of axially symmetric stationary vacuum gravitational fields. In this paper, we used a single auxiliary linear operator in the method.

Chapter 3 covers the equation used to describe the nonlinear evolution of a vector potential of an electromagnetic pulse propagating in an arbitrary pair plasma with temperature asymmetry. In this paper, the linear operator used is the linear part of the nonlinear operator (which does not always work).

In Chapter 4, the equation derived from a nonlinear σ model is discussed. The nonlinear sigma model is, among other things, a tool to use field theory to describe particles. Two different linear operators are chosen based on their solution types.

In Chapter 5, the Cahn-Hilliard equation, the nonlinear evolution equation that describes the free energy of a binary alloy, is discussed. This paper was where we really tested a variety of different linear operators over many varying given initial data.

Chapter 6 covers a difficult PDE: the Hasegawa-Mima equation. This equation, which takes a long time to even write down, describes the electric potential due to a drift wave in a plasma . This was actually the first project the author ever worked on using the Homotopy Analysis Method. The first linear operator chosen, which is just the linear part of the problem, does not yield solutions that are valid. The second choice yielded approximations that were too complicated to be tested. After writing the Cahn-Hilliard paper, we decided to try a third and successful linear operator.

Chapter 7 is about the Hunter-Saxton equation, the nonlinear wave equation that is used to study a nonlinear instability in the director field of a nematic liquid crystal. The original research in this chapter shows that the method is not suitable for all nonlinear partial

differential operators. Similarity transforms were used to find solutions to the equation, given in the next chapter.

Chapter 8 is about the exact and self-similar solutions to the Hunter-Saxton equation. We find new separable exact solutions, and a self-similar transform is used to convert the PDE into an ODE. Homotopy Analysis is then used on this ODE, with a convenient choice of linear operator.

Finally, we find self-similar solutions to the Khokhlov-Zabolotskaya equation, describing the propagation of a sound beam in a nonlinear medium, in Chapter 9. We are able to find several self-similarity transforms, including one that has a travelling wave similarity in one variable as well as a self-similarity in another. We are able to somewhat generalize the results and get new solutions by transforming variables and reducing the equation to an ODE. All of these lead to new exact solutions to this equation.

CHAPTER 2

EXACT AND ANALYTIC SOLUTIONS OF THE ERNST EQUATION GOVERNING AXIALLY SYMMETRIC STATIONARY VACUUM GRAVITATIONAL FIELDS

The following results are taken from the paper [63].

2.1 Background

The Ernst equation is given by

$$\mathcal{R}\mathrm{e}(u)\nabla^2 u = (\nabla u)^2 . \tag{2.1}$$

If we assume axial symmetry, the Ernst equation, in cylindrical form, reads

$$\mathcal{R}\mathrm{e}(u)\left(\frac{\partial^2 u}{\partial r^2} + \frac{1}{r}\frac{\partial u}{\partial r} + \frac{\partial^2 u}{\partial z^2}\right) = \left(\frac{\partial u}{\partial r}\right)^2 + \left(\frac{\partial u}{\partial z}\right)^2 , \tag{2.2}$$

where $u = u(r, z)$ is a complex-valued function [2]. The equation serves as a model of axially symmetric stationary vacuum gravitational fields [3]-[6]. Harrison [7] shows that the Ernst equation admits a Bächlund transform.

Since (2.2) is a homogeneous quadratic equation, perturbation theory works nicely [2]. In [8], the Ernst equation is used to completely separate the vacuum Einstein equations for an arbitrary stationary axisymmetric space-time. In [9], the Virasoro algebra is shown to exist in the solution space of the Ernst equation. The Ernst equation is solved as a boundary value problem using inverse methods in [10]. Rational approximations of the flip angle dependence of an MRI signal are derived using half-angle trigonometric substitutions in the Ernst equation in [11]. In [117], the class of hyperelliptic solutions to the Ernst equation are derived using Riemann-Hilbert techniques. The inverse scattering method [12] and the algebro-geometric ideology [13] have also been discussed.

In the present paper, the Ernst equation is transformed to a real-valued system and then simplified to a reduced Ernst equation. Then, the homotopy analysis method is used to find approximate solutions to this reduced equation. Following this, an exact solution is found under weaker boundary conditions. For many physical applications, approximate solutions, while clearly less informative than exact solutions, are sufficient to describe the true solutions (assuming that the error is sufficiently small). The method of homotopy analysis [14]-[22] has recently been applied to the study of a number of non-trivial and traditionally hard to solve nonlinear differential equations, for instance nonlinear equations arising in heat transfer [23]-[26], fluid mechanics [27]-[34], solitons and integrable models [35]-[39], nanofluids [40]-[41], the Lane-Emden equation which appears in stellar astrophysics [42]-[45], and models frequently used in mathematical physics [46, 47], to name a few areas.

2.2 A real-valued system

Let us transform (2.2) into a real-valued system. To this end, let us write $u = \rho + i\sigma$, where $\rho, \sigma : \mathbb{R}^2 \to \mathbb{R}$. Then, (2.2) becomes

$$\begin{aligned} \rho M[\rho] &= \rho_r^2 + \rho_z^2 - \sigma_r^2 - \sigma_z^2 \,, \\ \rho M[\sigma] &= 2\left(\rho_r \sigma_r + \rho_z \sigma_z\right) \,, \end{aligned} \tag{2.3}$$

where we define the linear operator M by

$$M = \frac{\partial^2}{\partial r^2} + \frac{1}{r}\frac{\partial}{\partial r} + \frac{\partial^2}{\partial z^2} \,. \tag{2.4}$$

Taking the second equation in (2.3) and dividing by ρ^3, we obtain

$$\frac{\sigma_{rr}}{\rho^2} + \frac{1}{r}\frac{\sigma_r}{\rho^2} + \frac{\sigma_{zz}}{\rho^2} - \frac{2\rho_r\sigma_r}{\rho^3} - \frac{2\rho_z\sigma_z}{\rho^3} = 0 \,. \tag{2.5}$$

Rearranging terms, we find that a solution pair (ρ, σ) satisfies the PDE

$$\frac{\partial}{\partial r}\left(\frac{\sigma_r}{\rho^2}\right) + \frac{1}{r}\left(\frac{\sigma_r}{\rho^2}\right) + \frac{\partial}{\partial z}\left(\frac{\sigma_z}{\rho^2}\right) = 0 \,. \tag{2.6}$$

Due to such symmetry, a self-similar solution to (2.3) may be possible. To this end, let us consider a solution of the form

$$\rho(r, z) = f(\eta) \qquad \text{and} \qquad \sigma(r, z) = g(\eta) \,, \tag{2.7}$$

where

$$\eta = \frac{r}{z} \tag{2.8}$$

is the similarity variable. Then, (2.3) is put into the form

$$f\left((1+\eta^2)f'' + \frac{2\eta^2+1}{\eta}f'\right) = (1+\eta^2)\left(f'^2 - g'^2\right) \,, \tag{2.9}$$

$$f\left((1+\eta^2)g'' + \frac{2\eta^2+1}{\eta}g'\right) = 2(1+\eta^2)f'g'\,, \tag{2.10}$$

where the prime denotes differentiation with respect to the similarity variable η. Observe that equation (2.9) can be solved for g'^2, and upon differentiation we obtain

$$g'g'' = -\frac{1}{2}\frac{d}{d\eta}\left(f\left(f'' + \frac{2\eta^2+1}{\eta(1+\eta^2)}f'\right) + f'^2\right)\,. \tag{2.11}$$

Meanwhile, (2.10) can be written in the form

$$\frac{g''}{g'} = -\frac{2\eta^2+1}{\eta(1+\eta^2)} + 2\frac{f'}{f}\,. \tag{2.12}$$

Then,

$$2\frac{f'}{f} - \frac{2\eta^2+1}{\eta(1+\eta^2)} = \frac{g''}{g'} = \frac{-\frac{1}{2}\frac{d}{d\eta}\left(f\left(f'' + \frac{2\eta^2+1}{\eta(1+\eta^2)}f'\right) + f'^2\right)}{f\left(f'' + \frac{2\eta^2+1}{\eta(1+\eta^2)}f'\right) + f'^2}\,. \tag{2.13}$$

Rearranging (2.13) for f and its derivatives, we obtain

$$f''' + \left\{\frac{3(2\eta^2+1)}{\eta(1+\eta^2)} - 5\frac{f'}{f}\right\}f'' + \left\{4\left(\frac{f'}{f}\right)^2 - \frac{5(2\eta^2+1)}{\eta(1+\eta^2)}\frac{f'}{f} + \frac{6\eta^2+1}{\eta^2(1+\eta^2)}\right\}f' = 0\,. \tag{2.14}$$

We shall refer to the ordinary differential equation (2.14) as the reduced Ernst equation. This equation, while reduced, is still rather complicated. So, let us attempt to simplify the form of this equation through a number of transformations. First, assuming $f \neq 0$ aside from a set of measure zero, divide (2.13) by f. Then, upon defining a new function

$$w(\eta) = \frac{f'(\eta)}{f(\eta)} = \frac{d}{d\eta}\ln(f(\eta))\,, \tag{2.15}$$

we reduce the order of (2.13) to obtain

$$w'' + \left\{\frac{3(2\eta^2+1)}{\eta(1+\eta^2)} - 2w\right\}w' - \frac{2(2\eta^2+1)}{\eta(1+\eta^2)}w^2 + \frac{6\eta^2+1}{\eta^2(1+\eta^2)}w = 0\,. \tag{2.16}$$

Next, we make the substitution

$$w(\eta) = \frac{v(\eta)}{\eta}\,, \tag{2.17}$$

which reduces (2.16) to

$$v'' + \frac{4\eta^2+1}{\eta(1+\eta^2)}v' + \frac{2}{1+\eta^2}v - \frac{2}{\eta}vv' - \frac{2}{1+\eta^2}v^2 = 0\,. \tag{2.18}$$

Finally, let us make the substitution

$$v(\eta) = \frac{u(\sqrt{1+\eta^2})}{\sqrt{1+\eta^2}} = \frac{u(s)}{s}\,, \tag{2.19}$$

where

$$s = \sqrt{1+\eta^2}\,. \tag{2.20}$$

Then, (2.18) becomes

$$u'' + \frac{2s}{s^2-1}u' - \frac{2}{s^2-1}uu' = 0\,, \tag{2.21}$$

where prime denotes differentiation with respect to s. With a solution $u(s)$ to (2.21)-(2.24), we may recover a solution to (2.14) by reversing the substitutions. In terms of u, a solution f to (2.14) is given by

$$f(\eta) = f(0)\exp\left(\int_0^\eta \frac{u(\sqrt{1+\tau^2})}{\tau\sqrt{1+\tau^2}}d\tau\right)\,. \tag{2.22}$$

In terms of the original coordinate system,

$$\rho(r,z) = f\left(\frac{r}{z}\right) = f(0)\exp\left(\int_0^{r/z} \frac{u(\sqrt{1+\tau^2})}{\tau\sqrt{1+\tau^2}}d\tau\right)\,. \tag{2.23}$$

In the transformed coordinates, $s = 1$ is the singular boundary, while a non-singular solution would be found $s > 1$. We may renormalize the domain so that $s \in [1+\epsilon, \infty)$,

where $0 < \epsilon$ is a parameter. Meaningful boundary conditions are

$$u(1+\epsilon) = A \qquad \text{and} \qquad \lim_{s\to\infty} u(s) = 0\,, \tag{2.24}$$

where A is a constant.

2.3 Homotopy analysis for the reduced Ernst equation

We may apply the method of homotopy analysis to the reduced Ernst equation (2.21) with initial data (2.24). We shall select the linear operator

$$L[u] = u'' + \frac{2s}{s^2-1}u'\,. \tag{2.25}$$

The order zero solution is then governed by the boundary value problem

$$L[u_0] = 0\,, \qquad u_0(1+\epsilon) = A\,, \qquad \lim_{s\to\infty} u(s) = 0\,. \tag{2.26}$$

The order zero solution is then given by

$$u_0(s) = A\frac{\ln(s+1) - \ln(s-1)}{\ln(2+\epsilon) - \ln(\epsilon)}\,. \tag{2.27}$$

The following will be useful in computing the higher order terms. Consider the initial value problem

$$L[U(s)] = Y(s)\,, \qquad U(1+\epsilon) = 0\,, \qquad \lim_{s\to\infty} U(s) = 0\,. \tag{2.28}$$

Let us define the function

$$I(s;\epsilon) = \int_{1+\epsilon}^{s} \frac{1}{\zeta^2-1}\int_{1+\epsilon}^{\zeta} (\xi^2-1)Y(\xi)d\xi d\zeta\,. \tag{2.29}$$

The solution obeying the condition at $s = 1 + \epsilon$ takes the form

$$U(s) = I(s;\epsilon) + C\int_{1+\epsilon}^{s} \frac{d\xi}{\xi^2 - 1} = I(s;\epsilon) + \frac{C}{2}\left(\ln\left(\frac{s-1}{s+1}\right) - \ln\left(\frac{\epsilon}{2+\epsilon}\right)\right), \tag{2.30}$$

where C is a constant to be determined. Evaluating this as $s \to \infty$ and using the remaining boundary condition, we have

$$0 = \lim_{s\to\infty} I(s;\epsilon) - \frac{C}{2}\ln\left(\frac{\epsilon}{2+\epsilon}\right), \tag{2.31}$$

which gives

$$C = \frac{2I(\infty;\epsilon)}{\ln\left(\frac{\epsilon}{2+\epsilon}\right)}, \tag{2.32}$$

where the numerator is defined in the limiting sense. With this, we have the solution

$$\begin{aligned} U(s) &= I(s;\epsilon) + \frac{I(\infty;\epsilon)}{\ln\left(\frac{\epsilon}{2+\epsilon}\right)}\left(\ln\left(\frac{s-1}{s+1}\right) - \ln\left(\frac{\epsilon}{2+\epsilon}\right)\right) \\ &= I(s;\epsilon) - I(\infty;\epsilon) + \frac{I(\infty;\epsilon)}{\ln\left(\frac{\epsilon}{2+\epsilon}\right)}\ln\left(\frac{s-1}{s+1}\right). \end{aligned} \tag{2.33}$$

The Homotopy between the reduced Ernst equation and the auxiliary linear operator L, given in (2.25), is

$$0 \equiv \mathcal{H}[u, u_0; q] = (1-q)L[U - u_0] - hqN[U], \tag{2.34}$$

where $u_0(s)$ is an initial approximate solution, h is the so-called convergence control parameter, and

$$N[U] = L[U] - \frac{2}{s^2-1}U\frac{dU}{ds}. \tag{2.35}$$

As q varies between 0 and 1, the Homotopy (2.34) takes the auxiliary linear operator L ($q = 0$) and "continuously deforms" it into the non-linear operator N ($q = 1$). Note that $N[U] = 0$ is (2.21). Next, we assume that $U(s)$ has a Taylor expansion around q:

$$U(s) = u_0(s) + \sum_{j=1}^{\infty} u_j(s) q^j. \tag{2.36}$$

Then the goal is to put (2.36) into (2.34) and match powers of q. Each value of q gives a nominal deformation equation. If the series (2.36) converges when $q = 1$, we have succeeded. What we will do is calculate the first few terms and show that a version of (2.36) with only a few terms gives small error.

The zeroth order deformation equation has been solved and is (2.27).

Plugging (4.28) into (2.34), we get

$$L[u_0] + \sum_{j=1}^{\infty} \Big(L[u_j] - (1+h) L[u_{j-1}] \Big) q^j = -qh \frac{2}{s^2 - 1} UU'. \tag{2.37}$$

Through the use of (4.28), the right-hand side of (2.37) has the closed form

$$-qh \frac{2}{s^2 - 1} UU' = -\frac{2h}{s^2 - 1} \sum_{m=0}^{\infty} \sum_{k=0}^{m} u_k(s) u'_{m-k}(s) q^{m+1}. \tag{2.38}$$

Thus, for $j \geq 1$, we have the jth order deformation equation

$$L[u_j] = (1+h) L[u_{j-1}] - \frac{2h}{s^2 - 1} \sum_{m=0}^{j-1} \sum_{k=0}^{m} u_k(s) u'_{m-k}(s). \tag{2.39}$$

The first order deformation equation is

$$L[u_1] = -\frac{2h}{s^2 - 1} u_0(s) u'_0(s), \tag{2.40}$$

which simplifies to

$$L[u_1] = \frac{4hA^2}{\ln(\frac{2+\epsilon}{\epsilon})^2} \ln\left(\frac{s+1}{s-1}\right) \frac{1}{(s^2-1)^2} \tag{2.41}$$

upon using (2.27). The solution, according to (2.33), is

$$u_1(s) = -\frac{hA^2}{6\ln(\frac{\epsilon}{2+\epsilon})^2} \ln\left(\frac{s-1}{s+1}\right) \left\{ \ln\left(\frac{s-1}{s+1}\right)^2 - \ln\left(\frac{\epsilon}{2+\epsilon}\right)^2 \right\}. \tag{2.42}$$

The second order deformation equation is

$$L[u_2] = (1+h)L[u_1] - \frac{2h}{s^2-1}\left(u_0(s)u_1'(s) + u_1(s)u_0'(s)\right). \tag{2.43}$$

Using (2.41), (2.27), and (2.42), the solution is

$$\begin{aligned} u_2(s) = -\frac{hA^2}{90\ln(\frac{2+\epsilon}{\epsilon})^3} \Bigg\{ & \ln\left(\frac{2+\epsilon}{\epsilon}\right)\left(15(1+h) - 2Ah\ln\left(\frac{2+\epsilon}{\epsilon}\right)\right) \\ & + 3Ah\ln\left(\frac{s-1}{s+1}\right)^2 \Bigg\} \ln\left(\frac{s-1}{s+1}\right) \left\{ \ln\left(\frac{s-1}{s+1}\right)^2 - \ln\left(\frac{\epsilon}{2+\epsilon}\right)^2 \right\}. \end{aligned} \tag{2.44}$$

Therefore, the sum of the first three terms gives us the approximate solution

$$\widehat{U}(s,h,A,\epsilon) = u_0(s) + u_1(s) + u_2(s). \tag{2.45}$$

We run $\widehat{U}$ through the original nonlinear operator corresponding to (2.21), then we set $\epsilon = 1$ and define the residual error $V(s,h,A) = N[\widehat{U}(s,h,A,1)]$. To get the error over the interval $[2,\infty)$, we compute the sum of squared residual errors

$$E(h,A) := \int_2^\infty (V(s,h,A))^2 ds. \tag{2.46}$$

What we get is that $E(h,A)$ is an eighth-degree polynomial in h. To get numerical estimates of the error, care must be taken in using approximations in the coefficients of $E(h,A)$

when actually plotting the error numerically. When using 5 or 10 digits of accuracy for the coefficients of h, rounding errors can be very large. Upon explicit evaluation, (2.46) becomes

$$E(h, A) = \mu_8(A)h^8 + \mu_7(A)h^7 + \cdots + \mu_0(A)\,, \tag{2.47}$$

where

$$\begin{aligned}\mu_8(A) =& 0.000001560555921A^8 - 1.28774467310^{-7}A^9 - 4.45989219710^{-9}A^{12} \\ &+ 2.24681149510^{-8}A^{10} - 2.25972420410^{-9}A^{11}\,,\end{aligned} \tag{2.48}$$

$$\begin{aligned}\mu_7(A) =& -8.95576236010^{-8}A^{10} - 0.00001248444737A^8 + 7.72643298210^{-7}A^9 \\ &+ 1.15124225910^{-9}A^{11}\,,\end{aligned} \tag{2.49}$$

$$\begin{aligned}\mu_6(A) =& -0.0003678857985A^6 - 0.0001395930553A^7 + 9.30879353010^{-8}A^{10} \\ &+ 0.00003433785169A^8 - 0.000002098971004A^9\,,\end{aligned} \tag{2.50}$$

$$\begin{aligned}\mu_5(A) =& -0.002207314791A^6 - 0.0007070296652A^7 + 0.00004318678092A^8 \\ &- 0.000002061861306A^9\,,\end{aligned} \tag{2.51}$$

$$\begin{aligned}\mu_4(A) =& 0.02842111612A^4 + 0.02704542242A^5 - 0.0009323264697A^7 \\ &+ 0.00002971091894A^8 + 0.003085522661A^6\,,\end{aligned} \tag{2.52}$$

$$\begin{aligned}\mu_3(A) =& -0.0003648898599A^7 + 0.1136844645A^4 + 0.01132144650A^6 \\ &+ 0.08113626728A^5\,,\end{aligned} \tag{2.53}$$

$$\mu_2(A) = 0.1705266967A^4 + 0.08113626726A^5 + 0.006396494847A^6\,, \tag{2.54}$$

$$\mu_1(A) = 0.02704542242A^5 + 0.1136844645A^4\,, \tag{2.55}$$

$$\mu_0(A) = 0.02842111611A^4\,. \tag{2.56}$$

Similar forms of the sum of squared residual errors are obtained for other values of $\epsilon > 0$; we omit the general form here, since it is quite expansive for arbitrary positive ϵ.

From the form of (2.46), it is clear that (2.47) is non-negative for all h and all A. As such, we can minimize the polynomial (2.47) over $h \in \mathbb{R}$ for each fixed value of A; in particular, a finite minimizing value of h must exist. In Figure 2.1, we plot the residual errors as a function of the convergence control parameter. For instance, when $A = 1$ we have a minimum at $h = -0.982$. This gives the approximate solution of $\widehat{U}(s, -0.982, 1, 1)$ with a sum of squares residual error of $E(-0.982, 1) = 3.19 \cdot 10^{-5}$. The error increases with the value in A, however. When $A = 0.1$, the error is $3.46 \cdot 10^{-13}$, but when $A = 5$, the error is 0.567. This makes sense: given a larger value of A, the adjustable parameter ϵ is closer to the singularity, hence the singularity's effect is stronger.

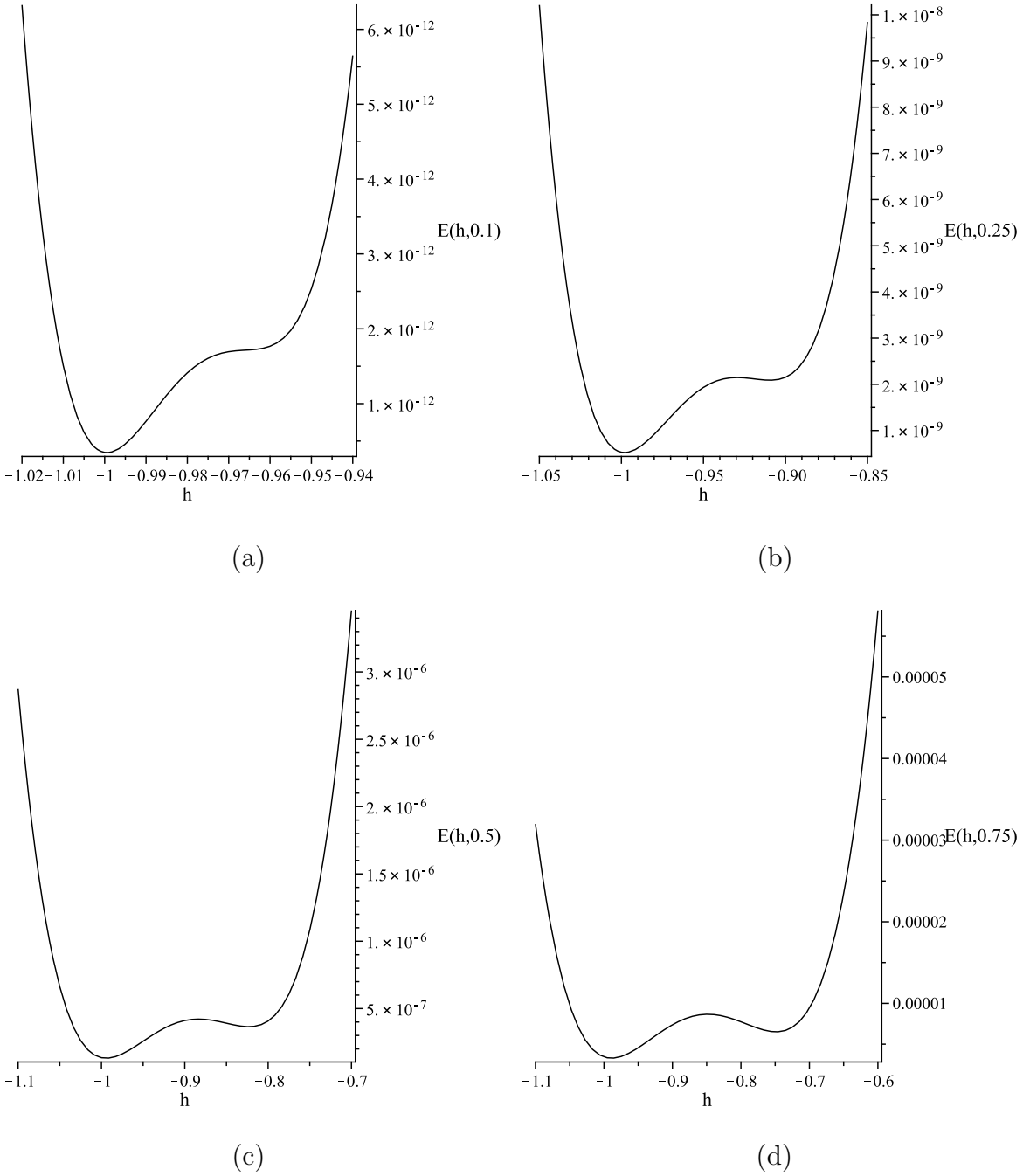

Figure 2.1: Plot of the function of residual errors $E(h, A)$ versus the convergence control parameter h for (a) $A = 0.1$, (b) $A = 0.25$, (c) $A = 0.5$, (d) $A = 1$.

To see the role increasing A has on making the solution more singular, note that the solution to our choice of linear operator L has Laurent expansion near $s = 1$ of the form

$$U(s) = \frac{C_\gamma}{(s-1)^\gamma} + \text{higher order terms}\,, \tag{2.57}$$

for arbitrary γ where C_γ is the leading order coefficient. Then, applying $A = u(1+\epsilon)$, we have

$$A = \frac{C_\gamma}{\epsilon^\gamma} \tag{2.58}$$

(neglecting higher order terms, since the singularity dominates near $s = 1$). If ϵ is small yet fixed, the parameter γ scales as $\gamma \sim \ln(A)$. So, as A becomes large, the strength of the singularity increases. For such strongly singular cases, the approximation method breaks down. However, for small or moderate values of A, the three-term expansions approximate the solutions remarkably well. In Figure 2, we plot the three term approximate solutions $\widehat{U}$ for various values of A. Included are the residual error minimizing values of the convergence control parameter, h.

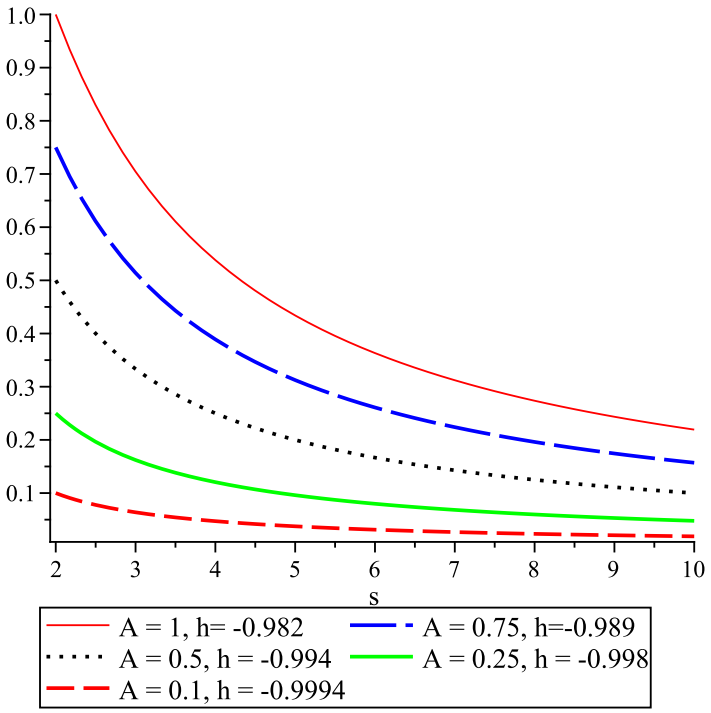

Figure 2.2: Plot of the three term approximation to the reduced Ernst equation (2.21) with initial data (2.24). We consider solutions for various values of A. The residual error minimizing value of the convergence control parameter, h, is indicated.

2.4 The connection between A and the singularity

The fact that the singularity present when using a homotopy solution with auxiliary linear operator L is stronger with increasing A can mean with the method induces the singularity, or the singularity is natural in the problem. Here we shall show that the singularity is natural, and that the homotopy analysis method solutions pick up on it. We shall see that for $A > 2$, the true solution develops an irregular singularity, while for smaller A a singularity is regular. This is in line with what we had in the previous section: for large A, the error in the homotopy solutions was large, while for small A, the approximate solutions gave very small error.

Let us begin with the exact equation (2.21). We may rewrite this as

$$\frac{u''}{u'} + \frac{2(s-u)}{s^2-1} = 0\,. \tag{2.59}$$

Integrating on the interval $[1+\epsilon, s]$, and then exponentiating, we find

$$u'(s) = C(\epsilon) \exp\left(\int_{1+\epsilon}^{s} \frac{2}{t^2-1} \left(u(t) - t\right) dt \right)\,. \tag{2.60}$$

Here $C(\epsilon)$ is a positive constant depending on ϵ. Let us write

$$u(t) - t = A - t + (u(t) - A) = A - t + (t - 1 - \epsilon)\Lambda(t)\,, \tag{2.61}$$

where $\Lambda(t)$ is analytic. The expression $u(t) - A = (t-1-\epsilon)\Lambda(t)$ follows from the fact that $u(1+\epsilon) = A$. Then, (2.60) becomes

$$u'(s) = C(\epsilon) \exp\left(2\int_{1+\epsilon}^{s} \frac{(t-1-\epsilon)\Lambda(t)}{t^2-1} dt \right) \exp\left(2\int_{1+\epsilon}^{s} \frac{A-t}{t^2-1} dt \right)\,. \tag{2.62}$$

Now,

$$\lim_{\epsilon\to 0^+}\int_{1+\epsilon}^{s}\frac{(t-1-\epsilon)\Lambda(t)}{t^2-1}dt=\int_1^s\frac{\Lambda(t)}{t+1}dt\,, \tag{2.63}$$

so the first integral in (2.62) is bounded on any compact interval since $\Lambda(t)$ is analytic. Next, consider

$$\begin{aligned}\int_{1+\epsilon}^{s}\frac{2(A-t)}{t^2-1}dt&=(A+1)\ln(2+\epsilon)-(A-1)\ln(\epsilon)+(A-1)\ln(s-1)-(A+1)\ln(s+1)\\&=(A+1)\ln\left(\frac{2+\epsilon}{1+s}\right)-(A-1)\ln\left(\frac{\epsilon}{s-1}\right)\\&=\ln\left[\left(\frac{2+\epsilon}{1+s}\right)^{A+1}\right]+\ln\left[\left(\frac{\epsilon}{s-1}\right)^{1-A}\right].\end{aligned} \tag{2.64}$$

So, this integral can become singular as $\epsilon\to 0^+$. Then, (2.62) becomes

$$u'(s)=C(\epsilon)\exp\left(2\int_{1+\epsilon}^{s}\frac{(t-1-\epsilon)\Lambda(t)}{t^2-1}dt\right)\left(\frac{2+\epsilon}{1+s}\right)^{A+1}(s-1)^{A-1}\epsilon^{1-A}\,. \tag{2.65}$$

Defining the analytic function

$$\Theta_\epsilon(s)=C(\epsilon)\exp\left(2\int_{1+\epsilon}^{s}\frac{(t-1-\epsilon)\Lambda(t)}{t^2-1}dt\right)\left(\frac{2+\epsilon}{1+s}\right)^{A+1}(s-1)^{A-1}\,, \tag{2.66}$$

($\Theta_\epsilon(s)$ is analytic for any choice of $\epsilon\geq 0$) we find that (2.65) becomes

$$u'(s)=\frac{\Theta_\epsilon(s)}{\epsilon^{A-1}}\,. \tag{2.67}$$

Now, the strength of the singularity determines whether or not it is regular. Here, we need $u'(s)\sim\epsilon^\nu$ where $\nu\geq -1$. Taking $\nu=-(A-1)$, we see that we need $A\leq 2$. Hence, for $A\leq 2$, we can have solutions with regular singular points. Meanwhile, for $A>2$, the strength of the singularity is too strong, and the solutions have irregular singular point at $s=1$.

We have therefore determined why the analytical approximations in Section 3 have poor error for large A: beyond $A = 2$, the solutions have an irregular singularity, and the problem as stated cannot be solved by an analytical method such as homotopy analysis. Even adding additional terms would not help for $A > 2$, since the analytical approximation cannot capture the strength of such a strong singularity. When regular singular solutions do exist ($0 < A < 2$), the analytical results are very good.

2.5 Exact solution for alternate boundary conditions

We've shown that approximate solutions with low residual error are possible for the conditions (2.24). A weaker set of conditions are possible, namely

$$u(1+\epsilon) = A \qquad \text{and} \qquad \lim_{s\to\infty} u'(s) = A, \tag{2.68}$$

where A is a constant. Under these different conditions, note that we obtain the exact solution $u(s) \equiv A$ to (2.21) for all $s \in (1, \infty)$. Then, we recover the quantities

$$v(\eta) = \frac{A}{\sqrt{1+\eta^2}} \qquad \text{and} \qquad w(\eta) = \frac{A}{\eta\sqrt{1+\eta^2}}\,. \tag{2.69}$$

Then,

$$\frac{f'(\eta)}{f(\eta)} = \frac{A}{\eta\sqrt{1+\eta^2}}\,, \tag{2.70}$$

which implies

$$\ln f(\eta) = B + A\int^{\eta} \frac{d\xi}{\xi\sqrt{1+\xi^2}} = B - A\tanh^{-1}\left(\frac{1}{\sqrt{1+\eta^2}}\right)\,. \tag{2.71}$$

Here B is another arbitrary constant. We then obtain the exact solution

$$f(\eta) = \exp\left\{B - A\tanh^{-1}\left(\frac{1}{\sqrt{1+\eta^2}}\right)\right\}. \tag{2.72}$$

Meanwhile, integrating (2.12) for $g'(\eta)$, we have

$$\ln g'(\eta) = C_1 - \ln\eta - \ln(1+\eta^2) - 2A\tanh^{-1}\left(\frac{1}{\sqrt{1+\eta^2}}\right). \tag{2.73}$$

We find that

$$g(\eta) = C_2 + \int_0^\eta \frac{\exp\left\{C_1 - A\tanh^{-1}\left(\frac{1}{\sqrt{1+\xi^2}}\right)\right\}}{\xi\sqrt{1+\xi^2}}. \tag{2.74}$$

Here C_1 and C_2 are constants. Putting these solutions back into the original coordinate systems, we find that a solution $u(r,z) = \rho(r,z) + i\sigma(r,z)$ is given by

$$\rho(r,z) = \exp\left\{B - A\tanh^{-1}\left(\frac{z}{\sqrt{r^2+z^2}}\right)\right\} \tag{2.75}$$

and

$$\sigma(r,z) = C_2 + \int_0^{r/z} \frac{\exp\left\{C_1 - A\tanh^{-1}\left(\frac{1}{\sqrt{1+\xi^2}}\right)\right\}}{\xi\sqrt{1+\xi^2}}, \tag{2.76}$$

where $r > 0$ and $z > 0$. To simplify $\sigma(r,z)$, make the change of variable

$$\nu = C_1 - A\tanh^{-1}\left(\frac{1}{\sqrt{1+\xi^2}}\right). \tag{2.77}$$

Then,

$$\sigma(r,z) = C_2 + \frac{1}{A}\int_{-\infty}^{\nu(r/z)} e^\nu d\nu = C_2 + \frac{1}{A}\exp\left\{C_1 - A\tanh^{-1}\left(\frac{z}{\sqrt{r^2+z^2}}\right)\right\}. \tag{2.78}$$

In Figure 3, we plot the modulus $|u(r,z)| = \sqrt{\rho(r,z)^2 + \sigma(r,z)^2}$ when $A = B = C_1 = 1$ and $C_2 = 0$. In the radial far-field case of $r >> z$ (i.e., $r/z \to \infty$), we have that $\rho \to e^A$ and

$\sigma \to C_2 + \frac{1}{A}e^{C_1}$, hence the modulus is bounded and satisfies

$$|u(r,z)| \approx \sqrt{e^{2A} + \left(C_2 + \frac{1}{A}e^{C_1}\right)^2} \qquad \text{for} \qquad r >> z\,. \tag{2.79}$$

This relation may then be used to calibrate the arbitrary integration constants. Further, when $A = B = C_1 = 1$ and $C_2 = 0$, taking $r \to 0^+$ and $z > 0$ fixed, we have $|u(r,z)| \to 0$ while if we take $z \to 0^+$ and $r > 0$ fixed, we have $|u(r,z)| \to \sqrt{2}$. This behavior is seen in Figure 2.3.

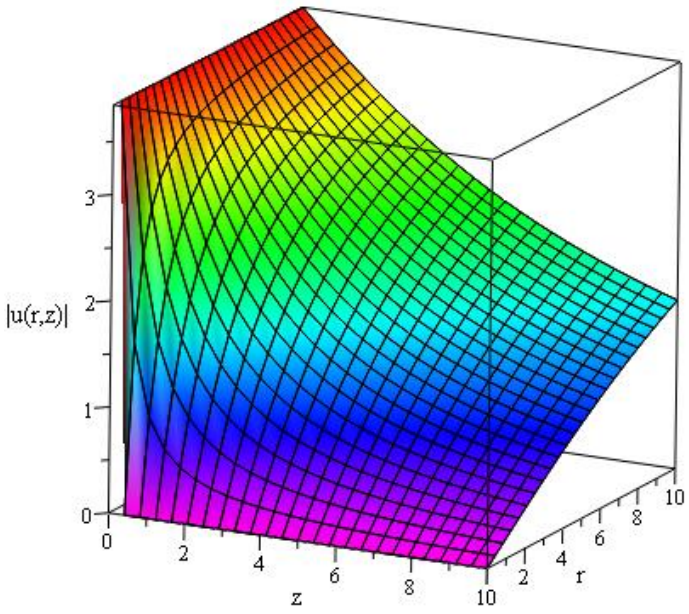

Figure 2.3: Plot of the modulus $|u(r,z)|$ of the exact solution $u(r,z)$ with real part $\rho(r,z)$ given by (2.75) and imaginary part $\sigma(r,z)$ given by (2.78). Here we select the arbitrary integration constants to satisfy $A = B = C_1 = 1$ and $C_2 = 0$.

2.6 Discussion

Upon transforming the cylindrical coordinate form of the Ernst equation into a real-valued system, we were able to apply the method of homotopy analysis to construct approximate solutions to the relevant nonlinear singular boundary value problem. Through an appropriate choice of the auxiliary linear operator, we were able to construct successive terms in the approximate solution, despite difficulties arising from the singular nature of the problem. Then, through an appropriate choice of the convergence control parameter we obtained three-term approximate solutions which have sufficiently small residual error. In particular, we selected the convergence control parameter so as to minimize the sum of squared residuals over the infinite domain. This method has recently been employed in order to control the residual error in a number of nonlinear problems [22, 48, 49, 50]. From here, the solution to the similarity ordinary differential equation can be mapped back to a solution of the Ernst partial differential equation, replacing $s = \sqrt{1+\eta^2}$ and then taking $\eta = r/z$.

For a related yet simpler boundary value problem (in the case where the near- and far-field conditions exactly agree), an exact solution was found to the boundary value problem. This solution was translated back into a solution of the full nonlinear PDE. Qualitatively, this solution agrees with the approximate solutions, though the latter are more complicated, owing to the more complicated boundary conditions. Both classes of solutions examined correspond to what one would expect physically. There exists a singularity as the radius

approaches zero ($r \to 0^+$), while, when the radius becomes large $r \to \infty$, the solutions asymptotically decay in an algebraic manner to some zero or positive limiting value.

With this, we have determined the behavior of two classes of solutions to the Ernst equation, which acts as a model of axially symmetric stationary vacuum gravitational fields, where the two classes are differentiated from one another in their far-field behavior. Regarding future work, recall that Harrison [7] showed that the Ernst equation admits a Bächlund transform. Hence, it may be possible to generate multi-hump soliton solutions for other reductions of the Ernst equations. Here, the exp-function, tanh or sech methods could prove useful; see, for instance [51].

CHAPTER 3

PEAKED SOLUTIONS FOR THE NONLINEAR EVOLUTION OF A VECTOR POTENTIAL OF AN ELECTROMAGNETIC PULSE PROPAGATING IN AN ARBITRARY PAIR PLASMA WITH TEMPERATURE ASYMMETRY

The following results are from the article [112].

3.1 Background

The nonlinear wave equation

$$2i\omega_0\frac{\partial A}{\partial t}+\frac{(2-\epsilon)}{\omega_0^2}\frac{\partial^2 A}{\partial \xi^2}+\frac{\partial^2 A}{\partial x^2}+\frac{\partial^2 A}{\partial y^2}+f(|A|^2)A=0 \tag{3.1}$$

describes the nonlinear evolution of a vector potential of an electromagnetic pulse propagating in an arbitrary pair plasma with temperature asymmetry [52, 53]. Here A is the slowly varying amplitude of a circularly polarized EM pulse with mean frequency ω_0 and mean wave number k_0, and $\xi = z - v_g t$ is the co-moving coordinate with group velocity v_g. Under

appropriate renormalization [52], the above equation takes the form

$$i\frac{\partial A}{\partial t} + \frac{\partial^2 A}{\partial \xi^2} + \frac{\partial^2 A}{\partial x^2} + \frac{\partial^2 A}{\partial y^2} + f(|A|^2)A = 0\,. \tag{3.2}$$

Appropriate forms of f include the cubic-quintic model

$$f(|A|^2) = |A|^2 - |A|^4 \tag{3.3}$$

and the more complicated focusing-defocusing model

$$f(|A|^2) = \frac{|R|^2}{(1+|R|^2)^2}\,. \tag{3.4}$$

Making the simplifying assumptions of [52], converting (x, y) to polar coordinates (r, θ), and taking $A = R(r)\exp(i\lambda t + im\theta)$ (where the integer m defines the topological charge of vortices and λ is the nonlinear frequency shift) we obtain

$$\frac{d^2R}{dr^2} + \frac{1}{r}\frac{dR}{dr} - \left(\frac{m^2}{r^2} + \lambda\right)R + F(R) = 0\,, \tag{3.5}$$

where

$$F(R) = R^3 - R^5 \qquad \text{or} \qquad F(R) = \frac{R^3}{(1+R^2)^2} \tag{3.6}$$

as needed. Natural boundary conditions are

$$R(0) = 0\,, \tag{3.7}$$

$$\left.\frac{d^mR}{dr^m}\right|_{r=0} = A_0\,, \tag{3.8}$$

$$\lim_{r\to\infty} R(r) = 0\,. \tag{3.9}$$

Note that there are three conditions, yet our equation is of second order. We shall see that one condition results in a restriction on the parameter regime for λ. To this end, note taking $m = 1$ and considering the linearized equation

$$R_0'' + \frac{1}{r}R_0' - \left(\frac{1}{r^2} + \lambda\right) R = 0\,, \tag{3.10}$$

we have the exact solution in terms of Bessel's function of the first kind

$$R_0(r) = \frac{2A_0}{\sqrt{-\lambda}} J_1(\sqrt{-\lambda}r) \tag{3.11}$$

provided that $\lambda < 0$. For $\lambda = 0$, we obtain a stationary state. The stationary state allows for a better understanding of the nonlinear structure, as it permits us to focus on the nonlinearity without also having to contend with stability or instability due to temporal perturbations. So, in what follows, we shall take $\lambda = 0$.

Solitons are thought to be better than current transmission of information methods [54]. It has been shown that the pair plasma with small temperature asymmetry is a suitable candidate for a stable soliton structure [52]. Also, electromagnetic soliton structures have been created due to asymmetries of different source [55]. In [53], numerical methods as well as a variational method are used for (3.2) to study light bullets in saturating media. Pair plasmas also have applications to astrophysics [55].

Note that (3.5) is too complicated to admit an exact solution. For many physical applications, approximate solutions, while clearly less informative than exact solutions, are sufficient to describe the true solutions (assuming that the error is sufficiently small). Taylor series solutions would likely only be valid in a small region near the origin. In the present

paper, we shall apply the method of homotopy analysis to study peaked solutions to equation (3.5) governing nonlinear evolution of a vector potential of an electromagnetic pulse propagating in an arbitrary pair plasma with temperature asymmetry. Peaked solutions have previously been considered in a number of applications. When working with integrable models, such solutions are usually referred to as peakons [56]-[58].

The method of homotopy analysis [14]-[22] has recently been applied to the study of a number of non-trivial and traditionally hard to solve nonlinear differential equations, for instance nonlinear equations arising in heat transfer [23]-[26], fluid mechanics [27]-[34], solitons and integrable models [35]-[39], nanofluids [40]-[41], the Lane-Emden equation which appears in stellar astrophysics [42]-[45], and models frequently used in mathematical physics [46, 47], to name a few areas. In the present paper, we apply a form of homotopy analysis known as the so-called "optimal homotopy analysis method." In this method, one chooses the convergence control parameter so as to minimize a function of the residual error over the domain. This method has been successfully applied to a number of problems in mathematical physics; see [48] - [63]. Using this method, we are able to construct peaked solutions valid over the whole semi-infinite interval corresponding to $r \in [0, \infty)$.

3.2 Homotopy analysis for the cubic-quintic model with topological charge $m = 1$

Here we solve the boundary value problem

$$\frac{d^2R}{dr^2} + \frac{1}{r}\frac{dR}{dr} - \frac{1}{r^2}R + R^3 - R^5 = 0\,, \tag{3.12}$$

subject to

$$R(0) = 0\,, \qquad R'(0) = A_0\,, \qquad \lim_{r\to\infty} R(r) = 0\,. \tag{3.13}$$

An appropriate choice of linear operator shall be

$$L = \frac{d^2}{dr^2} + \frac{1}{r}\frac{d}{dr} - \frac{1}{r^2}\,. \tag{3.14}$$

Then, for arbitrary constants c_1 and c_2 we have

$$L\left[c_1 r + \frac{c_2}{r}\right] = 0\,. \tag{3.15}$$

Note that the conditions at $r = 0$ would cause $c_2 = 0$ while the conditions at $r \to \infty$ would cause $c_1 = 0$. So, the only global solution on $r \in (0, \infty)$ which is continuously differentiable is the zero solution. However, if we are willing to search for continuous yet weak solutions (weak in the sense that solutions are not continuously differentiable everywhere on the domain), we can apply matching. To this end, consider a function

$$R_0(r) = \begin{cases} c_1 r & 0 \le r \le r_*\,, \\ \\ \frac{c_2}{r} & r > r_*\,, \end{cases} \tag{3.16}$$

where $r_* > 0$ is a matching point. Then, the conditions at $r = 0$ imply $c_1 = A_0$ while the far-field condition $R \to 0$ as $r \to \infty$ is always satisfied. To ensure continuity at $r = r_*$, we have

$$A_0 r_* = \frac{c_2}{r_*} \Rightarrow c_2 = A_0 r_*^2 \,, \tag{3.17}$$

hence

$$R_0(r) = \begin{cases} A_0 r & 0 \le r \le r_* \,, \\ \frac{A_0 r_*^2}{r} & r > r_* \,, \end{cases} \tag{3.18}$$

is a weak solution to the linear problem $L[R_0] = 0$ which satisfies all three boundary conditions. Regarding regularity, observe that such a solution is $L^2((0,\infty))$ (L^2-integrable):

$$\int_0^\infty \left(R_0(r)\right)^2 dr = \int_0^{r_*} A_0^2 r^2 dr + \int_{r_*}^\infty \frac{A_0^2 r_*^4}{r^2} dr = \frac{4}{3} A_0^2 r_*^3 < \infty \,. \tag{3.19}$$

Taking the nonlinear operator

$$N[R] = \frac{d^2 R}{dr^2} + \frac{1}{r}\frac{dR}{dr} - \frac{1}{r^2} R + R^3 - R^5 = L[R] + R^3 - R^5 \,, \tag{3.20}$$

we construct the homotopy

$$\mathcal{H}(R; q) = (1 - q) L[R] + q h N[R] \,, \tag{3.21}$$

where $q \in [0, 1]$ is the embedding parameter such that $\mathcal{H}(R; 0) = 0$ implies $L[R] = 0$ and $\mathcal{H}(R; 1) = 0$ implies $N[R] = 0$, and h is the convergence control parameter. Setting $\mathcal{H}(R; q) \equiv 0$, and assuming a solution of the form

$$R(r) = R_0(r) + q R_1(r) + q^2 R_2(r) + \cdots \,, \tag{3.22}$$

we see that

$$L[R_0] = 0\,, \tag{3.23}$$

subject to

$$R_0(0) = 0\,, \qquad R_0'(0) = A_0\,, \qquad \lim_{r\to\infty} R_0(r) = 0\,, \tag{3.24}$$

$$L[R_1] = (1-h)L[R_0] - hR_0^3 + hR_0^5 = -hR_0^3 + hR_0^5\,, \tag{3.25}$$

subject to

$$R_1(0) = 0\,, \qquad R_1'(0) = 0\,, \qquad \lim_{r\to\infty} R_1(r) = 0\,, \tag{3.26}$$

$$L[R_2] = (1-h)L[R_1] - 3hR_0^2R_1 + 5hR_0^4R_1\,, \tag{3.27}$$

subject to

$$R_2(0) = 0\,, \qquad R_2'(0) = 0\,, \qquad \lim_{r\to\infty} R_2(r) = 0\,. \tag{3.28}$$

We see that $R_0(r)$ is the function given by (3.18). While r_* denotes the position of the peak, we can (with an appropriate scaling of r) select $r_* = 1$, as this will greatly simplify computations. On $r \in (0,1)$, we have

$$L[R_{1-}] = -hA_0^3r^3 + hA_0^5r^5\,, \tag{3.29}$$

and therefore

$$R_{1-}(r) = \frac{hA_0^3}{48}r^5\left(A_0^2r^2 - 2\right)\,. \tag{3.30}$$

Meanwhile, for $r > 1$,

$$L[R_{1+}] = -hA_0^3r^{-3} + hA_0^5r^{-5}\,, \tag{3.31}$$

and we obtain

$$R_{1+}(r) = \frac{c_2}{r} + \frac{hA_0^3}{2}\frac{\ln r}{r} + \frac{hA_0^5}{8}\frac{1}{r^3}\,. \tag{3.32}$$

Matching $R_{1-}(1) = R_{1+}(1)$, we have

$$c_2 = -\frac{hA_0^3}{48}\left(5A_0^2 + 2\right)\,. \tag{3.33}$$

Putting this together, we have

$$R_1(r;h) = \begin{cases} \frac{hA_0^3}{48} r^5 \left(A_0^2 r^2 - 2\right) & \text{for } \; 0 \le r \le 1\,, \\ -\frac{hA_0^3}{48}\left(5A_0^2+2\right)\frac{1}{r} + \frac{hA_0^3}{2}\frac{\ln r}{r} + \frac{hA_0^5}{8}\frac{1}{r^3} & \text{for } \; r > 1\,, \end{cases} \tag{3.34}$$

We continue the process to obtain higher order terms. For the order two approximation $R(r;h) = R_0(r) + R_1(r;h) + R_2(r;h)$ we calculate the residual error $N[R(r;h)]$. To measure the error over the domain $r \in [0,\infty)$, we use the integral of squared residual errors

$$\begin{aligned} E(h) &= \int_0^\infty \left(N[R(r;h)]\right)^2 dr \\ &= \int_0^1 \left(N[A_0 r + R_{1-}(r;h) + R_{2-}(r;h)]\right)^2 dr \\ &+ \int_1^\infty \left(N[\frac{A_0}{r} + R_{1+}(r;h) + R_{2+}(r;h)]\right)^2 dr. \end{aligned} \tag{3.35}$$

We find that the error function $E(h)$ exists when $N[R(r;h)]$ is L^2-integrable, and by construction E is convex in h. So, a minimizer h^* exists, such that $E(h^*) < E(h)$ for all $h \neq h^*$. Taking $A_0 = 1$, we find that $h^* = \text{argmin}_{h\in\mathbb{R}} E(h) = 0.45014$. In Figure 3.1, we plot the error function $E(h)$ as it depends on the convergence control parameter, h. We find that the minimal value is $E(h^*) = 0.011$. Hence, the accumulated squared residual error over the whole domain is of order 10^{-2}, which is very good considering the domain is infinite. In Figure

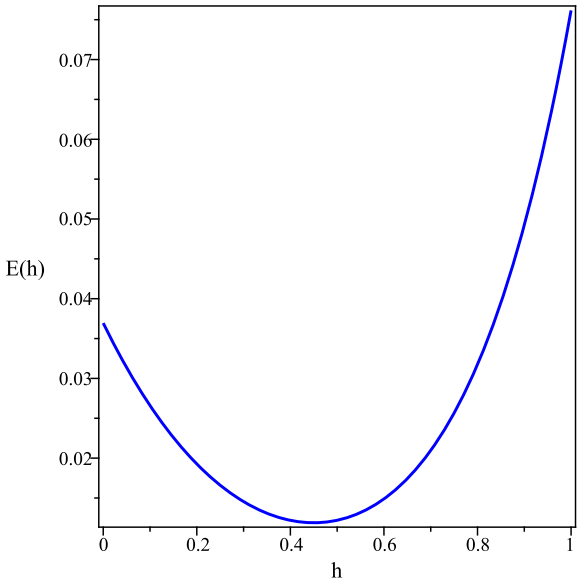

Figure 3.1: Plot of $E(h)$, the accumulated sum of squared residual error over the infinite domain $r \in [0, \infty)$, as a function of h, the convergence control parameter. The error function has minimum $E(h^*) = 1.1 \times 10^{-2}$ where $h^* = 0.45014$.

3.2, we plot the second order solution $R(r; h) = R_0(r) + R_1(r; h) + R_2(r; h)$. We observe the peaked behavior of the continuous approximate solution. So, the homotopy analysis method has allowed us to obtain the required weak solution, which is a piecewise-continuous peaked solution with peak at $r_* = 1$ and algebraic decay as $r \to \infty$.

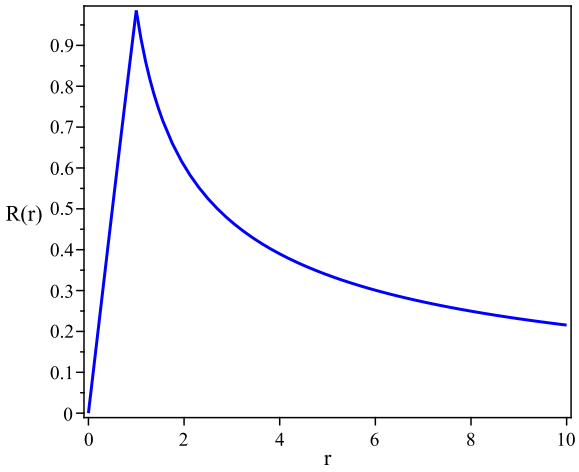

Figure 3.2: Plot of the three-term approximate solution to $R(r)$ when $h^* = 0.45014$, for the cubic-quintic model with topological charge $m = 1$. Here the initial condition is taken as $A_0 = 1$, and the peak occurs at $r_* = 1$.

3.3 Homotopy analysis for the cubic-quintic model with topological charge $m = 2$

Here we solve the boundary value problem

$$\frac{d^2R}{dr^2} + \frac{1}{r}\frac{dR}{dr} - \frac{4}{r^2}R + R^3 - R^5 = 0\,, \tag{3.36}$$

subject to

$$R(0) = 0\,, \qquad R''(0) = A_0\,, \qquad \lim_{r\to\infty} R(r) = 0\,. \tag{3.37}$$

An appropriate choice of linear operator shall be

$$L = \frac{d^2}{dr^2} + \frac{1}{r}\frac{d}{dr} - \frac{4}{r^2}\,. \tag{3.38}$$

Then, for arbitrary constants c_1 and c_2 we have

$$L\left[c_1 r^2 + \frac{c_2}{r^2}\right] = 0\,. \tag{3.39}$$

Note that the conditions at $r = 0$ would cause $c_2 = 0$ while the conditions at $r \to \infty$ would cause $c_1 = 0$. So, the only global solution on $r \in (0, \infty)$ which is continuously differentiable is the zero solution. Allowing continuous yet weak solutions, consider a function

$$R_0(r) = \begin{cases} c_1 r^2 & 0 \le r \le r_*\,, \\ \\ \frac{c_2}{r^2} & r > r_*\,, \end{cases} \tag{3.40}$$

where again $r_* > 0$ is a matching point. Then, the conditions at $r = 0$ imply $c_1 = A_0/2$ while the far-field condition $R \to 0$ as $r \to \infty$ is always satisfied. To ensure continuity at $r = r_*$, we have

$$\frac{A_0}{2} r_*^2 = \frac{c_2}{r_*^2} \Rightarrow c_2 = \frac{A_0}{2} r_*^4\,, \tag{3.41}$$

hence

$$R_0(r) = \begin{cases} \frac{A_0}{2} r^2 & 0 \le r \le r_*\,, \\ \\ \frac{A_0 r_*^4}{2} \frac{1}{r^2} & r > r_*\,, \end{cases} \tag{3.42}$$

is a weak solution to the linear problem $L[R_0] = 0$ which satisfies all three boundary conditions. Regarding regularity, observe that such a solution is $L^2((0,\infty))$ (L^2-integrable):

$$\int_0^\infty \left(R_0(r)\right)^2 dr = \int_0^{r_*} \frac{A_0^2}{4} r^4 dr + \int_{r_*}^\infty \frac{A_0^2 r_*^8}{4r^4} dr = \frac{2}{15} A_0^2 r_*^5 < \infty\,. \tag{3.43}$$

Taking the nonlinear operator to be $N[R] = L[R] + R^3 - R^5$, we construct the homotopy

$$\mathcal{H}(h; q) = (1 - h)L[R] - hqN[R]. \tag{3.44}$$

For $H(h;q) \equiv 0$, we assume the expansion

$$R(r) = \sum_{j=0}^{\infty} R_j(r) q^j. \tag{3.45}$$

Doing so and working this back into $H(h;q) = 0$ and matching powers of q yields

$$L[R_0] = 0, \qquad R_0(0) = 0, \qquad R_0''(0) = A_0, \qquad \lim_{r\to\infty} R_0(r) = 0, \tag{3.46}$$

$$L[R_1] = (1+h)L[R_0] + h(R_0^3 - R_0^5), \qquad R_1(0) = 0, \qquad R_1''(0) = 0, \qquad \lim_{r\to\infty} R_1(r) = 0, \tag{3.47}$$

and

$$L[R_2] = (1+h)L[R_1] + h\left(-5R_0^4 R_1 + 3R_0^2 R_1\right), \qquad R_2(0) = 0,\ R_2''(0) = 0, \qquad \lim_{r\to\infty} R_2(r) = 0. \tag{3.48}$$

For simplicity we take $r_* = 1$. Since we already found $R_0(r)$ in (3.42), we have

$$R_0(r) = \begin{cases} \frac{A_0}{2} r^2 & 0 \le r \le 1\,, \\ \\ \frac{A_0}{2r^2} & r > 1. \end{cases} \tag{3.49}$$

Next, for $0 \le r \le 1$, (3.47) becomes

$$L[R_{1-}] = h\left(\frac{A_0^3}{8} r^6 - \frac{A_0^5}{32} r^{10}\right), \tag{3.50}$$

which after using $R_{1-}(0) = 0$ and $R_{1-}'(0) = 0$ solves to

$$R_{1-}(r) = \frac{-hA_0}{4480} r^8 \left(A_0^2 r^4 - \frac{28}{3}\right). \tag{3.51}$$

Let $R_{1-}(1) = \kappa$. For $r > 1$, we have

$$L[R_{1+}] = h\left(\frac{A_0^3}{8r^6} - \frac{A_0^5}{32r^10}\right). \tag{3.52}$$

We want to match the functions at $r = 1$ for continuity, so we get the condition $R_{1+}(1) = \kappa$ in addition to $\lim_{r\to\infty} R_{1+}(r) = 0$. This gives us the two conditions we need to completely solve and get

$$R_{1+}(r) = \frac{A_0^3 h}{13,440r^8}\left(-112r^6 + 4A_0^2r^6 + 140r^4 - 7A_0^2\right). \tag{3.53}$$

We put this together for

$$R_1(r) = \begin{cases} \frac{-hA_0}{4480}r^8\left(A_0^2r^4 - \frac{28}{3}\right) & 0 \le r \le 1\,, \\ \frac{A_0^3 h}{13,440r^8}\left(-112r^6 + 4A_0^2r^6 + 140r^4 - 7A_0^2\right) & r > 1. \end{cases} \tag{3.54}$$

The work is similar to find $R_2(r)$.

Armed with the three-term expansion, we can calculate the error involved. First, we define $V(A_0, r, h) := R_0(r) + R_1(r) + R_2(r)$. Next, define $E_-(A_0, h, r) := N[R_{0-}(r) + R_{1-}(r) + R_{2-}(r)]$ and $E_+(A_0, h, r) := N[R_{0+}(r) + R_{1+}(r) + R_{2+}(r)]$. Consider the case when $A_0 = 1$. We calculate the sum of squared residual error

$$E(h) := \int_0^1 E_-(1, h, r)^2 dr + \int_1^\infty E_+(1, h, r)^2 dr. \tag{3.55}$$

The minimum value of this function is 3.14×10^{-11}, obtained at $h^* = -1.0018$. The plot of this error function is given in Figure 3.3, and the resulting three-term approximation with minimizing h-value $V(1, r, h^*)$ is given in Figure 3.4. The error here is much smaller than in the previous section due to the fact that the coefficients of the solution are cut in half. As these numbers are taken to higher powers through the nonlinear operator and squared to find the error, we are getting the same degree polynomial in h over the same interval, with much smaller coefficients.

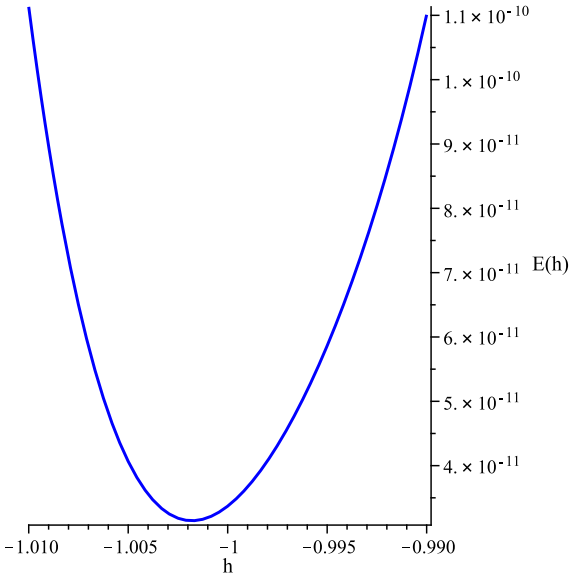

Figure 3.3: Plot of $E(h)$, the accumulated sum of squared residual error over the infinite domain $r \in [0, \infty)$, as a function of h, the convergence control parameter. The error function has minimum $E(h^*) = 3.14 \times 10^{-11}$ where $h^* = -1.0018$.

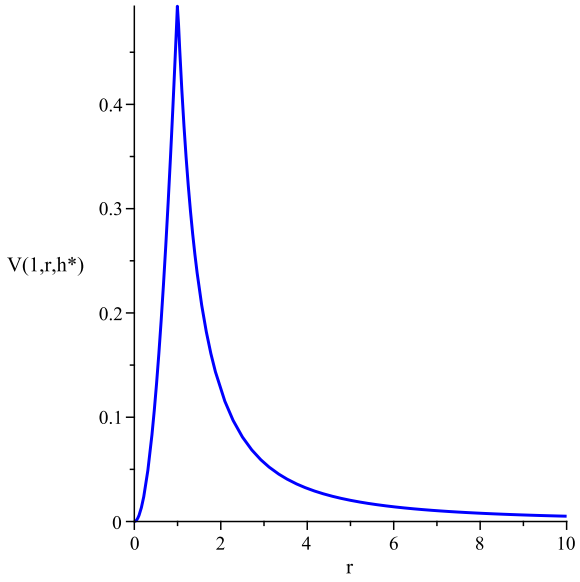

Figure 3.4: Plot of the three-term approximate solution to $V(r)$ to $R(r)$ when $h^* = -1.0018$, for the cubic-quintic model with topological charge $m = 2$. Here the initial condition is taken as $A_0 = 1$, and the peak occurs at $r_* = 1$.

3.4 Homotopy analysis for the cubic-quintic model with topological charge $m = 3$

In this section, we consider the boundary-value problem

$$\frac{d^2R}{dr^2} + \frac{1}{r}\frac{dR}{dr} - \frac{9}{r^2}R + R^3 - R^5 = 0\,, \tag{3.56}$$

subject to

$$R(0) = 0, \qquad R'''(0) = 1, \qquad \lim_{r\to\infty} R(r) = 0. \tag{3.57}$$

Considering the linear operator

$$L = \frac{d^2}{dr^2} + \frac{1}{r}\frac{d}{dr} - \frac{9}{r^2}, \tag{3.58}$$

we observe for arbitrary constants c_1 and c_2 that

$$L\left[c_1 r^3 + \frac{c_2}{r^3}\right] = 0. \tag{3.59}$$

As in the previous two sections, we will consider a weak solution such as

$$R_0(r) = \begin{cases} c_1 r^3 & 0 \le r \le r_*\,, \\ \\ \frac{c_2}{r^3} & r > r_*. \end{cases} \tag{3.60}$$

To ensure continuity, we will match the values of (3.60) at $r = r_*$. As before, let us take $r_* = 1$ for simplicity so we have

$$R_0(r) = \begin{cases} \frac{A_0}{6} r^3 & 0 \le r \le 1\,, \\ \\ \frac{A_0}{6r^3} & r > 1. \end{cases} \tag{3.61}$$

The homotopy for equation (3.56) is

$$\mathcal{H}(q;h) = (1-q)L[R] - qhN[R]. \tag{3.62}$$

We will set (3.62) identically to zero and assume an expansion

$$R(r) = \sum_{j=0}^{\infty} R_j(r)q^j. \tag{3.63}$$

Plugging this into (3.62) set to zero and equating powers of q on both sides leads to the first few equations

$$L[R_0] = 0, \qquad R_0(0) = 0, \qquad R_0'''(0) = A_0, \qquad \lim_{r\to\infty} R_0(r) = 0, \tag{3.64}$$

$$L[R_1] = h\left(R_0^3 - R_0^5\right), \tag{3.65}$$

subject to

$$R_1(0) = 0, \qquad R_1'''(0) = 0, \qquad \lim_{r\to\infty} R_1(r) = 0, \tag{3.66}$$

and

$$L[R_2] = (1+h)L[R_1] + h\left(-5R_0^4R_1 + 3R_0^2R_1\right), \tag{3.67}$$

subject to

$$R_2(0) = 0, \qquad R_2'''(0) = 0, \qquad \lim_{r\to\infty} R_2(r) = 0. \tag{3.68}$$

We already have $R_0(r)$ given in (3.61), so we next solve (3.65). If we consider $0 \le r \le 1$, we have

$$L[R_{1-}] = h\left(\left(\frac{A_0r^3}{6}\right)^3 - \left(\frac{A_0r^3}{6}\right)^5\right), \tag{3.69}$$

subject to

$$R_{1-}(r) = 0, \qquad R'''_{1-}(0) = 0. \tag{3.70}$$

The solution is

$$R_{1-}(r) = -\frac{A_0 h r^{11}}{2,177,280}\left(A_0^2 r^6 - 90\right). \tag{3.71}$$

To get the solution for $r > 1$, we let $\beta = R_{1-}(1)$ so we can match $R_{1+}(r)$ with $R_{1-}(r)$ at $r = 1$. Thus we are solving

$$L[R_{1+}] = h\left(\left(\frac{A_0}{6r^3}\right)^3 - \left(\frac{A_0}{6r^3}\right)^5\right), \tag{3.72}$$

subject to

$$R_{1+}(1) = \beta, \qquad \lim_{r\to\infty} R_{1+}(r) = 0. \tag{3.73}$$

Then we have

$$R_{1+}(r) = \frac{A_0^3 h}{8,709,120 r^{13}}\Big((3A_0^2 - 648)r^{10} + 1,008r^6 - 7A_0^2\Big). \tag{3.74}$$

And so we have the solution to (3.65) with (3.71) and (3.74). The process is the same to find $R_2(r)$.

With the three-term approximation, we can now estimate the error. If we define $R_-(A_0, r, h) = R_{0-}(r) + R_{1-}(r) + R_{2-}(r)$ and $R_+(A_0, r, h) = R_{0+}(r) + R_{1+}(r) + R_{2+}(r)$, the three-term approximation is then

$$M(A_0, r, h) = \begin{cases} R_-(A_0, r, h) & 0 \le r \le 1, \\ \\ R_+(A_0, r, h) & r > 1. \end{cases} \tag{3.75}$$

We then compute the residual error $N[R_-(A_0, r, h)]$ and $N[R_+(A_0, r, h)]$, and calculate the sum of squared residual errors

$$E(A_0, h) = \int_0^1 N[R_-(A_0, r, h)]^2 dr + \int_1^\infty N[R_+(A_0, r, h)] dr. \tag{3.76}$$

The minimum value of $E(h, 1)$ is found to be 8.7×10^{-20}, and occurs at $h^* = -0.99985$. The graph of $E(h, 1)$ is given in Figure 3.5 and the corresponding approximation $M(1, r, h^*)$ is given in Figure 3.6. As in the previous section, the error was better than before because we are integrating the same-degree polynomial with much smaller coefficients. In these three sections considering the cubic-quintic model, the sum of squared residual errors has been a polynomial in h of degree 20. However, the leading term's coefficient of the polynomial: $E(h)$ given in (3.35) was on the order of 10^{-8}, $E(h)$ given in (3.55) was of order 10^{-29}, and $E(1, h)$ derived from (3.76) was on the order of 10^{-46}.

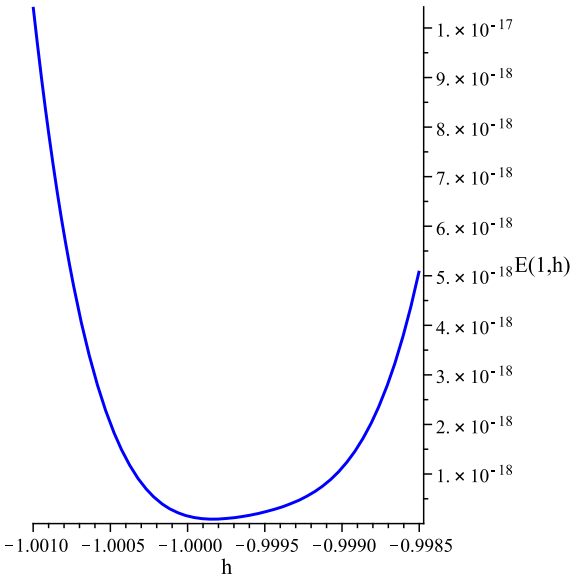

Figure 3.5: Plot of $E(1, h)$, the accumulated sum of squared residual error over the infinite domain $r \in [0, \infty)$, as a function of h, the convergence control parameter. The error function has minimum $E(1, h^*) = 8.7 \times 10^{-20}$ where $h^* = -0.99985$.

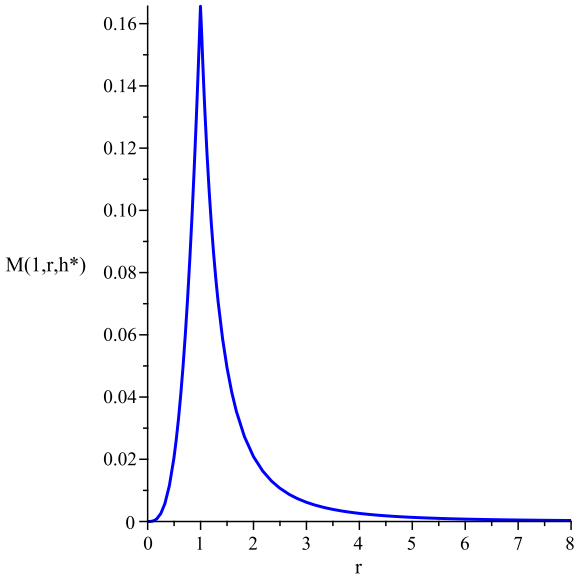

Figure 3.6: Plot of the three-term approximate solution $M(r)$ to $R(r)$ when $h^* = -0.99985$, for the cubic-quintic model with topological charge $m = 3$. Here the initial condition is taken as $A_0 = 1$, and the peak occurs at $r_* = 1$.

3.5 Homotopy analysis for the focusing-defocusing model with topological charge $m = 1$

Here we solve the boundary value problem

$$\frac{d^2R}{dr^2} + \frac{1}{r}\frac{dR}{dr} - \frac{1}{r^2}R + \frac{R^3}{(1+R^2)^2} = 0\,, \tag{3.77}$$

subject to

$$R(0) = 0\,, \qquad R'(0) = A_0\,, \qquad \lim_{r\to\infty} R(r) = 0\,. \tag{3.78}$$

Since the only difference will be in the nonlinear operator, we take the same linear operator as in section 2:

$$L = \frac{d^2}{dr^2} + \frac{1}{r}\frac{d}{dr} - \frac{1}{r^2}. \tag{3.79}$$

The nonlinear operator will be

$$N[R] = L[R] + \frac{R^3}{(1+R^2)^2}. \tag{3.80}$$

The homotopy for (3.77) can be set up as

$$\mathcal{H}(h;q) = (1-h)L[R] - qhN[R]. \tag{3.81}$$

We set $\mathcal{H}(h;q) \equiv 0$ and assume the expansion

$$R(r) = \sum_{j=0}^{\infty} R_j(r)q^j. \tag{3.82}$$

Plugging (3.82) into $\mathcal{H}(h;q) \equiv 0$ and matching powers of q gives the first three equations of the expansion

$$L[R_0] = 0, \qquad R_0(0) = 0, \qquad R_0'(0) = A_0, \qquad \lim_{r\to\infty} R_0(r) = 0, \tag{3.83}$$

$$L[R_1] = (1+h)L[R_0] + h\left(\frac{R_0^3}{(1+R_0^2)^2}\right) \tag{3.84}$$

subject to

$$R_1(0) = 0, \qquad R_1'(0) = 0, \qquad \lim_{r\to\infty} R_1(r) = 0, \tag{3.85}$$

and

$$L[R_2] = (1+h)L[R_1] + h\left(\frac{-4R_0^4R_1}{(1+R_0^2} + \frac{3R_0^2R_1}{(1+R_0^2)^2}\right) \tag{3.86}$$

subject to

$$R_2(0) = 0, \qquad R_2'(0) = 0, \qquad \lim_{r\to\infty} R_2(r) = 0. \tag{3.87}$$

As in section 2, we will consider a weak solution

$$R_0(r) = \begin{cases} c_1 r & 0 \le r \le r_*\,, \\ \\ \frac{c_2}{r} & r > r_*, \end{cases} \tag{3.88}$$

for r_* some point on the interval $(0,\infty)$. We will take $r_* = 1$, and solving (3.83) we have

$$R_0(r) = \begin{cases} A_0 r & 0 \le r \le 1, \\ \\ \frac{A_0}{r} & r > 1. \end{cases} \tag{3.89}$$

For $0 \le r \le 1$, (3.84) becomes

$$L[R_{1-}] = h\left(\frac{(A_0 r)^3}{(1+(A_0 r)^2)^2}\right). \tag{3.90}$$

Using the first two conditions in (3.85), this solves to

$$R_{1-}(r) = \frac{h\left\{(A_0^2r^2+2)\ln(1+A_0^2r^2) - 2A_0^2r^2\right\}}{4A_0^3 r}. \tag{3.91}$$

Note that $\lim_{r\to 0} R_{1-}(r) = 0$ so the boundary condition is satisfied.

As in previous sections, for the function $R_{1+}(r)$ defined for $r \in (1, \infty)$, we will match up the value at $r_* = 1$ to the value of $R_{1-}(1) = \rho$. Then solving

$$L[R_{1+}] = h \left(\frac{\left(\frac{A_0}{r}\right)^3}{\left(1 + \left(\frac{A_0}{r}\right)^2\right)^2} \right) \tag{3.92}$$

subject to

$$R_{1+}(1) = \rho, \qquad \lim_{r \to \infty} R_{1+}(r) = 0, \tag{3.93}$$

we have the solution

$$R_{1+}(r) = \frac{h\left(-A_0^6 \ln(r^2 + A_0^2) + (2 + A_0^2 + 2A_0^6)\ln(1 + A_0^2) - 2A_0^2\right)}{4A_0^3 r}. \tag{3.94}$$

The same process is used to develop $R_{2-}(r)$ and $R_{2+}(r)$, and we can find the three-term approximation. Let us define $M(A_0, r, h) = R_0(r) + R_1(r) + R_2(r)$. For r in the interval $[0, 1]$, we define $R_-(A_0, r, h) = R_{0-}(r) + R_{1-}(r) + R_{2-}(r)$. And for $r \in (1, \infty)$, we define $R_+(A_0, r, h) = R_{0+}(r) + R_{1+}(r) + R_{2+}(r)$. In what follows, let us take $A_0 = 1$ and so we will define $R_m(r, h) = R_-(1, r, h)$ and $R_p(r, h) := R_+(1, r, h)$. In the cubic-quintic model, we were able to integrate to find the sum of squared residual errors and minimize accordingly with respect to h. This is difficult in the focusing-defocusing model with the rational functions involved in the approximation. Instead of performing the integration

$$\int_0^1 N[R_m(r, h)]^2 dr + \int_1^\infty N[R_p(r, h)]^2 dr, \tag{3.95}$$

we use a finite number of values for r on the domain and compute a sum. This allows us to accumulate the error through the use of absolute value, rather than squaring. The accumulated error is then divided by the number of points used to weight each point evenly.

Taking a geometric spread of points, we first calculate

$$E_1(h) = \frac{1}{50}\left\{|N[R_m(0.25,h)| + \sum_{j=1}^{49}\left|N\left[R_p\left(0.25+1.1^j,h\right)\right]\right|\right\}. \tag{3.96}$$

This polynomial in h has a minimum value of 1.6478×10^{-2} occuring at $h_1 = -0.39997$.

If we want to use more points that lie in our approximation for $r \in [0,1]$, we can use

$$E_2(h) = \frac{1}{50}\left\{\sum_{j=1}^{20}\left|N\left[R_m\left(\frac{j}{20},h\right)\right]\right| + \sum_{j=1}^{30}\left|N\left[R_p(1.5^j,h)\right]\right|\right\}. \tag{3.97}$$

This gives an error of 6.185×10^{-3} at $h_2 = -0.8772$.

Doubling the number of points, we have the counterparts to $E_1(h)$ and $E_2(h)$:

$$E_3(h) = \frac{1}{100}\left\{|N[R_m(0.25,h)| + \sum_{j=1}^{99}\left|N\left[R_p\left(0.25+1.1^j,h\right)\right]\right|\right\}, \tag{3.98}$$

with a minimum of 8.24×10^{-3} at $h_3 = -0.39958$, and

$$E_4(h) = \frac{1}{100}\left\{\sum_{j=1}^{40}\left|N\left[R_m\left(\frac{j}{40},h\right)\right]\right| + \sum_{j=1}^{60}\left|N\left[R_p(1.5^j,h)\right]\right|\right\}, \tag{3.99}$$

with a minimum of 3.229×10^{-3} obtained at $h_4 = -0.9238$.

To get an even spread over $r \in [1,100]$ as well as values up to $r = 100 + 1.1^{100} \approx 13,880$, we define

$$E_5(h) = \frac{1}{200}\left\{|N[R_m(1,h)]|\sum_{j=1}^{99}|N[R_p(j,h)]| + \sum_{j=1}^{100}|N[R_p(100+1.1^j,h)]|\right\}, \tag{3.100}$$

which gives a minimum of 2×10^{-3} at $h_5 = -0.423$.

The largest r-domain covered, having size 3×10^{10}, is by $E_4(h)$. So to get a geometric spread over an r-domain of size 4×10^{52}, we define

$$E_6(h) = \frac{1}{300}\left\{|N[R_m(1,h)]| + \sum_{j=1}^{299}|N[R_p(1.5^j,h)]|\right\}, \tag{3.101}$$

which gives an error of 7.83×10^{-4} at $h_6 = -0.6192$.

The graphs of these error functions are given in Figures 3.7 - 3.12. The corresponding h value giving the least error, h_6, is used in a graph of the corresponding three-term approximation $M(1, r, h_6)$ in Figure 3.13.

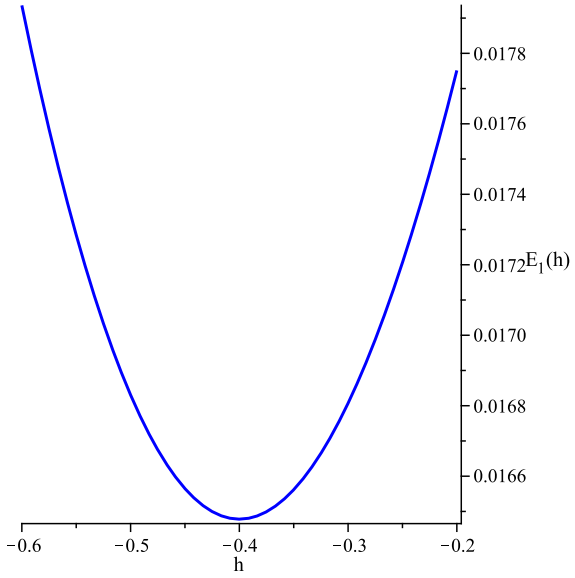

Figure 3.7: Plot of $E_1(h)$, the error along a geometric sequence of 50 values of r as a function of h. This function has minimum $E(h_1) = 1.6478 \times 10^{-2}$ where $h_1 = -0.3997$.

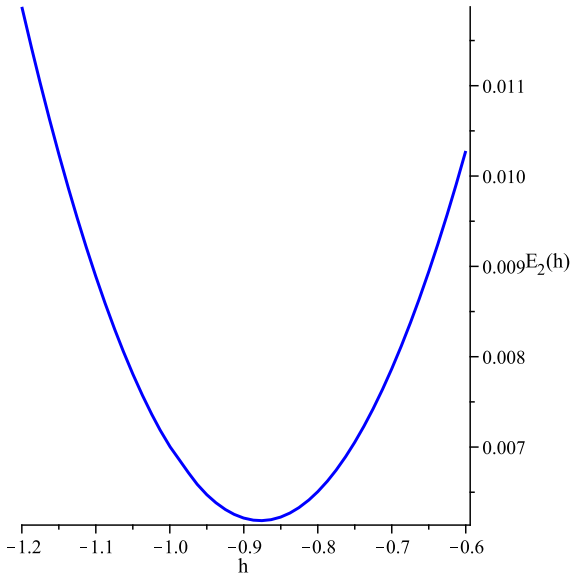

Figure 3.8: Plot of $E_2(h)$, the error using 20 evenly spaced values for $r \in [0, 1]$ and 30 more along a geometric sequence for $r > 1$, as a function of h. This function has minimum $E_2(h_2) = 6.185 \times 10^{-3}$ where $h_2 = -0.8772$.

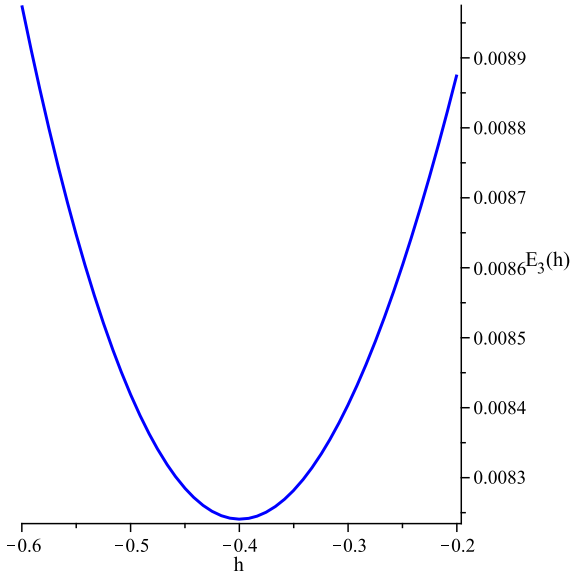

Figure 3.9: Plot of $E_3(h)$, the error along a geometric sequence of 100 values of r as a function of h. This function has minimum $E_3(h_3) = 8.24 \times 10^{-3}$ where $h_3 = -0.39958$.

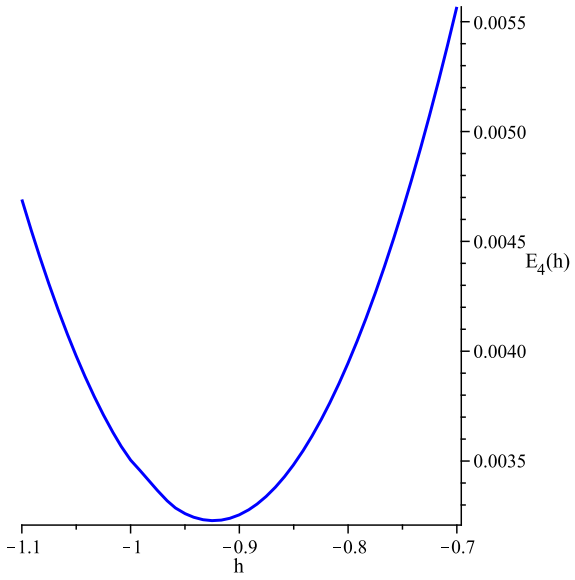

Figure 3.10: Plot of $E_4(h)$, the error the error using 40 evenly spaced values for $r \in [0, 1]$ and 60 more along a geometric sequence for $r > 1$, as a function of h. This function has minimum $E_4(h_4) = 3.229 \times 10^{-3}$ where $h_4 = -0.9238$.

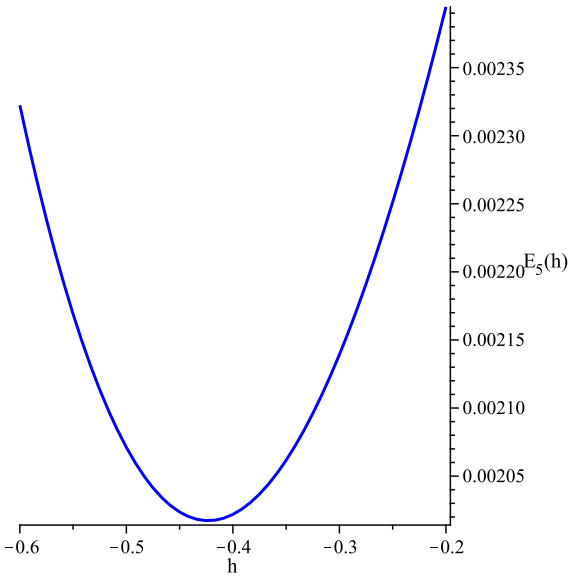

Figure 3.11: Plot of $E_5(h)$, the error the error using 100 evenly spaced values for $r \in [0, 100]$ and 100 more along a geometric sequence for $r > 1$ up to $r \approx 13,880$, as a function of h. This function has minimum $E_5(h_5) = 2 \times 10^{-3}$ where $h_5 = -0.423$.

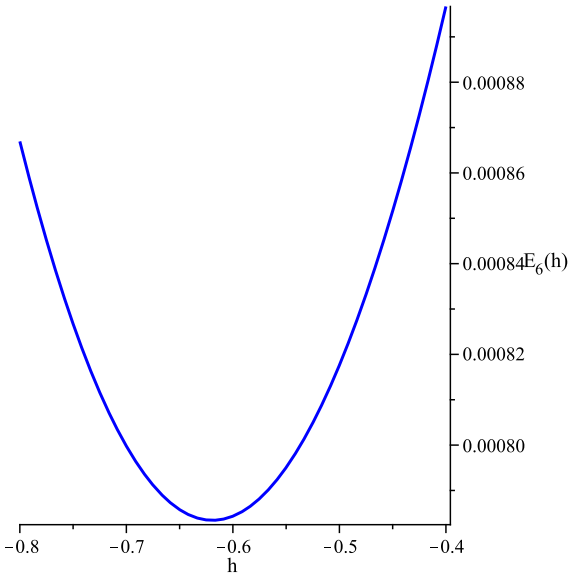

Figure 3.12: Plot of $E_6(h)$, the error along a geometric sequence of 300 values of r up to $r \approx 4 \times 10^{52}$, as a function of h. This function has minimum $E_6(h) = 7.83 \times 10^{-4}$ where $h_6 = -0.6192$.

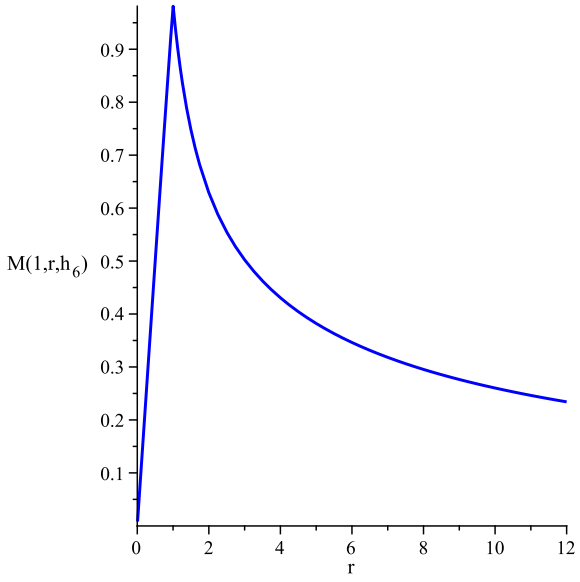

Figure 3.13: Plot of the three-term approximate solution $M(A_0, r, h)$ to $R(r)$ when $h = h_6 = -0.6192$, for the focus-defocusing model with topological charge $m = 1$. Here the initial condition is taken as $A_0 = 1$, and the peak occurs at $r_* = 1$.

3.6 Discussion

In this paper we considered the equation that governs the vector potential of an electromagnetic pulse. We sought to find analytical solutions through the use of the Homotopy Analysis Method. Under a stationary assumption, the linear part of the resulting equation yielded solutions that did not satisfy the boundary conditions. So a solution was assumed to the linear operator in the guise of a piece-wise defined function. On the first part the conditions at zero are satisfied, and for the far-field part of the equation the condition at infinity in satisfied. This created a weak solution, in that we could match the two different functions at a certain point r_* to obtain continuity, but the solution would not be differentiable there.

For the cubic-quintic model the error decreased quickly because of the topological charge as we moved up in cases where $m = 1, 2, 3$. There was a geometric decrease in error as $m = 1$ yielded error on the order of 10^{-2}, $m = 2$ on the order of 10^{-11}, and $m = 3$ on the order of 10^{-20}.

The technique of computing the residual error and finding the sum of squared residual errors proved to be difficult for the focusing-defocusing model. The structure of the equation does not lend itself well to integration. However, some estimates using sums show that these analytic approximations are still viable. The error was less than three decimal places using 300 points along a geometric progression of values.

Originally when writing this paper, we considered the case where $\lambda \neq 0$, which yielded a solution of the linear operator in terms of Bessel functions. This proved to be unwieldy,

and was abandoned due to lack of results. Perhaps a different linear operator could be used to generalize the results given here.

Physically, these results demonstrate the existence of peaked pulse solutions in the pair plasma model. Such solutions are shown to decay algebraically from the peak, and the analysis demonstrates that such solutions are valid for multiple values of the topological charge m. Furthermore, the peaked structures exist for multiple forms of the nonlinearity $F(R)$. However, the nonlinearity will determine how such peaked pulses propagate and decay.

CHAPTER 4

EXACT AND ANALYTICAL SOLUTIONS FOR A NONLINEAR SIGMA MODEL

The following results are from the paper [113].

4.1 Background

We consider the nonlinear σ-model

$$\mathbf{v}_{xt} + (\mathbf{v}_x \cdot \mathbf{v}_t)\mathbf{v} = 0\,, \tag{4.1}$$

where $\mathbf{v} : \mathbb{R}^2 \to \mathbb{R}^n$ is assumed to be $C^2(\mathbb{R}^2)$. As we are interested in travelling wave solutions to (4.1), we assume a solution of the form $\mathbf{v}(x,t) = \mathbf{V}(z)$ where $z = x - ct$ and $c \neq 0$. Under such an assumption, (4.1) becomes

$$\mathbf{V}'' + (\mathbf{V}' \cdot \mathbf{V}')\mathbf{V} = 0\,, \tag{4.2}$$

where prime denotes differentiation with respect to z. Note that the travelling wave equation is invariant under c. Let us write $\mathbf{V}$ component-wise as $\mathbf{V} = (f_1, f_2, \ldots, f_n)$, where each

$f_k \in C^2(\mathbb{R})$ for all $k = 1, 2, \ldots, n$. Then, (4.2) results in the n dimensional system

$$f_k'' + \left(\sum_{j=1}^{n} f_j'^2 \right) f_k = 0 \,, \tag{4.3}$$

for all $k = 1, 2, \ldots, n$.

As a remark on the structure of this system, let us define the operator L by

$$L[U] = U'' + \left(\sum_{j=1}^{n} f_j'^2 \right) U \,. \tag{4.4}$$

Then, (4.3) implies that for any linear combination $\alpha_1 f_1 + \alpha_2 f_2 + \cdots + \alpha_n f_n$, we have that

$$L\left[\alpha_1 f_1 + \alpha_2 f_2 + \cdots + \alpha_n f_n\right] = 0 \,. \tag{4.5}$$

In physics, nonlinear σ models are a tool to use field theory to describe particles [64]. Sigma model methods are extended to spin ladders in [65], which leads to the analysing of the magnetic and electronic structure of $(VO)_2P_2O_7$ vanadyl pyrophosphate [66]. The nonlinear σ model is used over the linear σ model in [67], where the nonlinear σ model incorporates a σ particle (whereas the linear σ model does not) and is used in a Padé calculation of $\pi\pi$ phase shifts. Also in particle physics, the nonlinear σ model is used in [68] to present a unified view of the two-dimensional half-filled Hubbard model at low temperature for any value of the Coulomb repulsion. Mass generation is retained in using the noncommutative supersymmetric $O(N)$ nonlinear σ model [69]. In relativity, the nonlinear σ model shares similar behavior with some black hole critical phenomena [64]. The nonlinear σ model is also used in string theory [70]-[72]. In string theory, the modified $O(N)$ σ model has a non-trivial fixed point, which presents interesting consequences [73].

The goal of this paper will be to provide exact (when possible) and analytical solutions to the system (4.3) governing the propagation of waves in the nonlinear σ-model (4.1). For the analytical solutions, we apply the homotopy analysis method, as it provides a clear way by which we may control the error in approximate solutions. In particular, making use of two distinct auxiliary linear operators, we are able to demonstrate that differing linear operators permit differing rates of convergence of the solutions. Furthermore, the convergence control parameter is selected in such a manner so as to minimize the residual errors arising in the approximate solutions. We observe that the optimal value of the convergence control parameter is actually dependent on the choice of linear operator selected. Finally, the qualitative behavior of the approximate solutions agree nicely with the exact solutions valid in a specific case.

For many physical applications, approximate solutions, while clearly less informative than exact solutions, are sufficient to describe the true solutions (assuming that the error is sufficiently small). The method of homotopy analysis [14]-[22] has recently been applied to the study of a number of non-trivial and traditionally hard to solve nonlinear differential equations. Examples include nonlinear equations arising in heat transfer [23]-[26], fluid mechanics [27]-[34], solitons and integrable models [35]-[39], nanofluids [40]-[41] and the Lane-Emden equation which appears in stellar astrophysics [42]-[45], to name a few areas.

4.2 The one-dimensional case: an exact solution

In the case of a one-dimensional model, (4.3) reduces to the nonlinear ODE

$$f'' + f'^2 f = 0\,. \tag{4.6}$$

Dividing through by f' and integrating, we arrive at the first integral

$$\ln f' + \frac{1}{2} f^2 = \ln C\,, \tag{4.7}$$

where $C > 0$ is a constant of integration. Separating variables we have

$$\exp\left(\frac{1}{2} f^2\right) f' = C\,, \tag{4.8}$$

and integrating once we recover

$$\int_0^f e^{\frac{1}{2}\xi^2} d\xi = Cz\,. \tag{4.9}$$

We may write this relation as

$$\operatorname{erf}\left(\frac{\sqrt{2}if}{2}\right) = \frac{2Ci}{\sqrt{2\pi}} z\,. \tag{4.10}$$

Here $\operatorname{erf}(q)$ denotes the error function. The inverse error function is given by

$$\operatorname{erf}^{-1}(q) = \sum_{k=0}^{\infty} \frac{\alpha_k}{2k+1} \left(\frac{\sqrt{\pi}}{2} q\right)^{2k+1}\,, \tag{4.11}$$

where

$$\alpha_0 = 1 \qquad \text{and} \qquad \alpha_k = \sum_{m=0}^{k-1} \frac{\alpha_m \alpha_{k-1-m}}{(m+1)(2m+1)}\,. \tag{4.12}$$

From this representation, it is clear that $\operatorname{erf}^{-1}(q)$ is an odd function. Inverting (4.10), we have

$$g(z) = -\frac{i}{\sqrt{2}} \operatorname{erf}^{-1}\left(\frac{2Ci}{\sqrt{2\pi}} z\right)\,, \tag{4.13}$$

which is a real-valued function. We have the natural boundary conditions $f(0) = 0$ and $f'(0) = C$.

4.3 Results for the general n-dimensional system

Let $f_1, f_2, \ldots, f_n$ be a set of solutions to (4.3) satisfying $f_k(0) = 0$ and $f_k'(0) = A_k$. If we construct a Taylor series solution for each, we find that the solutions all take the form $f_k(z) = A_k F(z)$, where $F(0) = 0$ and $F'(0) = 1$. Then, (4.3) is reduced to

$$F'' + \left(A_1^2 + A_2^2 + \cdots + A_n^2\right) F'^2 F = 0\,. \tag{4.14}$$

For simplicity, we introduce the scaling

$$g(z) = \sqrt{A_1^2 + A_2^2 + \cdots + A_n^2}\,F(z) \tag{4.15}$$

so that

$$g'' + g'^2 g = 0\,. \tag{4.16}$$

Applying the results of the previous section, with $g(0) = 0$ and

$$g'(0) = \sqrt{A_1^2 + A_2^2 + \cdots + A_n^2}\,. \tag{4.17}$$

From (4.10), we may write the solution to (4.16) as

$$\operatorname{erf}\left(\frac{\sqrt{2}ig(z)}{2}\right) = \frac{2\sqrt{A_1^2 + A_2^2 + \cdots + A_n^2}\,i}{\sqrt{2\pi}}z\,, \tag{4.18}$$

or, upon inversion,

$$g(z) = -\frac{i}{\sqrt{2}}\mathrm{erf}^{-1}\left(\frac{2\sqrt{A_1^2 + A_2^2 + \cdots + A_n^2}i}{\sqrt{2\pi}}z\right). \tag{4.19}$$

Then, $F(z)$ is given by

$$F(z) = -\frac{i}{\sqrt{2}\sqrt{A_1^2 + A_2^2 + \cdots + A_n^2}}\mathrm{erf}^{-1}\left(\frac{2\sqrt{A_1^2 + A_2^2 + \cdots + A_n^2}i}{\sqrt{2\pi}}z\right) \tag{4.20}$$

and each $f_k(z)$ reads

$$f_k(z) = -\frac{A_k i}{\sqrt{2}\sqrt{A_1^2 + A_2^2 + \cdots + A_n^2}}\mathrm{erf}^{-1}\left(\frac{2\sqrt{A_1^2 + A_2^2 + \cdots + A_n^2}i}{\sqrt{2\pi}}z\right). \tag{4.21}$$

This is an exact relation for the solution to (4.1) under the travelling wave assumption; $\mathbf{V}(z) = (f_1(z), f_2(z), \ldots, f_n(z))$ where $\mathbf{V}(0) = \mathbf{0}$ and $\mathbf{V}'(0) = (A_1, A_2, \ldots, A_n)$.

4.4 Homotopy analysis for obtaining accurate approximations

While we can arrive at exact implicit relations and series solutions for the the nonlinear sigma model, note that these solutions are computable in terms of Taylor series, which can converge rather slowly depending upon the domain of definition. As such, alternate methods for obtaining approximate solutions to the travelling wave system for the nonlinear sigma model are of interest.

Here we apply the method of homotopy analysis to the initial value problem

$$g'' + g'^2 g = 0\,, \qquad g(0) = 0\,, \qquad \text{and} \qquad g'(0) = A\,. \tag{4.22}$$

With an approximate solution $g(z)$ to this equation, we will be able to recover the approximate solutions to the travelling wave system (4.3).

The first step is to determine a suitable linear operator for the homotopy. Looking at (4.13), we see

$$g(z) \approx \operatorname{erf}^{-1}(z) = \frac{\sqrt{\pi}}{2} z + \frac{1}{6}\left(\frac{\sqrt{\pi}}{2} z\right)^3 + \cdots . \tag{4.23}$$

So $g(z) \approx \frac{\sqrt{\pi}}{2} z + O(z^3)$, and $g'(z) \approx \frac{\sqrt{\pi}}{2} + O(z^2)$. Then we can write (4.22) as $g'' + (g'g)g' = 0$, and plugging in the approximations we get $g'g \approx \frac{\pi}{4} z$ (we drop the larger order terms now). And so one choice of a linear operator is

$$L_1[U] = U'' + \frac{\pi}{4} z U'. \tag{4.24}$$

Using the method of complete differential matching [21], another choice is

$$L_2[U] = U'' + U'. \tag{4.25}$$

For both linear operators, the corresponding nonlinear operator is

$$N[U] = U'' + U'^2 U. \tag{4.26}$$

Note that (4.22) is just $N[g] = 0$. In the following subsections, we consider separate homotopies for each auxiliary linear operator.

4.4.1 The operator L_1

The homotopy for this operator is

$$0 \equiv \mathcal{H}_1[U, u_0; q] = (1-q)L_1[U - u_0] - qhN[U], \tag{4.27}$$

where u_0 is the solution to the initial auxiliary operator equation, q is the homotopy parameter that lies in the interval $[0, 1]$, and h is the convergence control parameter. When $q = 0$ we start with the linear operator, and as q moves from 0 to 1, we obtain a continuous deformation of the linear operator into the nonlinear operator. When $q = 1$, we will have only the nonlinear operator left, and the convergence control parameter h will help us minimize the error obtained.

Next we assume a series expansion about q. That is, we assume

$$U(z) = u_0(z) + \sum_{j=0}^{\infty} u_j(z)q^j. \tag{4.28}$$

So if convergence occurs when $q = 1$, we recover the solution to (4.22). Now we will plug in (2.36) into (4.27) and match powers of q. This produces an infinite number of linear PDEs, but we will be able to find the error only computing a small number of terms.

4.4.1.1 Deformation equations associated to L_1

From (4.27), we have

$$(1-q)L_1[U - u_0] = qhN[U], \tag{4.29}$$

which becomes

$$(1-(1+h)q)L_1[U]-L_1[u_0]=qh\left(U'^2U-\frac{\pi}{4}zU'\right). \tag{4.30}$$

Using (2.36), the left-hand side of (4.30) becomes

$$L_1[u_0]+\sum_{j=1}^{\infty}\Big(L_1[u_j]-(1+h)L_1[u_{j-1}]\Big)q^j. \tag{4.31}$$

The right-hand side of (4.30) can be expanded as

$$h\sum_{j=1}^{\infty}N_{j-1}^1[u_0,...,u_j]q^j, \tag{4.32}$$

where each N_j^1 is a function of $u_0(z),...,u_j(z)$. Putting (4.30) back together, we match up powers of q on each side. And we have the zeroth order deformation equation is

$$L_1[u_0]=0, u_0(0)=0, u_0'(0)=A, \tag{4.33}$$

and the jth order deformation equation ($j\geq 1$) is

$$L_1[u_j]=(1+h)L_1[u_{j-1}]+hN_j^1[u_0,...u_j], \tag{4.34}$$

subject to $u_j(0)=0, u_j'(0)=0$.

Now we are able to start solving these equations. We find that (4.33) has the solution

$$u_0(z)=A\int_0^z e^{-\frac{\pi}{8}t^2}dt. \tag{4.35}$$

Before solving the other deformation equations, consider that we will be solving something in the form

$$L_1[u_j]=k(z). \tag{4.36}$$

Making the substitution $y = u_j'$, we have

$$y' + \frac{\pi}{4} zy = k(z). \tag{4.37}$$

Then solving and substituting back in u_j', we have

$$u_j'(z) = e^{-\frac{\pi}{8}z^2} \int_0^z k(t) e^{\frac{\pi}{8}t^2} dt. \tag{4.38}$$

Integrating again, we obtain the general form of the solution

$$u_j(z) = \int_0^z e^{-\frac{\pi}{8}y^2} \int_0^y k(t) e^{\frac{\pi}{8}t^2} dt dy. \tag{4.39}$$

For example, the first order deformation equation is

$$L_1[u_1] = h\Big(u_0(z) u_0'(z)^2 - \frac{\pi}{4} z u_0'(z)\Big), \tag{4.40}$$

which comes out to

$$L_1[u_1] = h\left(A^3\sqrt{2}\mathrm{erf}\left(\frac{\sqrt{2\pi}}{4}z\right) e^{-\frac{\pi}{4}z^2} - \frac{\pi}{4} A z e^{-\frac{\pi}{8}z^2}\right). \tag{4.41}$$

Since this is in the form (4.36), the solution prescribed by (4.39) is

$$u_1(z) = \frac{1}{6} Ah \left\{ 3z e^{-\frac{\pi}{8}z^2} - 3\sqrt{2}\mathrm{erf}\left(\frac{\sqrt{2\pi}}{4}z\right) + 2A^2\sqrt{2}\mathrm{erf}\left(\frac{\sqrt{2\pi}}{4}z\right)^3 \right\}. \tag{4.42}$$

The second order deformation equation is

$$L[u_2] = (1+h)L[u_1] + h\left(u_0'^2 u_1 + 2u_0' u_1' u_0 - \frac{\pi}{4} z u_1'\right). \tag{4.43}$$

The solution, using the same method as above, is

$$u_2(z) = -\frac{1}{8} h^2 A^3 \pi z^2 e^{-\frac{\pi}{8}z^2} \mathrm{erf}\left(\frac{\sqrt{2\pi}}{4}z\right). \tag{4.44}$$

4.4.1.2 Error Analysis on L_1

Now that we have the first three terms of the expansion (2.36), we can consider the error associated with it. Let

$$\widehat{U}(z,h,A) = u_0(z) + u_1(z) + u_2(z). \tag{4.45}$$

Next we run this back through (4.26) to compute the residual error $N[\widehat{U}]$. To study the error on the semi-infinite interval $[0,\infty)$, we construct the sum of squared residual errors

$$E_1(h,A) = \int_0^\infty \left(N[\widehat{U}(z,h,A)]\right)^2 dz. \tag{4.46}$$

$E_1(h,A)$ is a twelfth-degree polynomial in h. The minimum value of $E_1(h,\frac{1}{10})$ is 3.2858×10^{-3} at $h=-0.6034$. However, the minimum value of $E_1(h,1)$ is 0.058486 at $h=-0.4352$. The plots of squared residual error are given for $A=\frac{1}{10}$ and $A=1$ in Figures 4.1 and 4.2, respectively. Each is plotted with the corresponding graph of $E_2(h,A)$ (the error associated with the second linear operator, L_2).

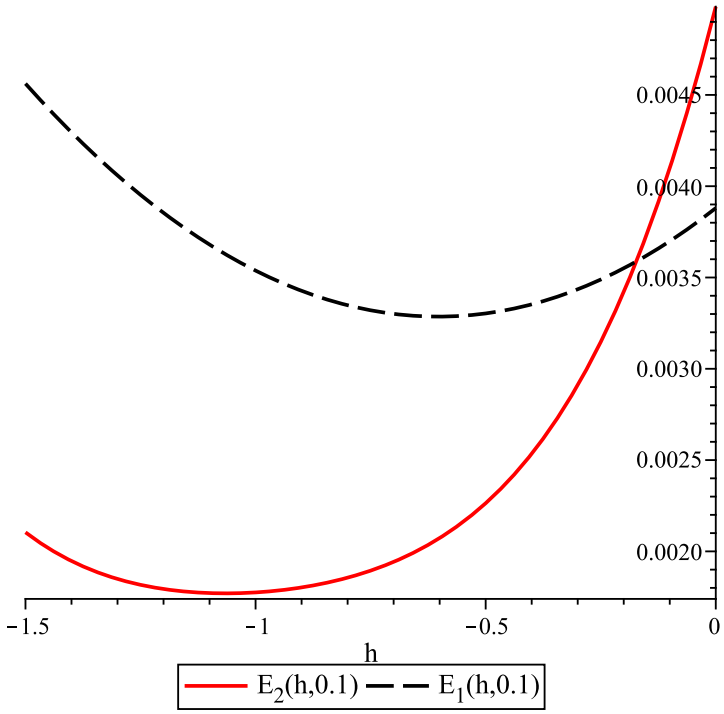

Figure 4.1: The plot of $E_1(h, 0.1)$ and $E_2(h, 0.1)$ over h. The minimum value of $E_1(h, 0.1)$ is 3.2858×10^{-3} which occurs at $h = -0.6034$. The minimum value of $E_2(h, 0.1)$ is 1.77×10^{-3} which occurs at $h = -1.065$. Hence, the auxiliary linear operator L_2 is superior to L_1 in terms of allowing us to control error.

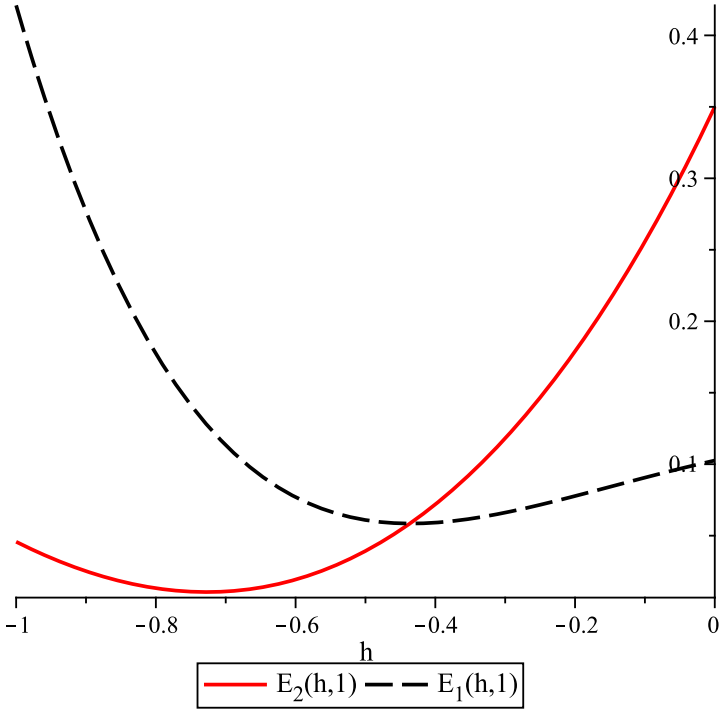

Figure 4.2: The plot of $E_1(h,1)$ and $E_2(h,1)$ over h. The minimum value of $E_1(h,1)$ is 0.058486 which occurs at $h = -0.4352$. The minimum value of $E_2(h,1)$ is 0.010556 which occurs at $h = -0.727$. Again, the auxiliary linear operator L_2 gives us more freedom to control residual error than does L_1.

4.4.2 The operator L_2

Now, we consider the simpler linear operator L_2 that was given by complete differential matching in (4.25). The homotopy for this operator is

$$0 \equiv \mathcal{H}_2[V, v_0; q] = (1-q)L_2[V - v_0] - qhN[V], \tag{4.47}$$

where v_0 is the solution to $L_2[v_0] = 0$, $q \in [0, 1]$ is the homotopy parameter, h is the convergence control parameter, and

$$V(z) = v_0(z) + \sum_{m=1}^{\infty} v_m(z) q^m. \tag{4.48}$$

4.4.2.1 Deformation equations associated to L_2

Simplifying (4.47) as before, we have

$$(1-q)L_2[V] = qhN[V], \tag{4.49}$$

which can be written as

$$(1-(1+h)q)L_2[V] = qh(-V' + V'^2 V). \tag{4.50}$$

Again we see that (4.50) can be written as

$$L_2[v_0] + \sum_{m=1}^{\infty} \Big(L_2[v_m] - (1+h)L_2[v_{m-1}] \Big) = h \sum_{m=1}^{\infty} N_{m-1}^2[u_0, ...u_m] q^m, \tag{4.51}$$

where each N_m^2 is a nonlinear function of $u_0(z), ..., u_m(z)$. Matching powers of q, we find the mth order deformation equation ($m \geq 1$) to be

$$L_2[v_m] = (1+h)L_2[v_{m-1}] + hN_m^2[u_0, ..., u_m]. \tag{4.52}$$

Now, the zeroth order is

$$L_2[v_0] = 0, v_0(0) = 0, v_0'(0) = A. \tag{4.53}$$

This is the ordinary differential equation $v_0'' + v_0' = 0$, which gives

$$v_0(z) = A(1 - e^{-z}). \tag{4.54}$$

Let us briefly mention that for the higher-order equations, we are solving something of the form

$$v_m''(z) + v_m'(z) = k(z), \tag{4.55}$$

which solves to

$$v_m(z) = \int_0^z e^{-y} \int_0^y e^t k(t) dt dy. \tag{4.56}$$

The first order deformation equation is

$$L[v_1] = h\big(v_0'(z)^2 v_0(z) - v_0'(z)\big). \tag{4.57}$$

This simplifies to

$$L[v_1] = -hA\left(e^{-z} - A^2 e^{-2z} + A^2 e^{-3z}\right). \tag{4.58}$$

The solution, according to (4.56), is

$$v_1(z) = -\frac{1}{6}Ah\left\{A^2 e^{-3z} - 3A^2 e^{-2z} + (3A^2 - 6z - 6)e^{-z} + 6 - A^2\right\}. \tag{4.59}$$

The second order deformation equation is

$$L[v_2] = (1+h)L[v_1] + h\big(v_0'^2 v_1 - v_1' + 2v_0' v_1' v_0\big), \tag{4.60}$$

which has solution governed by (4.56). We have

$$\begin{aligned} v_2(z) = {} & \frac{1}{120}Ah(7hA^4 - 40A^2h + 20A^2 - 120) \\ & - \frac{1}{24}Ah\left\{12hz^2 - 12(A^2h+2)z + 7hA^4 + 12A^2(1-2h) - 24\right\}e^{-z} \\ & + \frac{1}{12}A^3h(-12hz + 7A^2h - 12h + 6)e^{-2z} - \frac{1}{12}A^3h(-6hz + 7A^2h - 4h + 2)e^{-3z} \\ & + \frac{7}{24}h^2A^5e^{-4z} - \frac{7}{120}h^2A^5e^{-5z}. \end{aligned} \tag{4.61}$$

4.4.2.2 Error Analysis on L_2

As in the last error section, we will run the first few terms of our homotopy expansion back into the ODE to get the residual error. We will square this, integrate on $[0, \infty)$, and find the value of h that minimizes this sum of squared residual errors.

So let us define

$$\widehat{V}(z, h, A) = v_0(z) + v_1(z) + v_2(z). \tag{4.62}$$

Then the residual error is $N[\widehat{V}]$. Integrating its square, we obtain the sum of squared residual errors

$$E_2(h, A) = \int_0^\infty \Big(N[\widehat{V}(z, h, A)]\Big)^2 dz. \tag{4.63}$$

As before, $E_2(h, A)$ is a polynomial of degree 12 in h. We find that $E_2\left(h, \frac{1}{10}\right)$ has a minimum value of 1.77×10^{-3} which occurs at $h = -1.065$. Also $E_2(h, 1)$ has a minimum of 0.010556 at $h = -0.727$. The graphs of $E_2(h, A)$ are given for $A = 0.1$ and $A = 1$ in Figures 1 and 2, respectively. Also, the plots of the three-term approximate solution $\widehat{V}(z, h, A)$ are given for $A = 0.1$ and $A = 1$ in Figure 4.3. We take this to be the candidate approximate solution, since the error was better than $\widehat{U}(z, h, A)$ for all comparable values of A. Note that the plots in Figure 4.3 agree qualitatively with what we would expect from the one-dimensional exact solution.

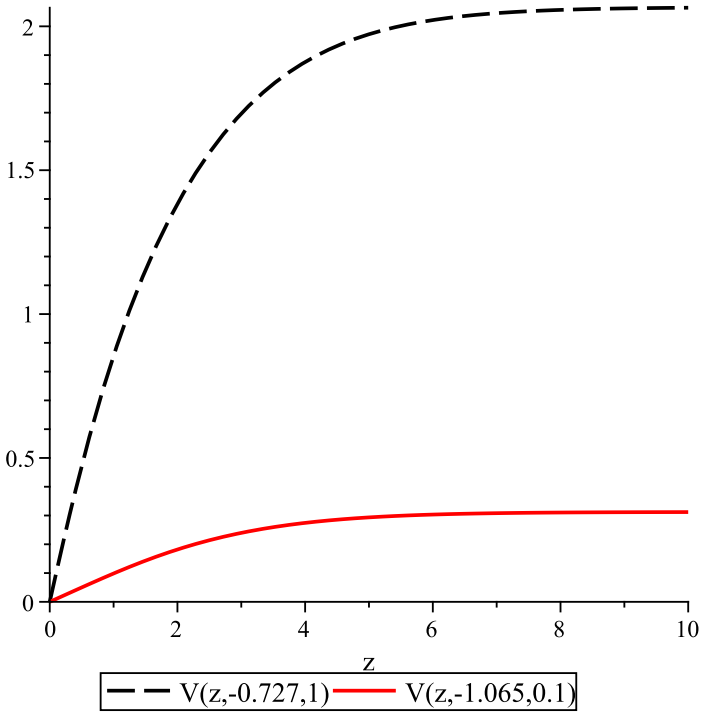

Figure 4.3: Plot of $\widehat{V}(z, -1.065, 0.1)$ and $\widehat{V}(z, -0.727, 1)$ over z. Both approximations have better error than their $\widehat{U}$ counterparts.

4.5 Discussion

In the case of one-dimension, the nonlinear σ model was solved exactly in terms of the inverse error function. Under a traveling-wave assumption, this solution was extended to n dimensions. However, such exact solution formulas involve the inversion of error functions, which can be computationally demanding. As such, we then considered approximate analytical solutions to the nonlinear σ model in n dimensions via homotopy analysis. In order to demonstrate the effectiveness of the method, we selected two different linear operators, one which would seemingly approximate the physical model, and then another which was selected by the method of complete differential matching as discussed in [21].

We found that the linear operator constructed through complete differential matching resulting in solutions with lower residual error (hence, the resulting solutions were more accurate). In order to find error-minimizing solutions, we treated the convergence control parameter as an unknown, and minimized the sum of squared residual errors. This is a useful method in controlling the error inherent in finite term approximations of PDEs by homotopy analysis, and had been employed recently on nonlinear PDEs [48, 50]. Indeed, through such a method, we are able to obtain accurate expressions which have relatively few terms, which means that our expansions will be very computationally efficient for the level of error control that they provide.

From the solution provided, one may plot the solution to the n dimensional model using a transform similar to (4.21). In particular, for each wave profile $f_k(z)$ with initial

value $f_k'(0) = A_k$, we have

$$f_k(z) = \frac{A_k}{\sqrt{A_1^2 + \cdots + A_n^2}} g(z)\,, \tag{4.64}$$

where $g(z)$ is the normalized homotopy solution developed in the previous section. For instance, consider the three wave system with initial amplitudes $f_1'(0) = 1$, $f_2'(0) = 2$, $f_3'(0) = 3$. We plot the dynamics for this system in Figure 4.4. Then, in Figure 4.5, we plot the dynamics for the four wave system $f_1'(0) = 1$, $f_2'(0) = 2$, $f_3'(0) = 3$, $f_4'(0) = 4$.

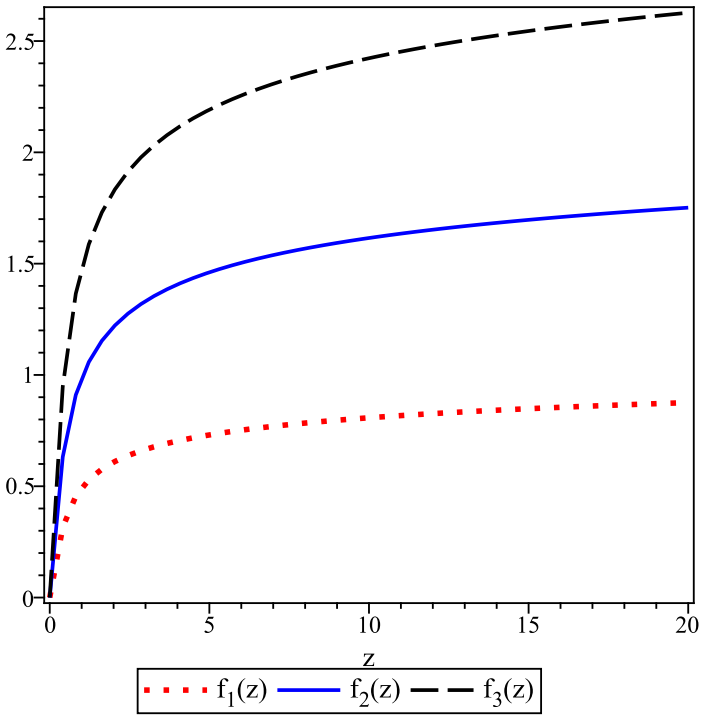

Figure 4.4: Plot of the three wave solution to the nonlinear sigma model with $f_1'(0) = 1$, $f_2'(0) = 2$, $f_3'(0) = 3$.

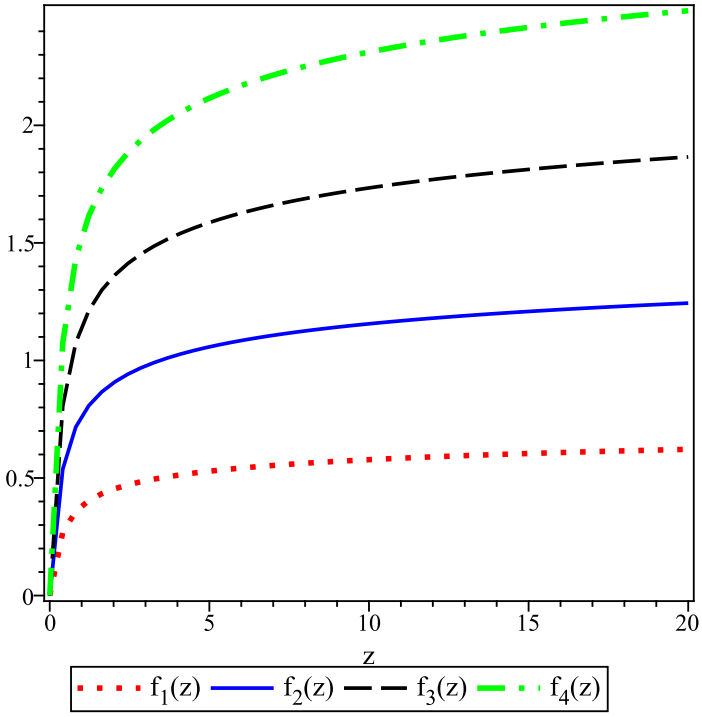

Figure 4.5: Plot of the four wave solution to the nonlinear sigma model with $f_1'(0) = 1$, $f_2'(0) = 2$, $f_3'(0) = 3$, $f_4'(0) = 4$.

CHAPTER 5

ON THE CHOICE OF AUXILIARY LINEAR OPERATOR IN THE OPTIMAL HOMOTOPY ANALYSIS OF THE CAHN-HILLIARD INITIAL VALUE PROBLEM

The following results are from the paper [87].

5.1 Background

The Cahn-Hilliard equation

$$u_t = \triangle(u^3 - u - \triangle u), \tag{5.1}$$

held subject to the initial data

$$u(\widetilde{x}, 0) = f(\widetilde{x}), \tag{5.2}$$

(where $u : \mathbb{R}^n \times \mathbb{R}_+ \to \mathbb{R}$ and $\widetilde{x} \in \mathbb{R}^n$) is a nonlinear evolution equation that describes the free energy of a binary alloy [74]. In 1958, Cahn and Hilliard re-derived the Van der Waals argument that a compressible fluid has its free energy at constant temperature dependent density gradient, while obtaining results on the interfacial energy between phases [75]. The

corresponding boundary value problem, wherein $0 < x < L$, $t > 0$, and $n = 1$, subject to $u_{xxx}(x,0) = u_{xxx}(L,0) = 0$ has its global existence or finite time blow up studied in [76].

If we consider the case when $n = 1$, then (5.1) becomes

$$u_t = 6uu_x^2 + 3u^2u_{xx} - u_{xx} - u_{xxxx}, \tag{5.3}$$

subject to

$$u(x,0) = f(x). \tag{5.4}$$

Numerical results exist in the literature. For instance, in [77], the Galerkin finite element method is used to study the corresponding boundary value problem. In [78], the asymptotics for the three-dimensional case has been considered. Existence and uniqueness of numerical solutions obtained using the finite element method are studied in [79]. A conservative finite difference scheme is employed, using a splitting potential with explicit and implicit time parts, along with free boundary conditions in [80].

In the present paper, we apply a type of optimal homotopy analysis method to obtain approximate analytical solutions to the nonlinear Cahn-Hilliard PDE and associated initial value problem given by (5.3)-(5.4). The method of homotopy analysis [14, 15, 16, 17, 18, 19, 20, 21, 81, 22] has recently been applied to the study of a number of non-trivial and traditionally hard to solve nonlinear differential equations, for instance nonlinear equations arising in heat transfer [23, 24, 25, 26], fluid mechanics [27, 28, 29, 30, 31, 32, 33, 34], solitons and integrable models [35, 36, 37, 38, 39], nanofluids [40, 41], the Lane-Emden equation which

appears in stellar astrophysics [42, 43, 44, 45], and models frequently used in mathematical physics [46, 51, 47], to name a few areas.

In order to best achieve our goals, we consider multiple types of auxiliary linear operators, so as to find an operator which permits rapid convergence of iterations. This, in turn, ensures computational efficiency, since we are able to obtain accurate results in relatively few iterations. We also make extensive use of the convergence control parameter, which we use to minimize the accumulated L^2-norm of the residual errors. This method has been employed to study optimal approximations for a number of nonlinear problems [48, 50, 49, 59, 60, 61, 62, 63]. To apply this method efficiently, we also provide a variety of different kinds of approximations to the L^2-norm, since approximate discrete sums are far easier to compute than square-integrals.

In each of the cases considered, we are able to pick the best auxiliary linear operator and the error minimizing convergence control parameter to obtain an accurate analytical approximation. In particular, we choose from three auxiliary linear operator:

(i) $L[U] = U_t + U$;

(ii) $L[U] = U_t - U_{xx}$;

(iii) $L[U] = U_t + U_x + U$.

In doing so, it is seen that although complicated auxiliary linear operators provide a greater fit to the original equation, they may slow the convergence of iterations while increasing the computational complexity of the problem. The latter observation follows from

the fact that more complicated linear operators are hard to invert, hence more computation time is needed to construct the higher order terms in the homotopy expansion.

We find that the optimal convergence control parameter is strongly influenced by the form of the auxiliary linear operator chosen. We present the results for various initial conditions, starting with the simple condition $u(x,0) = 1$, and then progressing to far more complicated conditions like $u(x,0) = \sin(x)$, $u(x,0) = \exp(-x^2)$ and even $u(x,0) = \text{ sech }(x)$. Despite such complicated initial conditions, we are still able to obtain accurate and physically reasonable analytical approximations which model the Cahn-Hilliard time-evolution of such initial data.

5.2 Preliminaries

The choice of linear operator is crucial in obtaining decent results with the Homotopy Analysis Method. Looking at equation (5.3), several choices arise. We could use operators depending only on t, like $\frac{\partial}{\partial t} + 1$. We could mix the two independent variables and use an example of the diffusion equation, like $\frac{\partial}{\partial t} - \frac{\partial^2}{\partial x^2}$, or something simpler, like $\frac{\partial}{\partial t} + \frac{\partial}{\partial x} + 1$.

The homotopy for general auxiliary linear operator $L[U]$ is

$$0 \equiv \mathcal{H}(U, u_0; q) = (1-q)L[U - u_0] - qhN[U], \tag{5.5}$$

where

$$N[U] = U_t + U_{xx} + U_{xxxx} - 6UU_x^2 - 3U^2U_{xx}, \tag{5.6}$$

$q \in [0,1]$ is the homotopy parameter, u_0 is the solution to $L[u_0] = 0$, and h is the convergence control parameter. Note that when $q = 0$ in (5.5) we obtain $L[U] = 0$, and when $q = 1$ we obtain $N[U] = 0$, which is (5.3). The idea is that the homotopy will continuously deform the linear operator into the nonlinear operator as q moves through the interval $[0,1]$.

Next, we assume an expansion of $U(x,t)$ around q, such as

$$U(x,t) = \sum_{j=0}^{\infty} u_j(x,t) q^j. \tag{5.7}$$

We move things around in (5.5) and make the substitution (5.7) to get

$$(1-q) \sum_{j=0}^{\infty} L[u_j(x,t)] q^j = hqN \left[\sum_{j=0}^{\infty} u_j(x,t) q^j \right]. \tag{5.8}$$

Re-indexing the sums on the left-hand side gives

$$L[u_0] + \sum_{j=1}^{\infty} \left(L[u_j - u_{j-1}] \right) q^j = hqN \left[\sum_{j=0}^{\infty} u_j(x,t) q^j \right]. \tag{5.9}$$

Making the substitution in the initial condition (5.4) yields

$$u_0(x,0) + u_1(x,0) q + u_2(x,0) q^2 + \cdots = f(x). \tag{5.10}$$

This, of course, implies that

$$u_0(x,0) = f(x) \qquad \text{and} \qquad u_k(x,0) = 0 \quad \text{for} \quad k \geq 1\,. \tag{5.11}$$

If we expand the right-hand side of (5.9) around q as a Taylor Series, we will match powers of q on each side of this equation. Every term on the right-hand side of (5.9) will have a q, so the $O(1)$ equation is

$$L[u_0] = 0, \tag{5.12}$$

subject to

$$u_0(x,0) = f(x). \tag{5.13}$$

For $m \geq 1$, we get the $O(q^m)$ equation to be

$$L[u_m] = L[u_{m-1}] + \frac{h}{(m-1)!}\left(\frac{\partial^{m-1}}{\partial q^{m-1}} N\left[\sum_{j=0}^{\infty} u_j q^j\right]\right)\Big|_{q=0}, \tag{5.14}$$

subject to

$$u_m(x,0) = 0. \tag{5.15}$$

Each instance of an equation like (5.14) is a so-called deformation equation. We mentioned before that when $q = 1$ we have the solution to $N[U] = 0$. When $q = 1$ in the expansion (5.7), the solution is

$$U(x,t) = \sum_{j=0}^{\infty} u_j(x,t). \tag{5.16}$$

If this sum converges, it will be a solution to our PDE. Note that the solution of every deformation equation (5.14) depends on the one prior to it. This means we can solve the deformation equations sequentially, and form an approximation to (5.16) with a finite number of terms. We can then perform error analysis on the approximation until we are satisfied with the results.

First, in section 3, we consider about the simple auxiliary linear operator $L[U] = U_t + U$, which permits basis functions involving decaying exponentials in t. Next, in section 4, we discuss the auxiliary linear operator $L[U] = U_t - U_{xx}$, which is the linear operator affiliated with the heat equation. Finally, in section 5, we discuss the operator $L[U] = U_t + U_x + U$, which typically describes solutions along characteristic curves. For each of

these, we shall determine the influence of the linear operator in the approximate analytical solutions obtained via homotopy analysis.

As we shall observe, another crucial choice is the initial data. In each section, multiple forms of initial data are considered for the function $f(x)$ given in (5.13). We find that the solutions process is highly dependent on the initial data, and that some auxiliary linear operators are better than others for specific forms of initial data.

5.3 Homotopy Analysis with linear operator $L[U] = U_t + U$

For the operator

$$L[U] = U_t + U, \tag{5.17}$$

we begin by solving (5.12). This is

$$u_{0t} + u_0 = 0, \tag{5.18}$$

subject to (5.13). The solution is

$$u_0(x,t) = f(x)e^{-t}. \tag{5.19}$$

Considering higher-order deformation equations, we are solving an equation of the form

$$L[u_m] = g_m(x,t), \tag{5.20}$$

subject to $u_m(x,0) = 0$. This equation has solution

$$u_m(x,t) = e^{-t}\int_0^t g_m(x,s)e^s ds. \tag{5.21}$$

Specifically, we have by (5.14), that

$$L[u_1] = h\left\{u_{0t} + u_{0xx} + u_{0xxxx} - 6u_0u_{0x}^2 - 3u_0^2u_{0xx}\right\}. \tag{5.22}$$

Using (5.19), we are solving

$$L[u_1] = h\left\{A(x)e^{-t} - 3B(x)e^{-3t}\right\}, \tag{5.23}$$

where

$$A(x) = f^{(4)}(x) + f''(x) - f(x) \tag{5.24}$$

and

$$B(x) = f''(x)f^2(x) + 2f(x)f'(x)^2. \tag{5.25}$$

By (5.21), the solution is

$$u_1(x,t) = he^{-t}\int_0^t \left(A(x) - 3B(x)e^{-2s}\right) ds. \tag{5.26}$$

Upon integrating, we find that

$$u_1(x,t) = he^{-t}\left\{\frac{3}{2}B(x)e^{-2t} + A(x)t - \frac{3}{2}B(x)\right\}. \tag{5.27}$$

We will compute one more term. By (5.14), we have

$$L[u_2] = L[u_1] + h\left(\frac{\partial}{\partial q}N\left[u_0 + u_1q + O(q^2)\right]\right)\Big|_{q=0}. \tag{5.28}$$

By (5.23), this is

$$\begin{aligned} L[u_2] &= h\left\{A(x)e^{-t} - 3B(x)e^{-3t}\right\} \\ &\quad + h\Big\{u_{1t} + u_{1xxxx} + u_{1xx} - 3u_{1xx}u_0^2 - 6u_1u_0u_{0xx} - 12u_{1x}u_{0x}u_0 - 6u_1u_0^2\Big\}. \end{aligned} \tag{5.29}$$

Using (5.19) and (5.27), this becomes

$$L[u_2] = C(x)e^{-5t} + D(x)te^{-3t} + E(x)e^{-3t} + F(x)te^{-t} + G(x)e^{-t}, \tag{5.30}$$

where

$$\begin{aligned}
C(x) &= -\frac{9h^2}{2}\left\{f(x)^2B''(x) + 2f'(x)^2B(x) + 4f(x)f'(x)B'(x) + 2f(x)f''(x)B(x)\right\},\\
D(x) &= -3h^2\left\{f(x)^2A''(x) + 4f(x)f'(x)A'(x) + 2f(x)f''(x)A(x) + 2h^2f''(x)^2A(x)\right\},\\
E(x) &= \frac{3}{2}\Big\{h^2B^{(4)}(x) + 6h^2f(x)f''(x)B(x) + 3h^2f(x)^2B''(x) + 12h^2f(x)f'(x)B'(x)\\
&\qquad + 6h^2f'(x)^2B(x) - 3h^2B(x) + h^2B''(x) - 2hB(x)\Big\},\\
F(x) &= h^2(A^{(4)}(x) + A''(x) - A(x)),\\
G(x) &= -\frac{3h^2}{2}\left(B^{(4)}(x) + B''(x) + B(x)\right) + h^2A(x) + hA(x).
\end{aligned} \tag{5.31}$$

Finally, solving (5.30), we obtain

$$\begin{aligned}
u_2(x,t) = &-\frac{1}{4}C(x)e^{-5t} + \left(-\frac{1}{4}D(x) - \frac{1}{2}E(x)\right)e^{-3t} - \frac{1}{2}D(x)t^3e^{-t}\\
&+ \frac{1}{2}F(x)t^2e^{-t} + G(x)te^{-t} + \left(\frac{1}{4}C(x) + \frac{1}{4}D(x) + \frac{1}{2}E(x)\right)e^{-t}.
\end{aligned} \tag{5.32}$$

5.3.1 Error analysis of the case with initial condition $f(x) = \mathbf{sech}\ x$

Here we take the initial data $u_0(x,0) = f(x) = \mathrm{sech}(x)$

$$u_0(x,t) = e^{-t}\mathrm{sech}\ x. \tag{5.33}$$

Let us call the three-term approximation

$$A(x,t;h) = u_0(x,t) + u_1(x,t) + u_2(x,t). \tag{5.34}$$

Normally when computing error, we define the residual error

$$V(x,t;h) = N[A(x,t;h)], \tag{5.35}$$

where N was defined in (5.6). To get a sense of how good the error is, we usually compute the sum of squared residual error

$$\int_0^\infty \int_{-\infty}^\infty V(x,t;h)^2 dxdt. \tag{5.36}$$

There are two reasons why we do not use this formulation of the error. First, the integration of the sum of squared residual error is very difficult, if possible at all. More importantly, the temporal domain is infinite, so small residuals can lead to arbitrarily large error as $t \to \infty$.

There are alternatives to integrating. We will use a sum of the form

$$\sum_{k=1}^{K} \sum_{j=1}^{J} \frac{|V(\alpha(j), \beta(k); h)|}{KJ}, \tag{5.37}$$

where α and β are chosen below. There are two benefits of using summations, and one drawback. The first benefit being that we can now use absolute value instead of squaring in our error. This is computationally less demanding. The second benefit is that we are considering x and t in a compact subset of $\mathbb{R}^2$. Thus we are guaranteed the sum will converge, meaning the sum written above will be a function of h. Not only a function, but a sum of absolute values of polynomials in h. Thus (5.37) can be minimized by the convergence control parameter h at some particular h^*.

The drawback is the lack of information we can use. We are limited by the number of points we can handle. Then there is the question of how spread apart the x-values and t-values should be.

Looking at the form of the solution to the deformation equations (5.21), we see that each term in the approximation (and therefore the error) will have a factor of e^{-t}. It stands to reason that large t-values will contribute negligibly to the error calculation.

For our first sum, we will define

$$E_1(h) = \frac{1}{25}\sum_{k=1}^{5}\sum_{j=1}^{5}|V(j,k;h)|. \tag{5.38}$$

This error function uses 25 points close to the origin. It has minimum value 4.06×10^{-2}, obtained at $h_1 = 2.13396 \times 10^{-3}$. Its plot is given in Figure 5.1.

For x- and t-values in a geometric progression, we can take

$$E_2(h) = \frac{1}{25}\sum_{k=1}^{5}\sum_{j=1}^{5}|V(5^j,5^k;h)|. \tag{5.39}$$

This yields an error of 3.7977×10^{-13} at $h_2 = -4.055 \times 10^{-2}$. The plot of $E_2(h)$ is given in Figure 5.2.

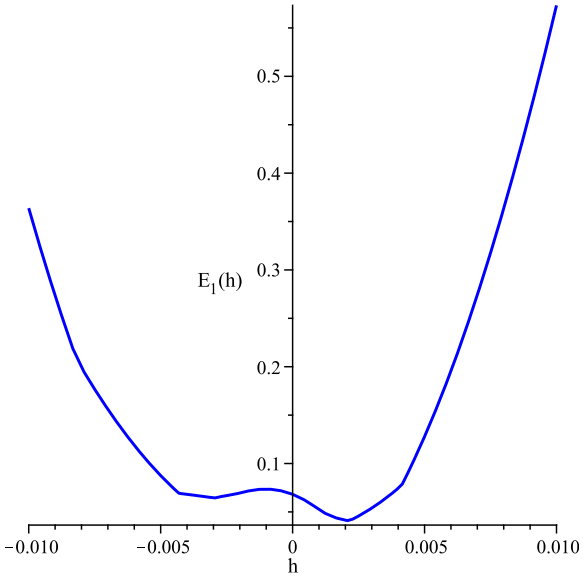

Figure 5.1: Plot of $E_1(h)$, the sum of absolute residual error over 25 points in the square $x \in [1, 5]$, $t \in [1, 5]$ as a function of h, the convergence control parameter. The error function has minimum $E_1(h_1) = 4.06 \times 10^{-2}$ where $h_1 = 2.13396 \times 10^{-3}$.

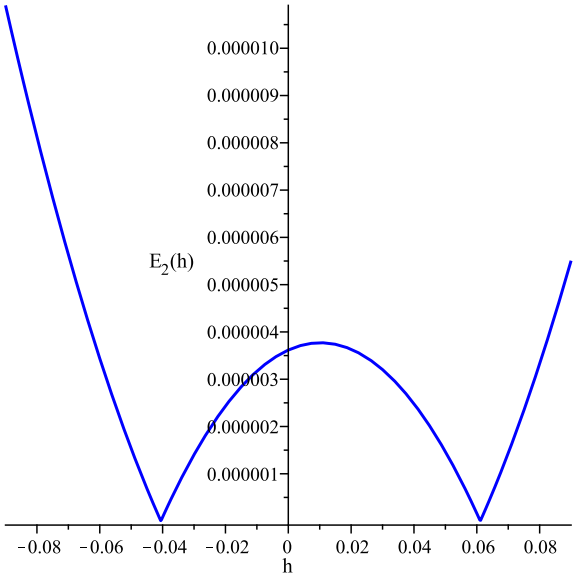

Figure 5.2: Plot of $E_2(h)$, the sum of absolute residual error over 25 points in a geometric x and t progression as a function of h, the convergence control parameter. The error function has minimum $E_2(h_2) = 3.7977 \times 10^{-13}$ where $h_2 = -4.055 \times 10^{-2}$.

The previous function used positive x-values, so the corresponding negative x-value summation is

$$E_3(h) = \frac{1}{25}\sum_{k=1}^{5}\sum_{j=1}^{5}|V(-5^j, 5^k; h)|. \tag{5.40}$$

The minimum value of this function is 5.1038×10^{-13}, occurring at $h_3 = -4.055 \times 10^{-2}$. The plot is given in Figure 5.3. It may be the case that E_3 and E_2 are symmetric functions. This would follow from the fact that sech x is an even function, and the operations taken in the homotopy analysis preserve this property. Looking at equation (5.3), if $U(x,t)$ is a solution, then $U(-x,t)$ is a solution. The differences in the error between the functions $E_2(h)$ and $E_3(h)$ would then be explained by machine error on Maple. Note that $h_2 = h_3$.

We can take more points in our error calculations. If we use a spread of 100 points with x-values on the interval $[-1024, 3125]$ and t-values in $[5, 3125]$, we have

$$E_4(h) = \frac{1}{100}\sum_{k=1}^{5}\sum_{j=-4}^{5}|V(j^5, k^5; h)| \tag{5.41}$$

The minimum is 2.895×10^{-2} found at $h_4 = -8.067 \times 10^{-4}$. The plot of $E_4(h)$ is given in Figure 5.4.

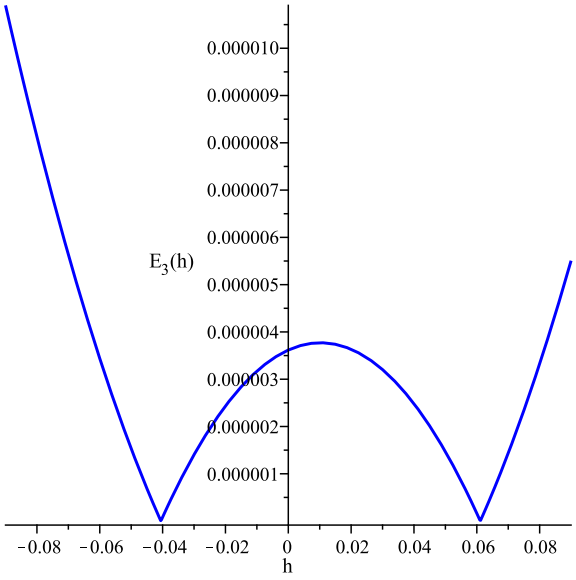

Figure 5.3: Plot of $E_3(h)$, the sum of absolute residual error over 25 points in negative x geometric progression as a function of h, the convergence control parameter. The error function has minimum $E_3(h_3) = 5.1038 \times 10^{-13}$ where $h_3 = -4.055 \times 10^{-2}$.

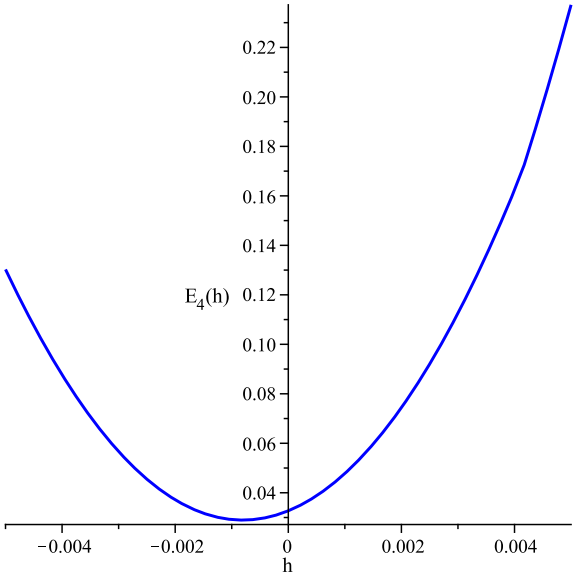

Figure 5.4: Plot of $E_4(h)$, the sum of absolute residual error over 100 points with $x \in [-1024, 3125]$ and $t \in [5, 3125]$ as a function of h, the convergence control parameter. The error function has minimum $E_4(h_4) = 2.895 \times 10^{-2}$ where $h_4 = -8.067 \times 10^{-4}$.

For the last approximation, we take a large spread of x-values, with small t-values. This computation is to see how large we can make the error using 100 points with small t-values. We define

$$E_5(h) = \frac{1}{100} \sum_{k=0}^{4} \sum_{j=-4}^{5} |V(j^5, k; h)|. \tag{5.42}$$

We indeed have the most error of 0.1785 obtained at $h_5 = -4.4 \times 10^{-4}$.

The plot of the three-term approximation, $A(x, t; h_5)$, is given in Figure 5.5.

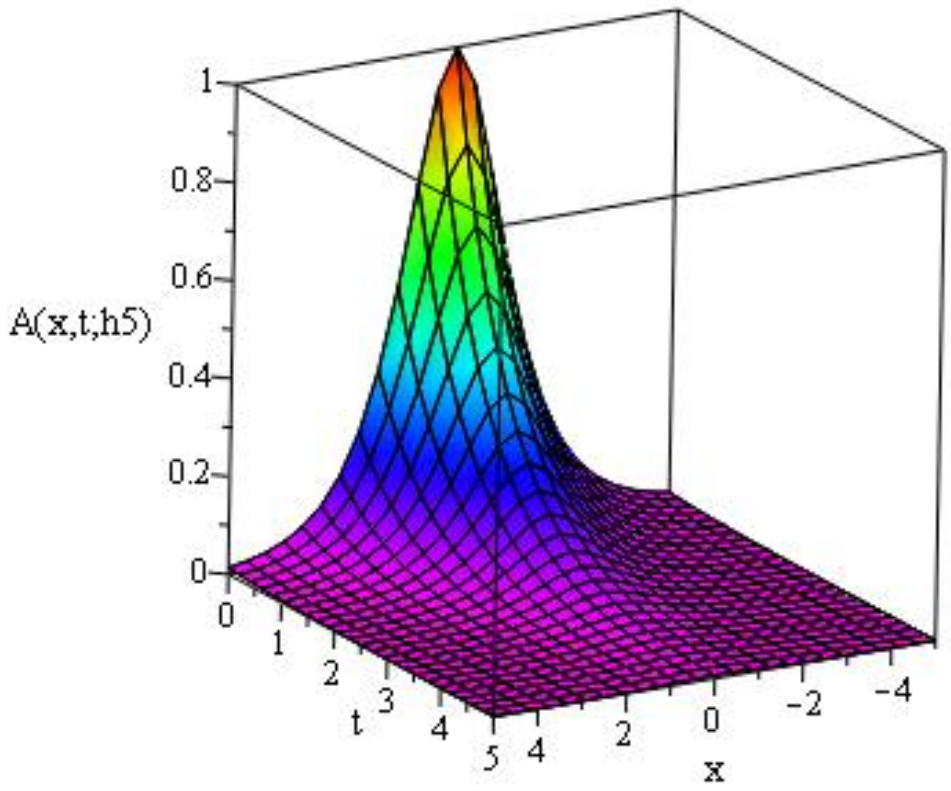

Figure 5.5: Plot of $A(x,t;h_5)$, the three-term approximation to (5.3) using $u(x,0) = \text{sech } x$ and linear operator $L[U] = U_t + U$.

5.3.2 Error analysis of the case with initial condition $f(x) = 1$

We now consider the case when $u(x, 0) = f(x) = 1$. Here

$$u_0(x, t) = e^{-t}, \tag{5.43}$$

$$u_1(x, t) = -hte^{-t}, \tag{5.44}$$

and

$$u_2(x, t) = te^{-t}\left(\frac{1}{2}h^2t - h^2 - h\right). \tag{5.45}$$

We define $B(x, t; h) = u_0(x, t) + u_1(x, t) + u_2(x, t)$, and let $Y(x, t; h) = N[B(x, t)]$.

Let us begin by using the same error functions as in the previous section. The function

$$E_6(h) = \frac{1}{25}\sum_{k=1}^{5}\sum_{j=1}^{5}|Y(j, k; h)|. \tag{5.46}$$

gives a minimum error 8.178×10^{-2} at $h_6 = 0.4142$.

Since $Y(x, t)$ is only a function of t, we can consider t-values separated by a large margin, such as

$$E_7(h) = \frac{1}{25}\sum_{k=1}^{5}\sum_{j=1}^{5}|Y(j, k^5; h)|. \tag{5.47}$$

This function is not quite symmetric (see Figure 5.6) and has minimum 4.14×10^{-10} at $h_7 = 1.4142$.

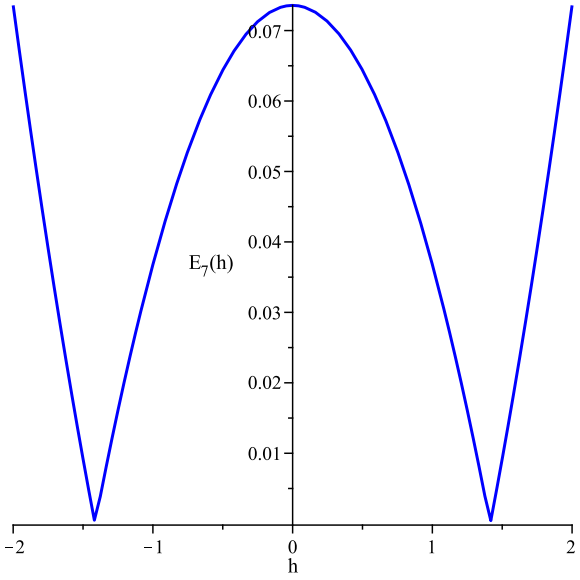

Figure 5.6: Plot of $E_7(h)$, the sum of absolute residual error over 25 points in a geometric t progression as a function of h, the convergence control parameter. The error function has minimum $E_7(h_7) = 4.14 \times 10^{-10}$ where $h_7 = 1.4142$.

The residual error $Y(x,t;h)$ is simple enough to integrate in the temporal variable, giving rise to

$$E_8(h) = \int_0^\infty Y(x,t;h)^2 dt. \tag{5.48}$$

This yields a polynomial in h, and we can get an idea of what the error is for x lying in a compact set. Suppose x lies in a compact set with diameter M. Then the sum of squared residual error is

$$E_9(h;M) = M(E_8(h)) = M\left(\frac{3}{16}h^4 + \frac{3}{4}h^3 + \frac{5}{4}h^2 + h + \frac{1}{2}\right). \tag{5.49}$$

For example, if $M = 1$, the minimum value of the polynomial is 0.1875 at $h_8 = -1$. Since these calculations are much simpler, we can arrive at higher order terms in the approximation. In fact,

$$u_3(x,t) = -\frac{1}{6}hte^{-t}\left(h^2t^2 - 6h(h+1)t + 12h + 6\right). \tag{5.50}$$

If we run the four-term approximation through the nonlinear operator, let us call the result

$$Y_1(x,t;h) = N[u_0(x,t) + u_1(x,t) + u_2(x,t) + u_3(x,t)]. \tag{5.51}$$

The resulting sum of squared residual error is

$$E_{10}(h;M) = M\int_0^\infty Y_1(x,t;h)^2 dt, \tag{5.52}$$

where again we can only consider x in a compact set of diameter M. In the case where $M = 1$, we obtain a minimum error of 0.15625 at $h = -1$. Notice that going to the next term did not decrease the error significantly. The reason for this was given in the previous section. If

we integrate over an infinite domain, even if we have convergence, small contributions can add up leading to an undesirable error.

However, if we consider the sums as in (5.46) and (5.47), the corresponding values for the four-term approximation are more reasonable. The error function

$$E_{11}(h) = \frac{1}{25}\sum_{k=1}^{5}\sum_{j=1}^{5}|Y_1(j,k;h)| \tag{5.53}$$

has a minimum value of 0.07759 at $h = 0.2624$. The function

$$E_{12}(h) = \frac{1}{25}\sum_{k=1}^{5}\sum_{j=1}^{5}|Y_1(j,k^5;h)| \tag{5.54}$$

obtains its minimum 6.651×10^{-11} at $h = 0.71167$. The plots of $E_{11}(h)$ and $E_{12}(h)$ are given in Figures 5.7 and 5.8, respectively.

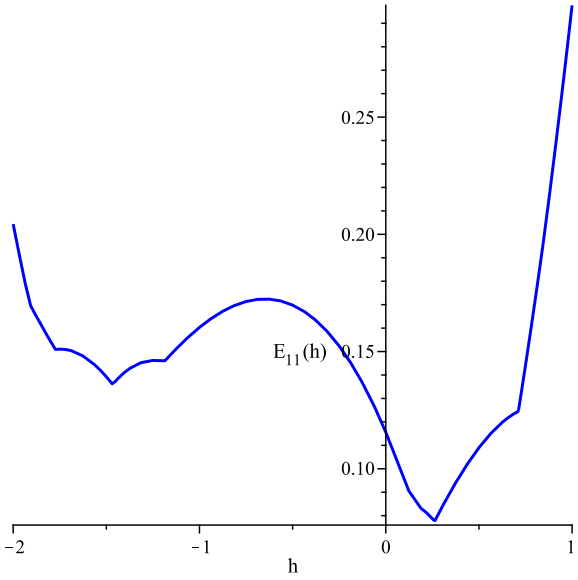

Figure 5.7: Plot of $E_{11}(h)$, the sum of absolute residual error over 25 points in the square $x \in [1, 5]$, $t \in [1, 5]$ as a function of h, the convergence control parameter. The error function has minimum $E_{11}(h) = 0.07759$ where $h = 0.2624$.

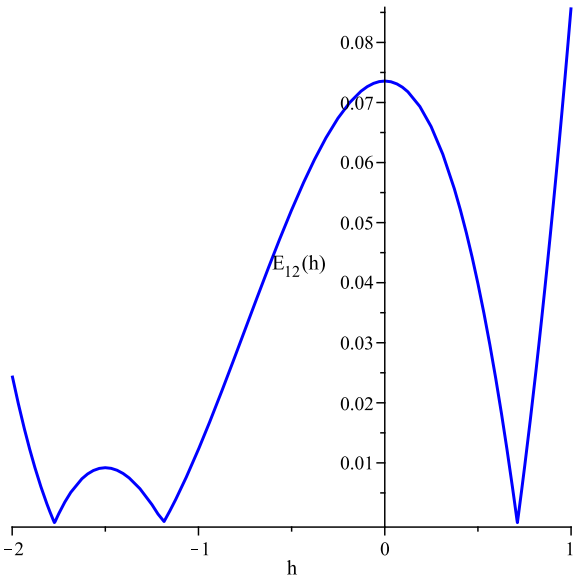

Figure 5.8: Plot of $E_{12}(h)$, the sum of absolute residual error over 25 points in a geometric t progression as a function of h, the convergence control parameter. The error function has minimum $E_{12}(h) = 6.651 \times 10^{-11}$ at $h = 0.71167$.

The ease of this case also affords being able to use more points to get an idea of what convergence control parameter to use when making a plot of our four-term approximation. We have

$$E_{13}(h) = \frac{1}{1000} \sum_{k=1}^{100} \sum_{j=1}^{10} \left| Y_1 \left(j, \frac{k}{5}; h \right) \right| \tag{5.55}$$

giving a minimum value of 0.04377 at $h^* = 0.116$. The plot of $E_{13}(h)$ is given in Figure 5.9, and the plot of the four-term approximation $Y_1(x, t; h^*)$ is given in Figure 5.10.

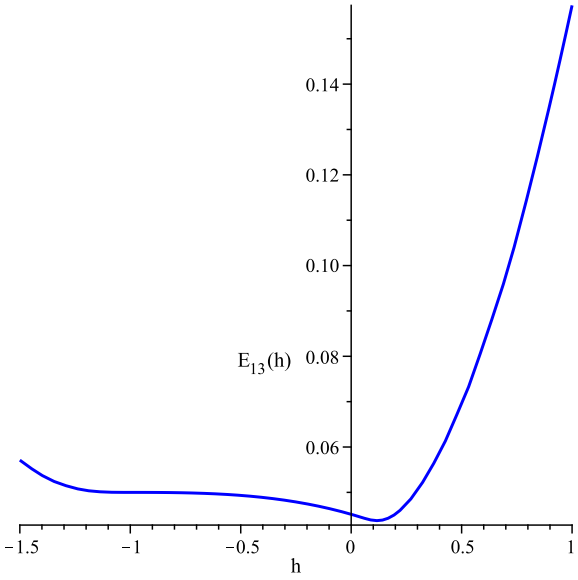

Figure 5.9: Plot of $E_{13}(h)$, the sum of absolute residual error over 1000 points with $x \in [1, 10]$, $t \in \left[\frac{1}{5}, 20\right]$ as a function of h, the convergence control parameter. The error function has minimum $E_{13}(h^*) = 4.377 \times 10^{-2}$ where $h^* = 0.116$.

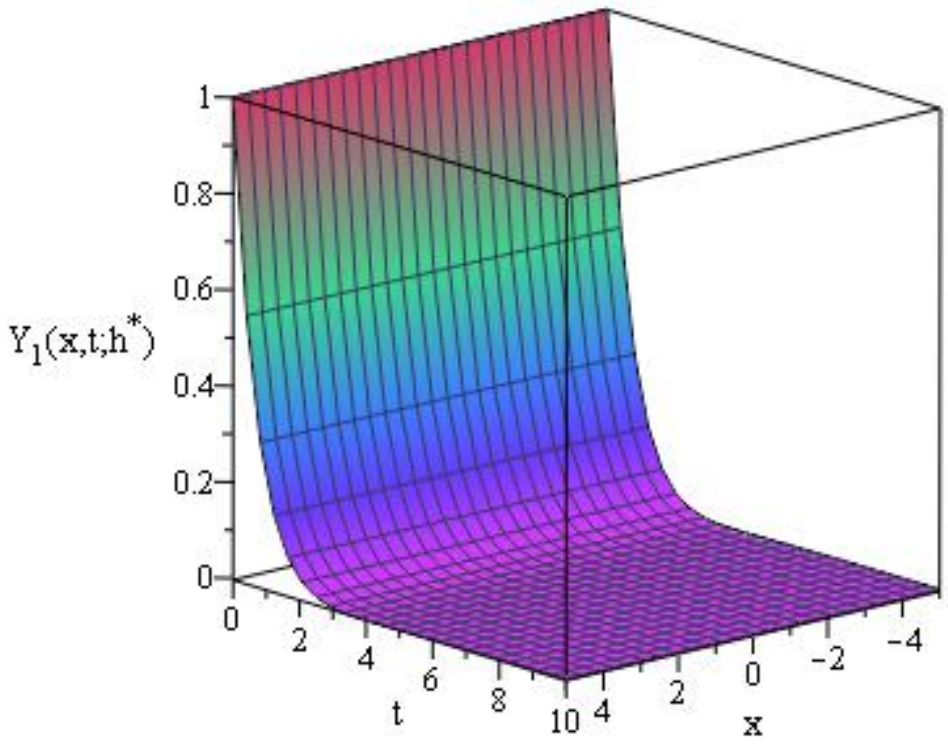

Figure 5.10: Plot of $Y_1(x,t;h^*)$, the three-term approximation to (5.3) subject to $u(x,0)=1$ and using linear operator $L[U]=U_t+U$.

5.3.3 Error analysis of the case with initial condition $f(x) = e^{-x^2}$

In this section we look at the case of initial data

$$u(x,0) = e^{-x^2}. \tag{5.56}$$

We have

$$u_0(x,t) = e^{-x^2-t} \tag{5.57}$$

and

$$u_1(x,t) = 16h\left\{te^{-x^2-t}\left(x^4 - \frac{11}{4}x^2 + \frac{9}{16}\right) + \frac{9}{8}e^{-3x^2}\left(e^{-3t} - e^{-t}\right)\left(x^2 - \frac{1}{6}\right)\right\}. \tag{5.58}$$

Again we will call $A(x,t;h) = u_0(x,t) + u_1(x,t) + u_2(x,t)$, and the residual error $V(x,t;h) = N[A(x,t;h)]$.

The function

$$E_{14}(h) = \frac{1}{25}\sum_{k=1}^{5}\sum_{j=1}^{5}|V(j,k;h)| \tag{5.59}$$

returns a minimum error of 0.14 at $h = -0.0032$. However, the function

$$E_{15}(h) = \frac{1}{25}\sum_{k=1}^{5}\sum_{j=1}^{5}|V(5^j,5^k;h)| \tag{5.60}$$

has minimum error 1.84×10^{-15} at $h = -0.0002$, and its plot is 5.11. To try and strike a balance between these vastly different error calculations, we use more data. Note again that the initial data (5.56) sits inside our approximation, and so contributes to the error. The highest error is close to the origin. So consider 200 lattice points relatively close to the

origin. The function

$$E_{16}(h) = \frac{1}{200} \sum_{k=1}^{20} \sum_{j=-4}^{5} |V(j,k;h)| \tag{5.61}$$

has a minimum error 0.06657 at $h_0 = -0.000976$. The plot of the three-term approximation $A(x,t;h_0)$ is given in Figure 5.12.

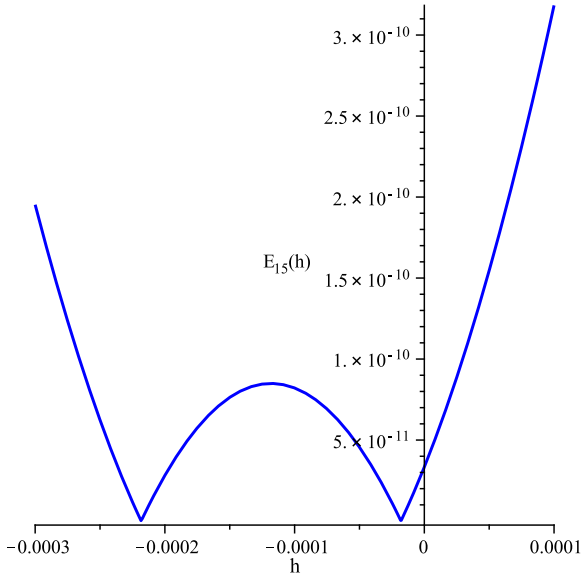

Figure 5.11: Plot of $E_{15}(h)$, the sum of absolute residual error over 25 points in a geometric x and t progression as a function of h, the convergence control parameter. The error function has minimum $E_{15}(h) = 1.84 \times 10^{-15}$ where $h = -2 \times 10^{-4}$.

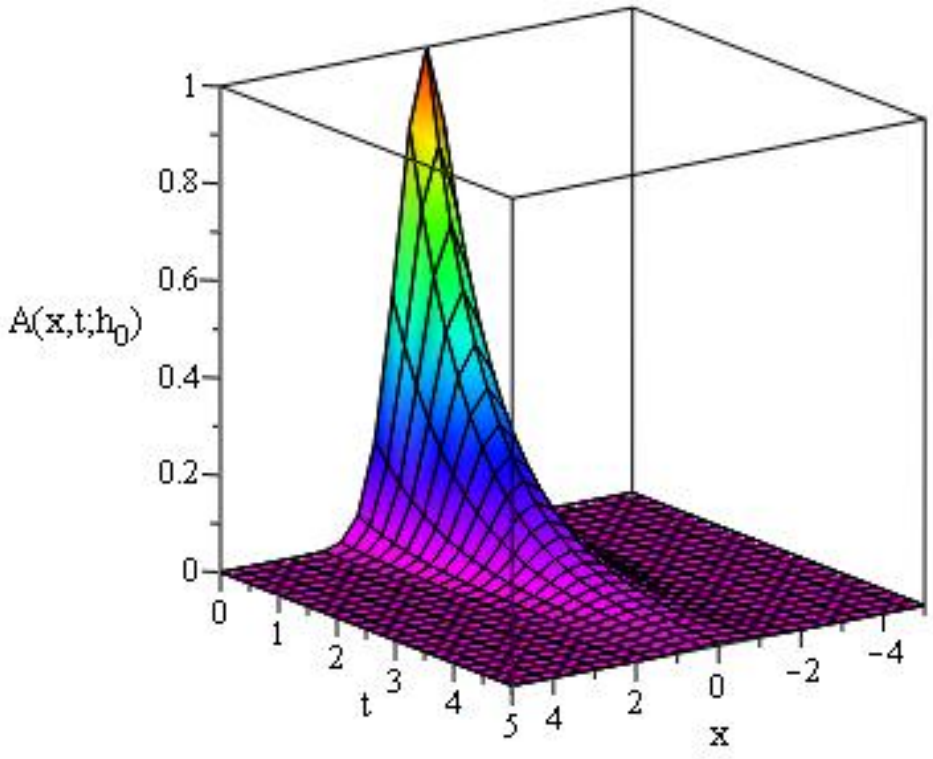

Figure 5.12: Plot of $A(x,t;h_0)$, the three-term approximation to (5.3) with initial condition $u(x,0) = e^{-x^2}$ using linear operator $L[U] = U_t + U$.

5.3.4 Error analysis of the case with initial condition $f(x) = \sin x$

We noted in section 2.1 that the solution to the original PDE (5.3) had to be symmetric in x, and that our homotopy approximation was then symmetric in x. So now we consider a case with inital datum that does not carry the same symmetry. We use

$$f(x) = \sin x. \tag{5.62}$$

We have

$$u_0(x,t) = e^{-t}\sin x, \tag{5.63}$$

and

$$u_1(x,t) = -\frac{1}{2}h\sin x\left\{3e^{-3t}(1-3\cos^2 x) + 2te^{-t} + 9e^{-t}\cos^2 x\right\}. \tag{5.64}$$

Let us define the three-term approximation

$$A(x,t;h) = u_0(x,t) + u_1(x,t) + u_2(x,t). \tag{5.65}$$

Then we consider the residual error

$$V(x,t;h) = N[A(x,t;h)]. \tag{5.66}$$

We have the error function

$$E_{17}(h) = \frac{1}{25}\sum_{k=1}^{5}\sum_{j=1}^{5}|V(j,k;h)|. \tag{5.67}$$

This function has a minimum 0.0777 at $h = -0.002486$. If we use the points that are spread out in a polynomial sequence, the function

$$E_{18}(h) = \frac{1}{25}\sum_{k=1}^{5}\sum_{j=1}^{5}|V(j^5,k^5;h)|. \tag{5.68}$$

gives an error of 0.0348 at $h = -0.0067$. Its plot is Figure 5.13. To use 100 points, we consider the function

$$E_{19}(h) = \frac{1}{100} \sum_{k=1}^{10} \sum_{j=-4}^{5} |V(10j, k; h)|. \tag{5.69}$$

It has minimum 0.0337 obtained at $h_9 = -0.00475$. The plot of the three-term approximation $V(x, t; h_9)$ is given in Figure 5.14.

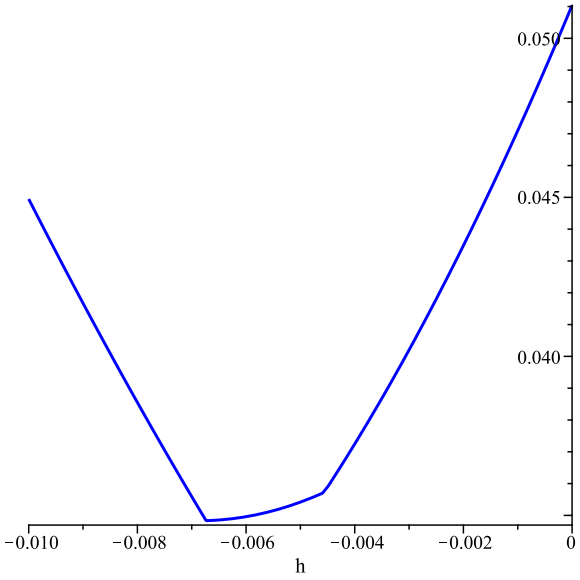

Figure 5.13: Plot of $E_{18}(h)$, the sum of absolute residual error over 25 points in a geometric x and t progression as a function of h, the convergence control parameter. The error function has minimum $E_{18}(h) = 3.48 \times 10^{-2}$ where $h = -6.7 \times 10^{-3}$.

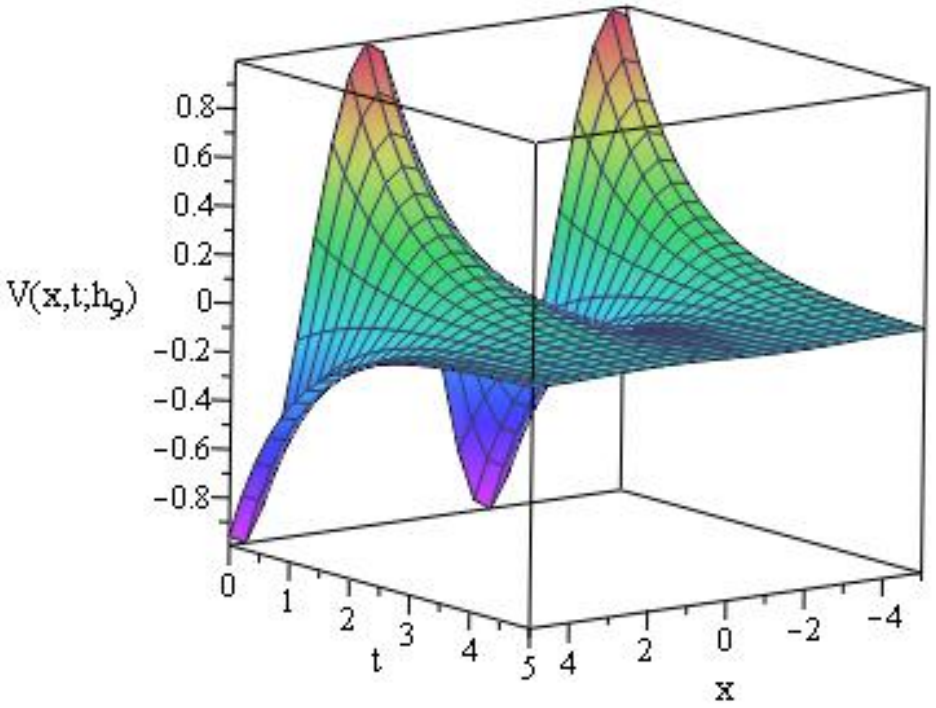

Figure 5.14: Plot of $V(x,t;h_9)$, the three-term approximation to (5.3) with $u(x,0) = \sin x$ using linear operator $L[U] = U_t + U$.

5.4 Homotopy Analysis with linear operator $L[U] = U_t - U_{xx}$

The diffusion operator $L[U] = U_t - U_{xx}$ is a natural choice since we know how to solve $L[U]$ set equal to zero (for the zeroth order deformation equation), as well as when $L[U]$ is set equal to some inhomogeneity (for the higher-order deformation equations). The solution to $L[u_0] = 0$ subject to $u_0(x, 0) = f(x)$ is

$$u_0(x,t) = \frac{1}{\sqrt{4\pi t}} \int_{-\infty}^{\infty} \exp\left(\frac{-(x-y)^2}{4t}\right) f(y)dy. \tag{5.70}$$

Looking at the higher order deformation equations, we see they are equivalent to solving the diffusion equation with a source,

$$u_{nt} - u_{nxx} = f_n(x,t), \tag{5.71}$$

subject to initial conditions $u_n(x, 0) = 0$. This equation has solution

$$u_n(x,t) = \int_0^t \int_{-\infty}^{\infty} \frac{1}{2\sqrt{\pi(t-s)}} \exp\left(\frac{-(x-y)^2}{4(t-s)}\right) f_n(y,s)dyds. \tag{5.72}$$

5.4.1 Error analysis of the case $f(x) = \sin x$

Using the initial condition $f(x) = \sin x$, we find

$$u_0(x,t) = e^{-t} \sin x, \tag{5.73}$$

$$u_1(x,t) = h \sin x \left\{ \left(\frac{3}{8} - \frac{3}{2}\cos^2 x\right) e^{-9t} + \frac{3}{2}e^{-3t}\cos^2 x + te^{-t} - \frac{3}{8}e^{-t} \right\}, \tag{5.74}$$

and $u_2(x, t)$ similarly using (5.72).

We call the approximation up to $O(q^2)$ by $a(x,t;h) = u_0(x,t) + u_1(x,t) + u_2(x,t)$. The residual error found by running through the original nonlinear operator is $V(x,t;h) = N[a(x,t;h)]$.

The function

$$G(h) = \frac{1}{25}\sum_{k=1}^{5}\sum_{j=1}^{5}|V(j,k;h)| \tag{5.75}$$

has minimum error 0.074 found at $h_{10} = -0.37$. If we use points spread out in a geometric sequence to approximate the error, we get a small result. The function

$$G_1(h) = \frac{1}{25}\sum_{k=1}^{5}\sum_{j=1}^{5}|V(5^j,5^k;h)| \tag{5.76}$$

has a minimum error of 1.88×10^{-3} at $h = 1.388 \times 10^{-17}$. The plot is given in Figure 5.15. If we use 100 points close to the origin in a 10 by 2 rectangle, we get an undesirable result. The function

$$G_2(h) = \frac{1}{100}\sum_{k=1}^{10}\sum_{j=-4}^{5}\left|V\left(j,\frac{k}{5};h\right)\right| \tag{5.77}$$

returns a minimum error of 0.46799 occurring at $h = -0.2985$. To get an idea of what our three-term approximation looks like, we use h_{10}, the minimizer for equation (5.75) in the plot. So $a(x,t;h_{10})$ is given in Figure 5.16. Compare this with Figure 14.

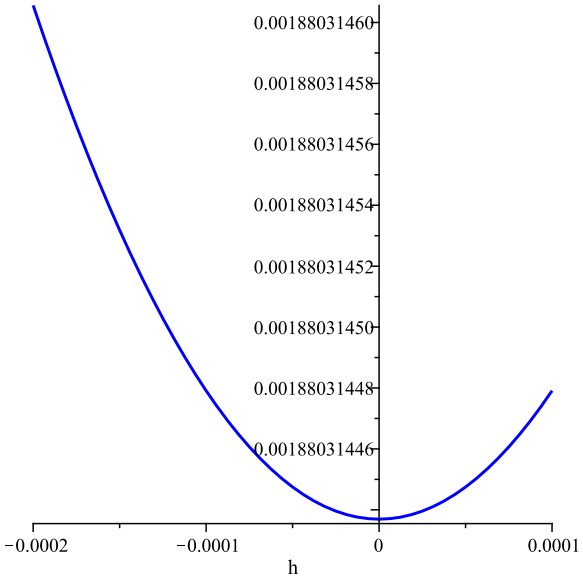

Figure 5.15: Plot of $G_1(h)$, the sum of absolute residual error over 25 points in a geometric x and t progression as a function of h, the convergence control parameter. The error function has minimum $G_1(h) = 1.88 \times 10^{-3}$ where $h = 1.388 \times 10^{-17}$.

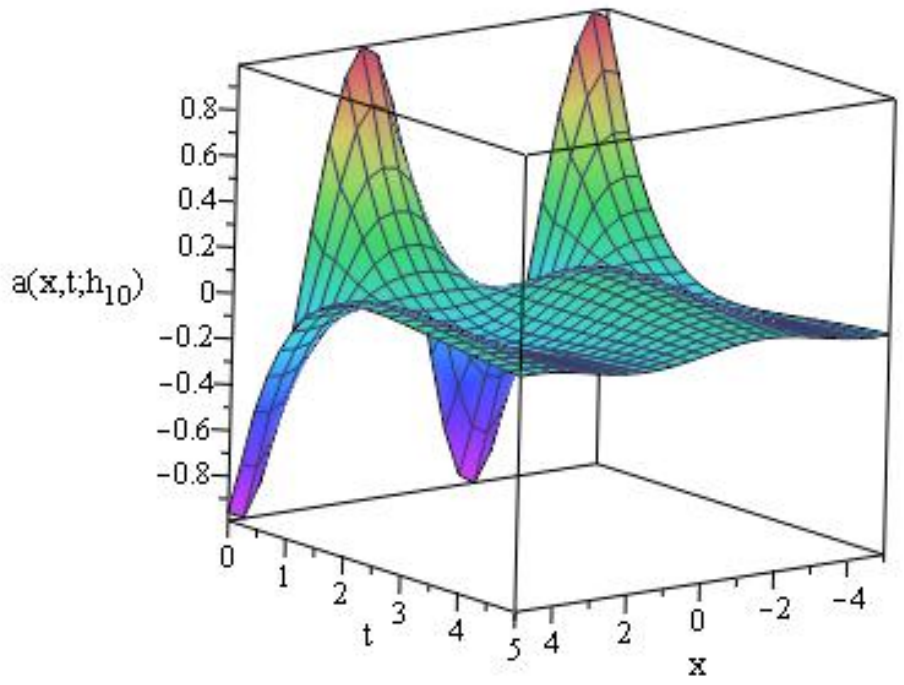

Figure 5.16: Plot of $a(x,t;h_{10})$, the three-term approximation to (5.3) with initial condition $u(x,0) = \sin x$ and linear operator $L[U] = U_t - U_{xx}$.

5.4.2 Comment on the $f(x) = 1$ case

We are primarily interested in solutions which decay to zero as $t \to \infty$. While other solutions exist, the solutions exhibiting temporal decay can more readily be studied in the context of the framework provided here, since the residual error of such solutions necessarily decays to zero as $t \to \infty$, as well. Some operators are compatible with this type of solution, for appropriate initial data.

Now, when $f(x) = 1$, the present choice of linear operator results in order zero term

$$u_0(x,t) = \frac{1}{\sqrt{4\pi t}} \int_{-\infty}^{\infty} \exp\left(\frac{-(x-y)^2}{4t}\right) dy = 1 \tag{5.78}$$

for all $t > 0$. Yet, $N[u_0(x,t)] = N[1] = 0$, hence $u_0(x,t)$ is an exact solution to the original problem. This is simply the constant solution $u(x,t) = 1$. From the form of the Cahn-Hilliard equation, we see that any function of the form $u(x,t) = C$, where C is a real-valued constant, is a solution. However, such a solution does not decay as $t \to \infty$. Obviously, for such solutions, we do not require the homotopy analysis method in the first place. Still, it is nice to see that, in certain trivial cases, the homotopy analysis solution at order zero reduces the the exact trivial solution of the form $u(x,t) = C$.

5.5 Homotopy Analysis with linear operator $L[U] = U_t + U_x + U$

In this section we consider $L[U] = U_t + U_x + U$. Solving

$$u_t + u_x + u = 0 \tag{5.79}$$

yields

$$u(x,t) = e^{-x}\varphi(t-x), \tag{5.80}$$

where φ is an arbitrary function defined along a characteristic. If we use the initial condition

$$u(x,0) = f(x), \tag{5.81}$$

we find that the arbitrary function φ satisfies $\varphi(x) = e^{-x}f(-x)$ and therefore

$$u_0(x,t) = e^{-t}f(x-t). \tag{5.82}$$

Suppose we want to solve the nth order equation

$$L[u_n] = u_{nt} + u_{nx} + u_n = g_n(x,t). \tag{5.83}$$

The solution is then given by

$$u_n(x,t) = e^{-x}\left\{\varphi(t-x) + \int e^x g_n(x,\nu+x)dx\right\}, \tag{5.84}$$

where φ is an arbitrary function and ν is a parameter in the integral along which we consider the characteristic curve. After the integration is complete, we take $\nu = t - x$. To use the initial condition toward finding φ, let us call

$$j(x,t) = \int e^x g_n(x,\nu+x)dx, \tag{5.85}$$

which will return to being a function of both x and t after the integration. The initial condition for $n \geq 1$ is that

$$u_n(x,0) = 0, \tag{5.86}$$

so we have

$$0 = e^{-x}(\varphi(-x) + j(x,0)), \tag{5.87}$$

so $\varphi(x) = -j(-x,0)$. So our solution is

$$u_n(x,t) = e^{-x}\left(-j(x-t,0) + j(x,t)\right). \tag{5.88}$$

This outlines the general method of inverting the operator L using characteristics. We shall make use of these results in the following subsections, where we consider specific initial data.

5.5.1 Error analysis of the case $f(x) = e^{-x^2}$

If we consider the initial data $u(x,0) = f(x) = e^{-x^2}$, then we recover the zeroth order approximation

$$u_0(x,t) = e^{-t-(x-t)^2}. \tag{5.89}$$

The first order approximation reads

$$\begin{aligned} u_1(x,t) = 16h\Bigg\{ & t\left(t - x + \frac{1}{2}\right) e^{-t^2+(2x-1)t-x^2} \Bigg\{ t^3 - \left(3x + \frac{1}{2}\right) t^2 \\ & + \left(3x^2 + x - \frac{5}{2}\right) t - x^3 - \frac{1}{2}x^2 + \frac{5}{2}x + \frac{9}{8} \Bigg\} \\ & + \frac{9}{8}\left(t^2 + x^2 - 2xt - \frac{1}{6}\right)\left(e^{-3t^2+(6x-3)t-3x^2} - e^{-3t^2+(6x-1)t-3x^2}\right) \Bigg\}, \end{aligned} \tag{5.90}$$

and $u_2(x,t)$ can be found similarly using (5.88).

We will call the three-term approximation $a(x,t;h) = u_0(x,t)+u_1(x,t)+u_2(x,t)$, and the resulting residual error $V(x,t;h) = N[a(x,t;h)]$. We next see how this approximation stands up to our first error function, that given by

$$J_1(h) = \frac{1}{25}\sum_{k=1}^{5}\sum_{j=1}^{5}|V(j,k;h)|. \tag{5.91}$$

For this measure of the error, we obtain a minimum error value of 0.38 at $h = 9.66 \times 10^{-4}$. If we take a geometric sequence of points for $x \in [5,5^5], t \in [5,5^5]$, we have

$$J_2(h) = \frac{1}{25}\sum_{k=1}^{5}\sum_{j=1}^{5}|V(5^j,5^k;h)|. \tag{5.92}$$

This function has minimum 1.548×10^{-3} at $h = 3.73 \times 10^{-4}$, and is plotted in Figure 5.17. To get an idea of how strong the error is, we can take 100 points close to the origin, as in

$$J_3(h) = \frac{1}{100}\sum_{k=1}^{10}\sum_{j=-4}^{5}|V(j,k;h)|. \tag{5.93}$$

This function has minimum 0.132 at $h_{11} = -0.001$. Figure 5.18 gives the plot of our three-term approximation $a(x,t;h_{11})$.

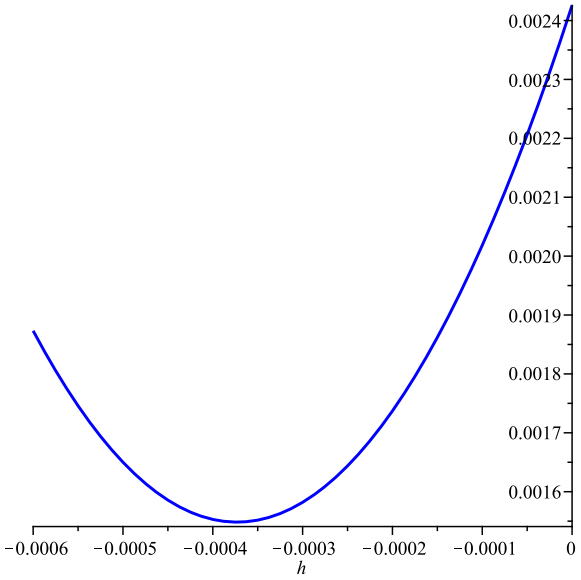

Figure 5.17: Plot of $J_2(h)$, the sum of absolute residual error over 25 points in a geometric progression in x and t as a function of h, the convergence control parameter. The error function has minimum $J_2(h) = 1.548 \times 10^{-3}$ where $h = 3.73 \times 10^{-4}$.

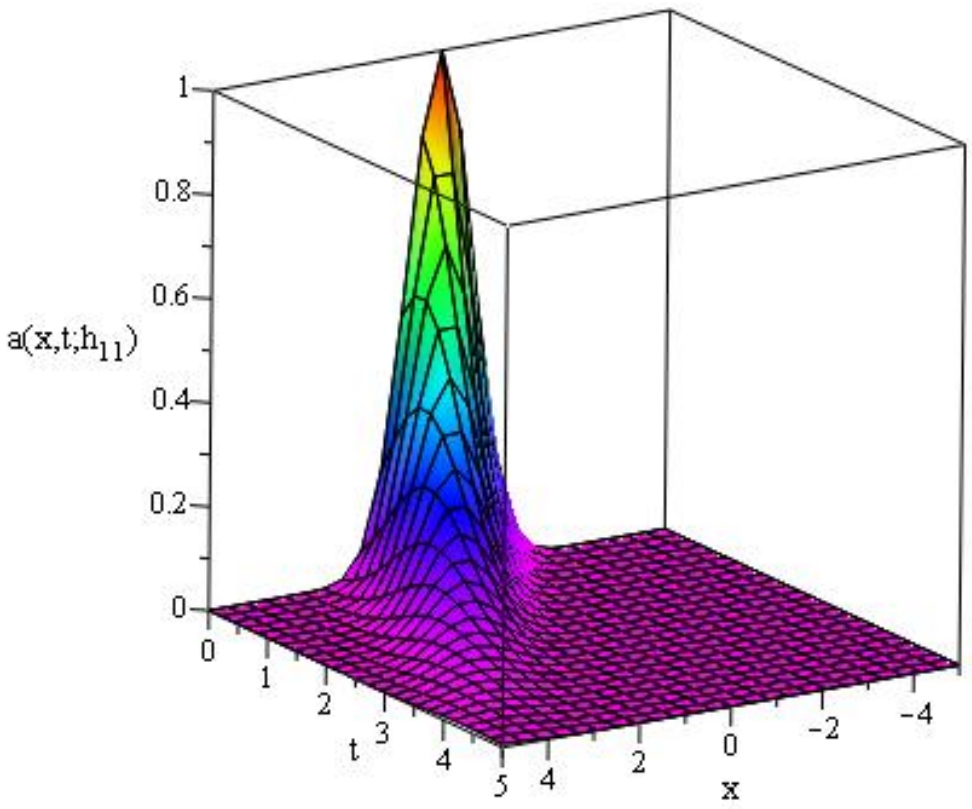

Figure 5.18: Plot of $a(x,t;h_{11})$, the three-term approximation to (5.3) with $u(x,0) = e^{-x^2}$ and linear operator $L[U] = U_t + U_x + U$.

5.5.2 Error analysis of the case $f(x) = \sin x$

We have

$$u_0(x,t) = e^{-t}\sin(x-t), \tag{5.94}$$

$$u_1(x,t) = hxe^{-t}\left(\sin(t-x) - \cos(t-x)\right) - he^{-t}\Bigg(\left(x - t - \frac{9}{2}\cos^2(t-x) + \frac{3}{2}\right)\sin(t-x) + (t-x)\cos(t-x)\Bigg) - \frac{3}{8}he^{-3t}\left(3\sin(3t-3x) - \sin(t-x)\right). \tag{5.95}$$

We can find $u_2(x,t)$ similarly, and set $a(x,t;h) = u_0(x,t) + u_1(x,t) + u_2(x,t)$. The residual error is again $V(x,t;h) = N[a(x,t;h)]$. Using our first error function

$$P_1(h) = \frac{1}{25}\sum_{k=1}^{5}\sum_{j=1}^{5}|V(j,k;h)|, \tag{5.96}$$

we have a minimum error of 0.107 at $h_{12} = 1.558 \times 10^{-3}$. If we use 25 points in a geometric progression in x and t, the function

$$P_2(h) = \frac{1}{25}\sum_{k=1}^{5}\sum_{j=1}^{5}|V(5^j, 5^k; h)| \tag{5.97}$$

returns an error of 1.66×10^{-3} at $h = -2.266\times10^{-3}$. Figure 5.19 is $P_2(h)$. We plot $a(x,t;h_{12})$ in Figure 5.20.

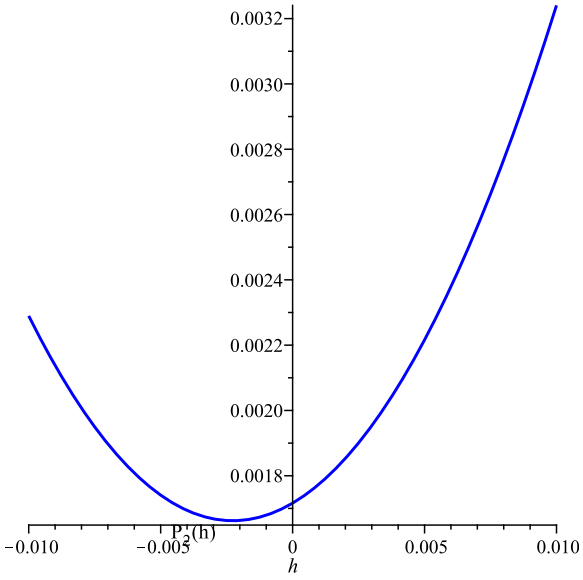

Figure 5.19: Plot of $P_2(h)$, the sum of absolute residual error over 25 points in a geometric x and t progression as a function of h, the convergence control parameter. The error function has minimum $P_2(h) = 1.66 \times 10^{-3}$ where $h = -2.266 \times 10^{-3}$.

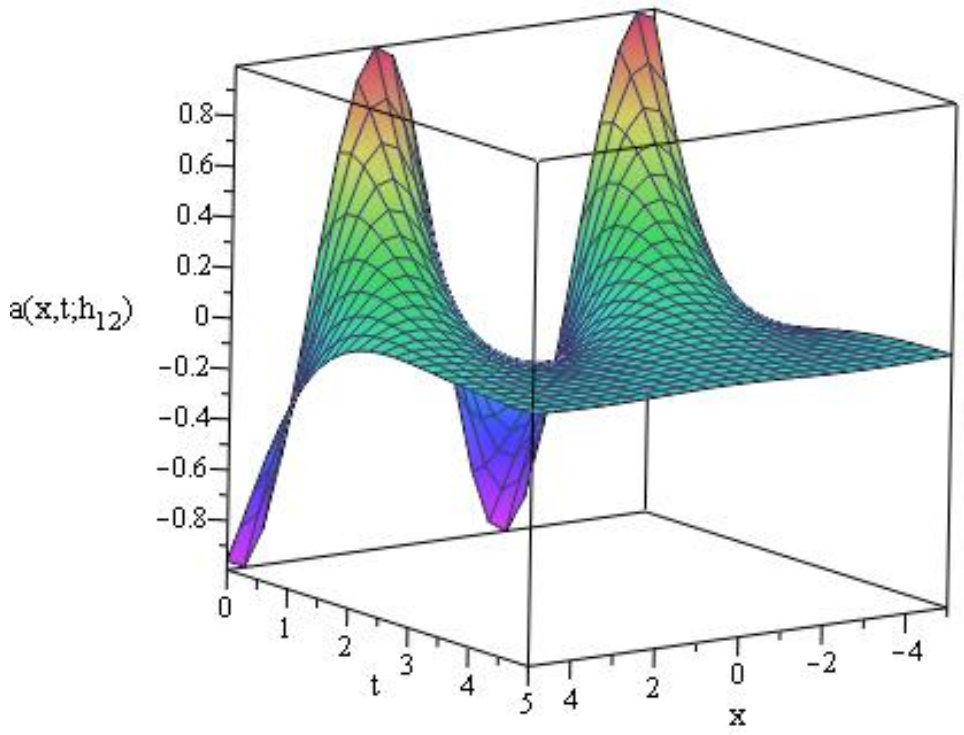

Figure 5.20: Plot of a(x,t;12), the three-term approximation to (5.3) with initial condition $u(x,0) = \sin x$ using linear operator $L[U] = U_t + U_x + U$.

5.5.3 Errror analysis of the case $f(x) = 1$

In the case $u(x, 0) = 1$, we have

$$u_0(x, t) = e^{-t}, \tag{5.98}$$

$$u_1(x, t) = -hte^{-t}, \tag{5.99}$$

and

$$u_2(x, t) = \frac{1}{2}h\left\{\left((t^2 - 2t + 3)h - 2t\right)e^{-t} - 6h\left(t + \frac{1}{2}\right)e^{-3t}\right\}. \tag{5.100}$$

Use $a(x, t; h) = u_0(x, t) + u_1(x, t) + u_2(x, t)$, and the residual error $V(x, t; h) = N[a(x, t; h)]$.

As in section 3.2, the residual error is square-integrable in the t variable. So if we take x to be in some compact set with diameter M, then

$$Q(h; M) = M\int_{-\infty}^{\infty} V(x, t; h)^2 dt \tag{5.101}$$

is the sum of squared residual error. This function has minimum value 0.225 at $h = -0.531$. This is because we are integrating over the entire temporal domain. If we instead use 1,000 points to approximate the function over $x \in [1, 10], t \in [\frac{1}{5}, 20]$, we have the function

$$Q_1(h) = \frac{1}{1000}\sum_{k=1}^{100}\sum_{j=1}^{10}\left|V\left(j, \frac{k}{5}; h\right)\right|. \tag{5.102}$$

Here we have a minimum of 4.385×10^{-2} at $h_{13} = 0.18$. The plot of $Q_1(h)$ is Figure 5.21. The plot of $a(x, t; h_{13})$ is given in Figure 5.22.

For reference, we include the sum using just 25 points in the square:

$$Q_2(h) = \frac{1}{25}\sum_{k=1}^{5}\sum_{j=1}^{5}|V(j, k; h)|. \tag{5.103}$$

The function $Q_2(h)$ has minimum value 8.12×10^{-2} occurring when $h = 0.519$.

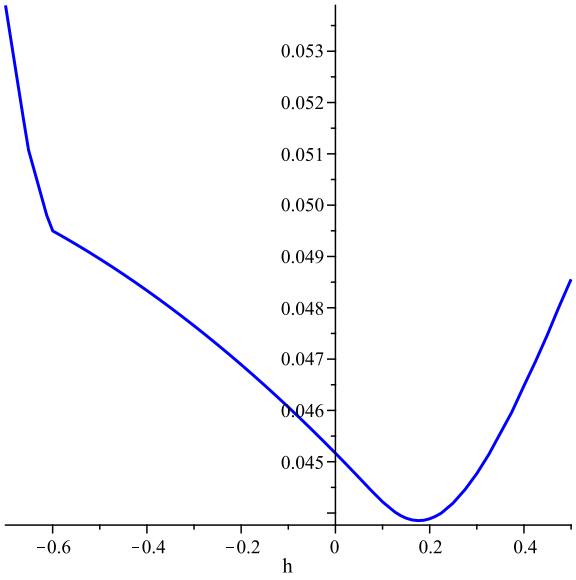

Figure 5.21: Plot of $Q_1(h_1)$, the sum of absolute residual error over 1000 points with x in the interval $[1, 10]$ and t in the interval $\left[\frac{1}{5}, 20\right]$ as a function of h, the convergence control parameter. The error function has minimum $Q_1(h_{13}) = 4.385 \times 10^{-2}$ where $h_{13} = 0.18$.

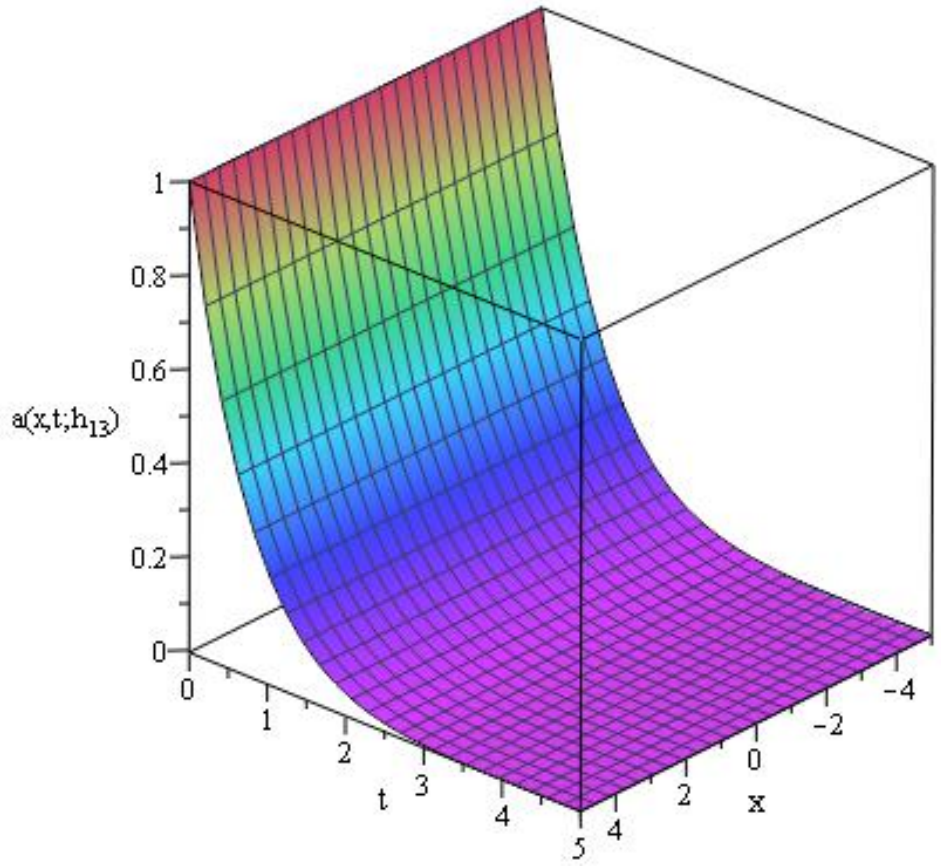

Figure 5.22: Plot of $a(x,t;h_{13})$, the three-term approximation to (5.3) with $u(x,0)=1$ and linear operator $L[U]=U_t+U_x+U$.

5.6 Discussion

We have applied an optimal form of the homotopy analysis method to obtain analytical approximations to the Cahn-Hilliard equation (5.3) with various forms of initial data. In constructing the homotopy, we have great freedom to select the auxiliary linear operator, and we demonstrate this by selecting three types of operators. It was shown that for different types of initial data, some operators allow us to obtain more accurate low-order approximations than others. However, there was no one operator that performed better than others. This makes sense, because for different kinds of initial conditions, we have different time evolution properties. Although the time evolution of the initial data is governed by the Cahn-Hilliard equation, drastically different initial data can induce various types of time evolution, since the right hand side of (5.3) involves not only $f(x) = u(x, 0)$ but also various derivatives of $f(x)$. Hence, it follows that various types of auxiliary operators pick up the different manners of time evolution induced by the initial data.

One point to be made is the fact that $L[U] = U_t + U$ gave reasonable results every time it was used as the auxiliary linear operator in the method. However, when using initial data $u(x, 0) = 1$, the three-term approximation under $L[U] = U_t + U_x + U$ gave almost the same error (the difference was in the ten-thousandths place) as the *four*-term approximation using $L[U] = U_t + U$. See (5.55) and (5.102). Thus, it appears as though simple auxiliary linear operators such as $L = U_t + U$ are reliable at giving solutions. More complicated

auxiliary operators can be used to obtain better solutions, but only some of the time (when they are efficient to use).

When working on an infinite domain, it is difficult to accurately measure how accurate an approximate solution is. For instance, let us compare the results of (5.59) and (5.60), where points used closer to the origin yield a marked difference in the error. Hence, in order to obtain more accurate measures of error, we should increase the number of points used, so that we get something like (5.61), which shows that the approximate solution is reasonable. The trade off is that, by using more points, we are forced to undertake more computations, which can become increasingly demanding as the number of terms used in the approximation increases.

What these results suggest is that, in addition to the form of the original nonlinear operator, it can prove fruitful to consider the form of the initial data when selecting the type of auxiliary nonlinear operator used. Note that this issue is particular to initial value problems for PDEs. When working with ODEs, the initial data is of course constant, so such considerations do not matter. Such considerations are of course important, since by selecting a proper auxiliary linear operator, we can greatly reduce the residual error inherent in a low-order homotopy approximation. This in turn is useful, since calculating higher order terms in the homotopy expansion of PDEs becomes very complicated, particularly in the case of strongly nonlinear PDEs.

CHAPTER 6

OPTIMAL ANALYTIC METHOD FOR THE NONLINEAR HASEGAWA-MIMA EQUATION

The following results are from the paper [114].

6.1 Background

The Hasegawa-Mima equation is a second order nonlinear partial differential equation that describes the electric potential due to a drift wave in a plasma [82, 83]. The equation reads

$$(1-\triangle)_t U - [U, \triangle U] + \kappa U_y + \nu U_{yy} - \beta[U, U_y] + T[U] = 0\,, \tag{6.1}$$

where the operator $[\cdot,\cdot]$ is defined by

$$[U, V] = U_x V_y - U_y V_x\,, \tag{6.2}$$

the operator $(1-\triangle)_t$ is given by

$$(1-\triangle)_t U = U_t - U_{xxt} - U_{yyt}\,, \tag{6.3}$$

$\triangle$ is the Laplacian operator on two space variables ($\triangle U = U_{xx} + U_{yy}$), and the operator $T[U]$ equals $-\delta\triangle^3 U$ or $\delta\triangle^2 U$ depending on whether we consider the case of hyper-viscous

damping or viscous dissipation, respectively. The terms $-U_t - [U, \triangle U]$ in the Hasegawa-Mima equation, which appear in the Navier Stokes equation, are the terms introduced by adding the polarization drift. In the limit where the wavelength of a perturbation of the electric potential is much smaller than the gyroradius based on the sound speed, the Hasegawa-Mima equations become the same as the two-dimensional incompressible fluid [82, 83].

The equation can be defined over the domain $\mathcal{D} \times [0, \infty)$, where $\mathcal{D} \subset \mathbb{R}^2$. In the present paper, we shall be interested in rectangular domains. Of course, with an appropriate scaling we can then take $\mathcal{D}$ to be a square of unit area. The equation is held subject to the initial condition

$$U(x, y, 0) = \Phi(x, y) \tag{6.4}$$

and the boundary conditions

$$\begin{aligned} U(0, y, t) &= 0 = U(1, y, t)\,, \\ U(x, 0, t) &= \Psi(x) = U(x, 1, t)\,. \end{aligned} \tag{6.5}$$

Here $\Phi(x, y)$ is the sufficiently smooth initial data, and $\Psi(x)$ is a sufficiently smooth function which constitutes a periodic boundary condition. (The boundary condition is periodic in the sense that we may glue multiple copies of $\mathcal{D} = [0, 1] \times [0, 1]$ together in order to obtain a continuous solution over a larger domain.) In order to maintain consistency, we restrict ourselves to initial data Φ satisfying

$$\begin{aligned} \Phi(0, y) &= 0 = \Phi(1, y)\,, \\ \Phi(x, 0) &= \Psi(x) = \Phi(x, 1)\,. \end{aligned} \tag{6.6}$$

There are few solutions of this equations in the literature, owning to both the nonlinearity and the number of terms in the equation. In the present paper, we apply the method of homotopy analysis to the study of the Hasegawa-Mima equation. The method of homotopy analysis [14]-[22] has recently been applied to the study of a number of non-trivial and traditionally hard to solve nonlinear differential equations, for instance nonlinear equations arising in heat transfer [23]-[26], fluid mechanics [27]-[34], solitons and integrable models [35]-[39], nanofluids [40]-[41] and the Lane-Emden equation which appears in stellar astrophysics [42]-[45], to name a few areas. In applying this type of method, we obtain analytical approximations to the Hasegawa-Mima equation over a bounded domain. This is important, since obtaining analytical approximations to such equations gives us some insight into the behavior of the solutions.

Interestingly, in order to obtain accurate appoximations, we needed to generalize one aspect of the method. One important feature of the homotopy analysis method is that it allows us to control the manner of convergence and the error of obtained approximate solutions through the so-called convergence control parameter. Choosing the convergence control parameter by using it it minimize residual error, we effectively perform what is known as "optimal homotopy analysis" and this method has recently been employed to great effect on a number of nonlinear equations [48]-[50]. However, we also find that it is possible to perform this type of optimization over a family of auxiliary linear operators parameterized by a constant. This parameter may also be used to minimize residual error. The parameter has the interpretation of being the decay rate of the solutions in time.

Interestingly, we obtain a method with two free parameters, both of which can be used to minimize residual errors due to the analytical approximations. For many examples considered, the sum of squared residual errors over the domain is less than order 10^{-15}, which is very good considering that we take a small number of terms in the homotopy expansion. A small number of terms increases the efficiency of the method, since for many complicated nonlinear partial differential equations the construction of higher-order terms in the homotopy solutions is computationally demanding. We consider five distinct concrete examples in order to demonstrate the utility of the method.

Using the analytical homotopy solutions, we show that the solutions to the Hasegawa-Mima equation (6.1) are rather localized, decaying for large time values. This is physically reasonable, and suggests that initial disturbances to the electric potential described by the model gradually decay in the cases we consider. This occurs for both the hyper-viscous damping and the viscous dissipation cases.

6.2 Preliminaries and homotopy analysis for the Hasegawa-Mima equation

In applying the method of homotopy analysis, suppose we take the term with the time derivative to be our linear operator. That is, suppose $\mathcal{L}[U] = (1 - \triangle)_t U$. Then in the zeroth order deformation equation, we would be solving the homogeneous case $\mathcal{L}[U] = 0$.

Let $V = U_t$ to get $(\triangle - 1)V = 0$. Then the solution is some $V^*(x, y)$, and solving back for U we see that $U(x, y, t) = V^*(x, y)t + c(x, y)$. This diverges as $t \to \infty$, even if the desired solution is bounded. Thus, we should avoid the seemingly obvious choice of the auxiliary linear operator.

Define the linear part of the nonlinear partial differential equation (6.1) by

$$L[U] = (1 - \triangle)_t U \,. \tag{6.7}$$

Furthermore, for notational simplicity, we define the operators

$$M[U] = \kappa U_y + \nu U_{yy} \,, \tag{6.8}$$

$$N[U] = -[U, \triangle U] - \beta[U, U_y] \,, \tag{6.9}$$

so that

$$\Omega[U] = L[U] + N[U] + M[U] + T[U] \tag{6.10}$$

is the original nonlinear operator. That is to say (6.1) is then equivalent to $\Omega[U] = 0$. Note that $N[U]$ has the nonlinear contribution. In many cases, $\kappa = \nu = 0$, which means that $M[U] = 0$. This is why we separate L and M: even though both are linear, L will always remain in the equation, whereas M will be omitted in some cases.

The homotopy $\mathcal{H}$ between the Hasegawa-Mima equation and the auxiliary linear operator $\mathcal{L}$ (which in general is distince from the linear part of Ω given by L) is then

$$0 \equiv \mathcal{H} = (1 - q)\mathcal{L}[U - u_0] - qh\Omega[U] \,. \tag{6.11}$$

Here, u_0 is an initial approximation to the solution and h is the so-called convergence control parameter. For all values of $q \in [0,1]$, (6.11) defines a partial differential equation for U. When $q = 0$, we have $U = u_0$, while when $q = 1$, we recover the original nonlinear partial differential equation $\Omega[U] = 0$. As is standard, we shall assume that

$$U(x,y,t) = u_0(x,y,t) + \sum_{m=1}^{\infty} u_m(x,y,t) q^m \,, \tag{6.12}$$

Thus, we have a Taylor series representation for U in powers of q, where the coefficients are arbitrary functions which must be determined. If this expansion converges at $q = 1$, then it is a solution to $\Omega[U] = 0$, which is what we desire.

6.3 Appropriate selection of the auxiliary linear operator, $\mathcal{L}$

We first explored taking $\mathcal{L} = L$, the linear part of Ω. However, this resulted in solutions which were bad in two ways. First of all, the resulting solutions are very complicated to obtain (we had to use a Green's function approach to solve each iterate u_m in the method, which became very complicated in light of the form of the nonlinearity in Ω). Secondly, once such solutions were obtained, they were found to have very poor error properties.

To remedy this, we looked for simpler auxiliary linear operators. We attempted $\mathcal{L}[U] = U_t$, however this resulted in solutions which grew as polynomials in time. Yet, a natural (physical) solution to the equation (6.1) should be finite in time, in many instances

exhibiting decay as time increases. So, such a simple auxiliary linear operator was not very effective, either.

We next considered an operator of the form $\mathcal{L}[U] = U_t + U$, which results in solutions that exponentially decay in time. With this we were on the right track, since the solutions ought to remain bounded in time. However, the residual errors were still rather high. As it turns out, for this choice of operator, we effectively prescribe the decay rate of the solutions in advance, since by choosing $\mathcal{L}[U] = U_t + U$ we have a rule of solution expression [15] that takes base functions of the form $e^{-t}, e^{-2t}, e^{-3t}, \ldots$.

To account for the poor error in these approximations, we tried a similar type of operator, of the form $\mathcal{L} = L_\alpha$, where

$$L_\alpha[U] = U_t + \alpha U. \tag{6.13}$$

Operators similar to this have been shown to produce decently accurate results that are computationally less severe [87]. Introducing another parameter α is just another way to tailor our approximation by minimizing residual errors. Since α effects the rule of solution expression, giving base functions $e^{-\alpha t}, e^{-2\alpha t}, e^{-3\alpha t}, \ldots$, it is clear that α can be used to change the rate of decay. We then used an approach analogous to the "optimal homotopy analysis method" (where one typically selects the convergence control parameter h by minimizing the residual errors), where we used both α and h to minimize residual errors.

If we consider single-mode initial data, then we assume

$$U(x, 0, t) = U(x, 1, t) = 0, \quad U(0, y, t) = U(1, y, t) = 0, \tag{6.14}$$

and the initial condition is

$$U(x, y, 0) = f(x, y) \tag{6.15}$$

If we create a homotopy as before, we have

$$0 \equiv \mathcal{H}(U, q) = (1 - q)L_\alpha[U] - qh\Omega[U]. \tag{6.16}$$

Assuming a series expansion of $U(x, y, t)$ around q gives

$$U(x, y, t) = \sum_{j=0}^{\infty} u_j(x, y, t)q^j. \tag{6.17}$$

Expanding this in our homotopy (6.16), we have

$$(1 - q)L_\alpha \left[\sum_{j=0}^{\infty} u_j(x, y, t)q^j\right] = qh\Omega \left[\sum_{j=0}^{\infty} u_j(x, y, t)q^j\right]. \tag{6.18}$$

This can be written as

$$\sum_{j=0}^{\infty} L_\alpha[u_j(x, y, t)]q^j = \sum_{j=0}^{\infty} L_\alpha[u_j(x, y, t)]q^{j+1} + qh\Omega \left[\sum_{j=0}^{\infty} u_j(x, y, t)q^j\right]. \tag{6.19}$$

Equating powers of q on each side, the zeroth order deformation equation is

$$L_\alpha[u_0] = 0, \quad u_0(x, y, 0) = f(x, y), \tag{6.20}$$

and the mth order deformation equation is

$$L_\alpha[u_m] = L_\alpha[u_{m-1}] + \frac{h}{(m-1)!} \left(\frac{\partial^{m-1}}{\partial q^{m-1}} \Omega \left[\sum_{j=0}^{\infty} u_j q^j\right]\right) \Big|_{q=0}, \tag{6.21}$$

subject to

$$u_m(0, y, t) = u_m(1, y, t) = 0, \qquad u_m(x, 0, t) = u_m(x, 1, t) = 0, \tag{6.22}$$

and

$$u_m(x, y, 0) = 0. \tag{6.23}$$

The solution to (6.20) is

$$u_0(x, y, t; h, \alpha) = f(x, y)e^{-\alpha t}. \tag{6.24}$$

If we consider the right-hand side of (6.21) as some $g_m(x, y, t)$, then the solution of (6.21) is

$$u_m(x, y, t; h, \alpha) = e^{-\alpha t} \int_0^t e^{\alpha \xi} g_m(x, y, \xi) d\xi. \tag{6.25}$$

We have the general three-term approximation when $q = 1$ in (6.16):

$$\hat{u}(x, y, t; h, \alpha) = u_0(x, y, t; h, \alpha) + u_1(x, y, t; h, \alpha) + u_2(x, y, t; h, \alpha). \tag{6.26}$$

We will use this information below by considering different single-mode initial data and computing residual errors for their approximations (6.26).

6.4 Error analysis

The Hasegawa-Mima equation is a complicated nonlinear partial differential equation, and as such we do not have the luxury of comparing approximate solutions with exact solutions. As such, we need to have some way of analysing the error inherent in our approximations. For any fixed combination of parameters and initial / boundary conditions, we shall consider a three-term approximation

$$\hat{u}(x, y, t) = u_0(x, y, t) + u_1(x, y, t; h) + u_2(x, y, t; h)\,. \tag{6.27}$$

Placing (6.27) into Ω, we obtain the residual error at a point:

$$\text{Res}(x, y, t; h) = \Omega[\hat{u}(x, y, t; h)] \,. \tag{6.28}$$

The spatial domain is compact, so it makes sense to integrate the absolute value of the residuals over $\mathcal{D}$ in order to determine the accumulated residual error over the domain. The time domain in unbounded, hence even small residuals can result in infinite accumulated error as $t \to \infty$. So, we should count the residuals up until some terminal point $t = t_{\text{final}}$. It will be most practical to approximate the temporal integral with a sum. We then have the accumulated residual error

$$\epsilon(h) = \sum_{i=0}^{t_{\text{final}}} \int_0^1 \int_0^1 |\text{Res}(x, y, i; h)| dy dx \delta_t \,, \tag{6.29}$$

where δ_t denotes the temporal step-size. Since the integration may be too challenging to perform, we consider two alternate formulations. First, instead of performing the spatial integration, we could consider approximating the integral with sums. We have the approximate residual error

$$\hat{E}(h) = \sum_{i=0}^{t_{\text{final}}} \sum_{j=0}^{J} \sum_{k=0}^{K} |\text{Res}(k, j, i; h)| \frac{\delta_t}{(J+1)(K+1)} \,. \tag{6.30}$$

Meanwhile, we may be able to compute the integral of the squared residuals, so we define the second error, the sum of squared residual error, by

$$E(h) = \int_0^{t_{\text{final}}} \int_0^1 \int_0^1 (\text{Res}(x, y, i; h))^2 dy dx dt \,. \tag{6.31}$$

The choice of the individual method of estimating the residual error will usually be dictated by the form of the approximate solutions. Note that both measures of error depend on the

choice of h, the convergence control parameter. In order to minimize error, we should then determine the value of h^* such that

$$h^* = \text{argmin}_{h\in\mathbb{R}}\hat{E}(h) \tag{6.32}$$

or

$$h^* = \text{argmin}_{h\in\mathbb{R}}E(h)\,, \tag{6.33}$$

depending on the choice of error (6.30) or (6.31), respectively.

6.5 Analytical approximations to (6.1) for several specific cases

In this section, we finally apply our method in order to construct residual error minimizing approximations to the equation (6.1) for various values of the model parameters and boundary data. By optimally selecting both α (the decay rate of solutions) and h (the convergence control parameter), we demonstrate that the error due to the approximations is rather small for most cases.

6.5.1 The case $f(x,y) = \sin(\pi x)\sin(\pi y)$ with $\nu = \kappa = \beta = 0$, $T[U] = \triangle^2 U$

First we consider viscous dissipation by taking the nonlinear operator of the form

$$\Omega[U] = \Omega_1[U] = (1-\triangle)_t U - [U, \triangle U] + \triangle^2 U \tag{6.34}$$

under the initial condition

$$f(x,y) = \sin(\pi x)\sin(\pi y). \tag{6.35}$$

Then by (6.24)

$$u_0(x,y,t;h,\alpha) = \sin(\pi x)\sin(\pi y)e^{-\alpha t}. \tag{6.36}$$

By (6.25)

$$u_1(x,y,t;h,\alpha) = h(4\pi^4 - 2\pi^2\alpha - \alpha)\sin(\pi x)\sin(\pi y)te^{-\alpha t}, \tag{6.37}$$

and

$$u_2(x,y,t;h,\alpha) = \frac{h}{2}(4\pi^4 - 2\pi^2\alpha - \alpha)\sin(\pi x)\sin(\pi y)(2+2h+4h\pi^2+4ht\pi^4-2h\pi^2\alpha t-h\alpha t)te^{-\alpha t}. \tag{6.38}$$

Then using the three-term approximation $\hat{u}(x,y,t;h,\alpha)$ we compute the squared residual error

$$E(h,\alpha) = \int_0^\infty \int_0^1 \int_0^1 \Omega_1[\hat{u}(x,y,t;h,\alpha)]^2 dxdydt. \tag{6.39}$$

This function has minimum 2.0379×10^{-17} at $h = -4.8238 \times 10^{-2}$, $\alpha = 18.7875$. The plot of $E(h,\alpha)$ is given in Figure 6.1. The plot of $\hat{u}(x,y,t;-4.8238,18.7875)$ for four different values of t is given in Figure 6.2.

We see that the accumulated residual error over the domain is actually very small, even though we consider an infinite time domain. This suggests that the method of optimally selecting both the convergence control parameter, h, and the decay rate parameter, α, is highly useful. Note that the value of h is rather small. This indicates that relatively small

corrections are needed to the initial approximation u_0, since the higher-order terms all depend on powers of h.

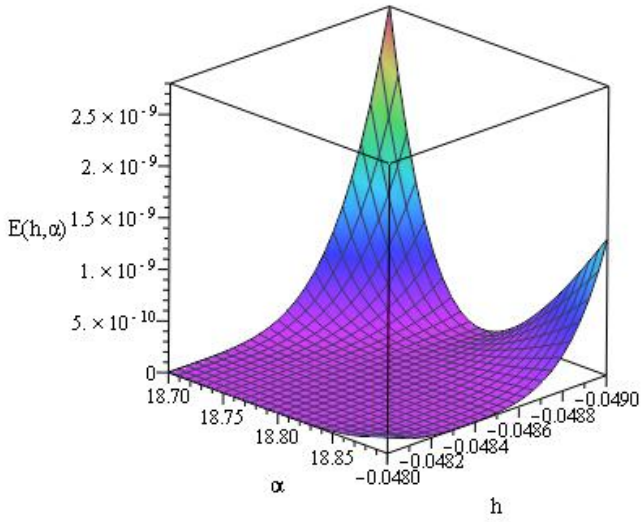

Figure 6.1: Plot of $E(h, \alpha)$, the squared residual error as a function of h and α, the convergence control parameter and the exponential coefficient. The error function has minimum $E(h, \alpha) = 2.0379 \times 10^{-17}$ obtained at $h = -4.8238 \times 10^{-2}, \alpha = 18.7875$.

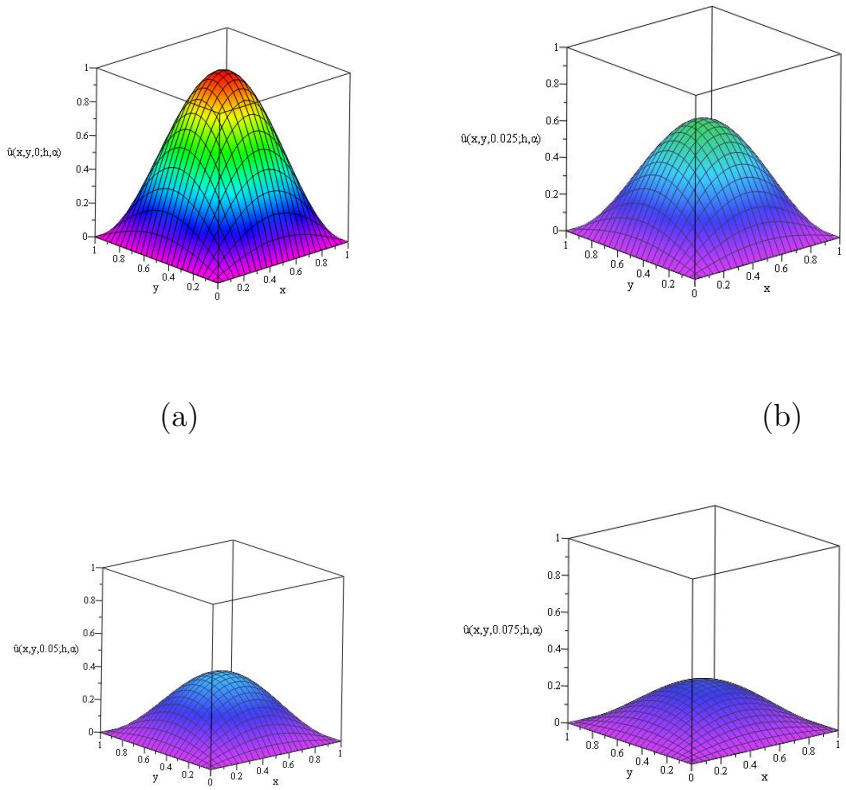

(a) (b)

(c) (d)

Figure 6.2: Plot of the approximate solution $\hat{u}(x, y, t, h, \alpha)$, the three-term approximation to $\Omega_1[u] = 0$ with initial condition $f(x, y) = \sin(\pi x)\sin(\pi y)$. The minimizing values of $h = -4.8238 \times 10^{-2}$ and $\alpha = 18.7875$ have been plugged in. We have taken the solution at various times: (a) $t = 0$, (b) $t = 0.025$, (c) $t = 0.05$, (d) $t = 0.075$.

6.5.2 The case $f(x,y) = \sin(\pi x)\sin(\pi y)$ with $\nu = \kappa = \beta = 0$, $T[U] = -\triangle^3 U$

Suppose we consider the case of hyper-viscous damping, where

$$\Omega[U] = \Omega_2[U] = (1 - \triangle)_t U - [U, \triangle U] - \triangle^3 U \tag{6.40}$$

subject to the same initial condition (6.35). The zeroth order term, according to (6.24), is

$$u_0(x, y, t; h, \alpha) = \sin(\pi x)\sin(\pi y)e^{-\alpha t}. \tag{6.41}$$

The first-order term is

$$u_1(x, y, t; h, \alpha) = h(8\pi^6 - 2\pi^2\alpha - \alpha)\sin(\pi x)\sin(\pi y)te^{-\alpha t}, \tag{6.42}$$

and the second-order term is

$$u_2(x, y, t; h, \alpha) = \frac{h}{2}(4h\pi^2+2+2h+8h\pi^6 t-\alpha ht-2\alpha h\pi^2 t)(8\pi^6-2\pi^2\alpha-\alpha)\sin(\pi x)\sin(\pi y)te^{-\alpha t}. \tag{6.43}$$

With the sum of these three terms $\hat{u}(x, y, t; h, \alpha)$ we have the squared residual error

$$E(h, \alpha) = \int_0^\infty \int_0^1 \int_0^1 \Omega_2[\hat{u}(x, y, t; h, \alpha)]^2 dxdydt. \tag{6.44}$$

The minimum of this function is 4.88×10^{-18} and occurs at $h = -4.821 \times 10^{-2}, \alpha = 370.85$. The plot of $E(h, \alpha)$ is given in Figure 6.3. The plot of $\hat{u}(x, y, t; -4.821 \times 10^{-2}, 370.85)$ for four different values of t is given in Figure 6.4.

Again, the method is very effective. Note that in the case of hyper-viscous damping, the decay rate is much larger, so the solutions should decay much faster. This behavior is seen when one compares the solution for the hyper-viscous damping (Figure 4) with that of the previous case (viscous dissipation, as shown in Figure 6.2).

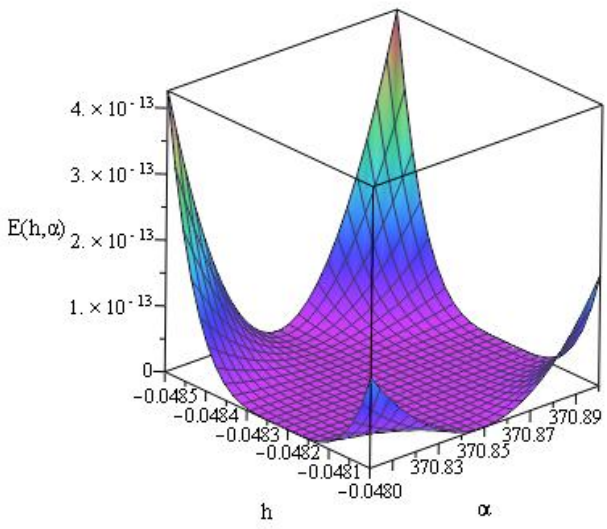

Figure 6.3: Plot of $E(h, \alpha)$, the squared residual error as a function of h and α, the convergence control parameter and the exponential coefficient. The error function has minimum $E(h, \alpha) = 4.88 \times 10^{-18}$ obtained at $h = -4.821 \times 10^{-2}, \alpha = 370.85$.

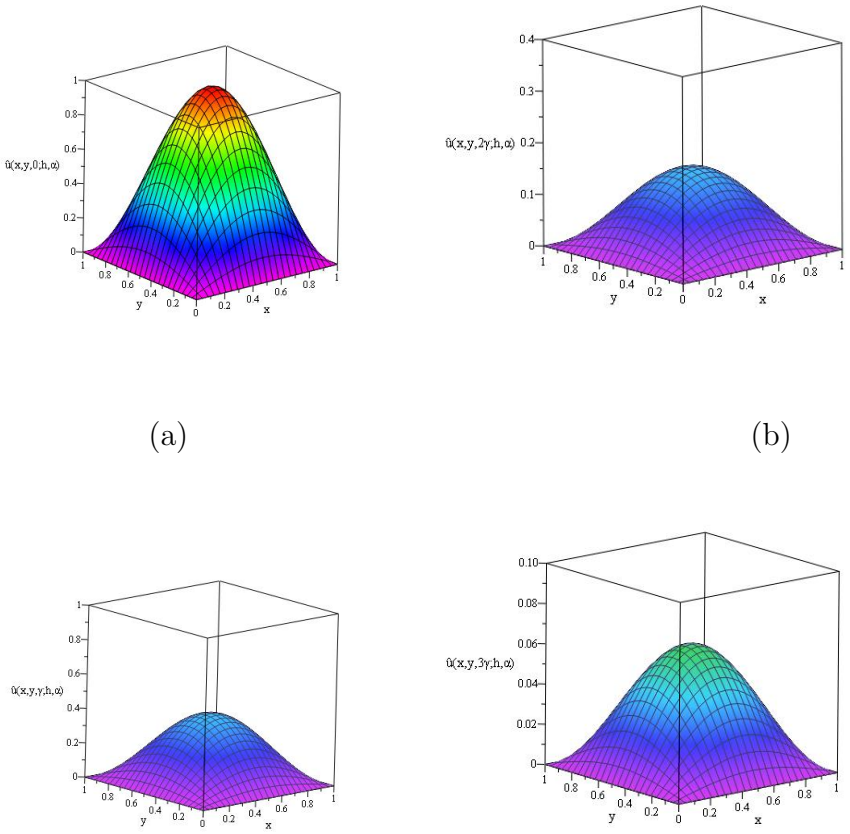

(a) (b)

(c) (d)

Figure 6.4: Plot of the approximate solution $\hat{u}(x, y, t, h, \alpha)$, the three-term approximation to $\Omega_2[u] = 0$ with initial condition $f(x, y) = \sin(\pi x)\sin(\pi y)$. The minimizing values of $h = -4.821 \times 10^{-2}$ and $\alpha = 370.85$ have been plugged in. We have taken the solution at various times: (a) $t = 0$, (b) $t = 0.0025$, (c) $t = 0.005$, (d) $t = 0.0075$. In the figure labels, $\gamma = 0.0025$ is a scaling factor.

6.5.3 The case $f(x,y) = \sin(2\pi x)\sin(2\pi y)$ with $\nu = \kappa = \beta = 0$, $T[U] = \triangle^2 U$

Suppose we consider viscous dissipation ($\Omega = \Omega_1[U]$) with the initial condition

$$f(x,y) = \sin(2\pi x)\sin(2\pi y). \tag{6.45}$$

Such a solution then consists of four extreme points, as opposed to one (as was the case in the previous initial conditions). The zeroth order term (6.24) is

$$u_0(x,y,t;h,\alpha) = \sin(2\pi x)\sin(2\pi y)e^{-\alpha t}. \tag{6.46}$$

The first order term, according to (6.25), is

$$u_1(x,y,t;h,\alpha) = h(64\pi^4 8\pi^2\alpha - \alpha)\sin(2\pi x)\sin(2\pi y)te^{-\alpha t}, \tag{6.47}$$

and the second order term is

$$\begin{aligned} u_2(x,y,t;h,\alpha) = \frac{h}{2}&(16h\pi^2 + 2h + 2 - 8\alpha h\pi^2 t - \alpha ht + 64h\pi^4 t)(64\pi^4 8\pi^2\alpha \\ &- \alpha)\sin(2\pi x)\sin(2\pi y)te^{-\alpha t}. \end{aligned} \tag{6.48}$$

With the sum of these three terms $\hat{u}(x,y,t;h,\alpha)$, we can take the squared residual error

$$E(h,\alpha) = \int_0^\infty \int_0^1 \int_0^1 \Omega_1[\hat{u}(x,y,t;h,\alpha)]^2 dxdydt. \tag{6.49}$$

The function $E(h,\alpha)$ has minimum 4.753×10^{-16} at $h = 1.125 \times 10^{-2}, \alpha = 77.97$. The plot of $E(h,\alpha)$ is given in Figure 6.5. The plot of $\hat{u}(x,y,t;1.125 \times 10^{-2}, 77.97)$ is given in Figure 6.6.

Even with the marginally more complicated initial condition, the method is still very accurate. Interestingly, the decay rate for the initial condition with four extreme points is

much greater than that which we found for the case where the initial condition with only one extreme point.

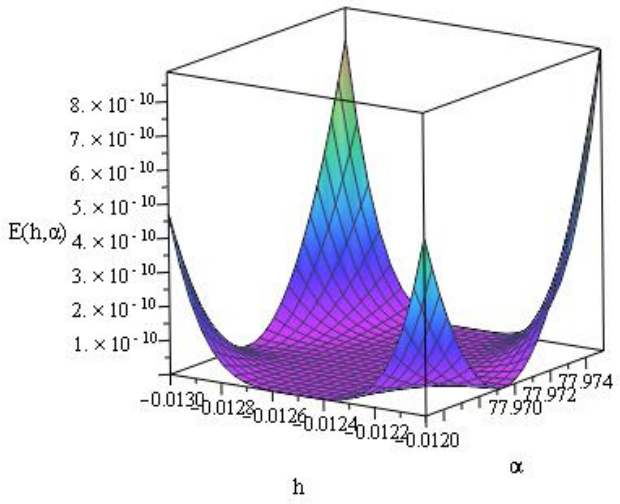

Figure 6.5: Plot of $E(h, \alpha)$, the squared residual error as a function of h and α, the convergence control parameter and the exponential coefficient. The error function has minimum $E(h, \alpha) = 4.753 \times 10^{-16}$ obtained at $h = 1.125 \times 10^{-2}, \alpha = 77.97$.

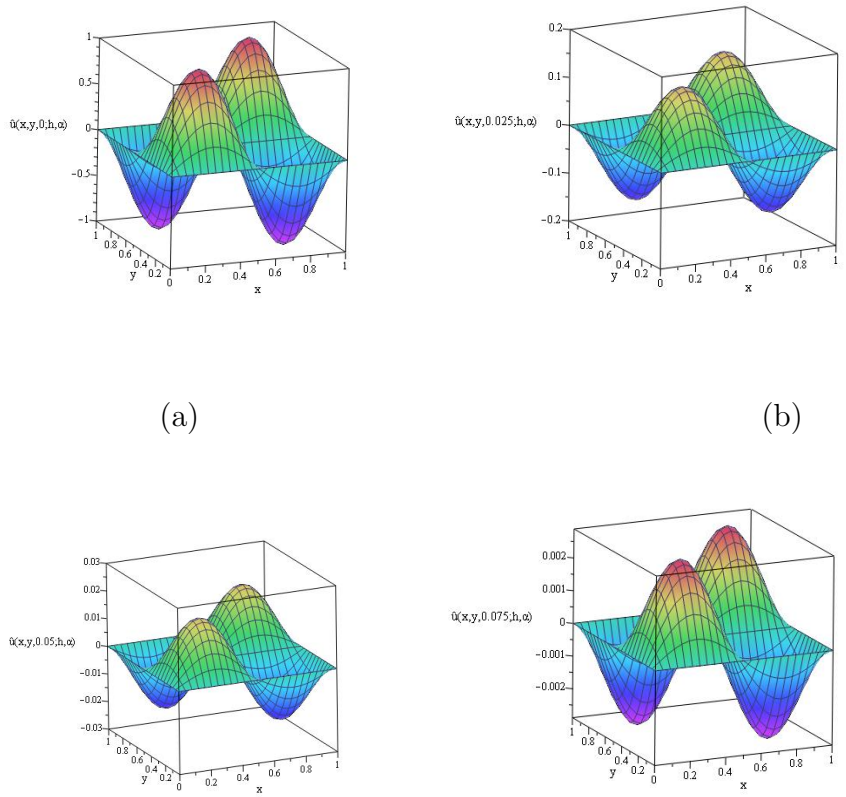

(a) (b)

(c) (d)

Figure 6.6: Plot of the approximate solution $\hat{u}(x, y, t, h, \alpha)$, the three-term approximation to $\Omega_1[u] = 0$ with initial condition $f(x, y) = \sin(2\pi x)\sin(2\pi y)$. The minimizing values of $h = 1.125 \times 10^{-2}$ and $\alpha = 77.97$ have been plugged in. We have taken the solution at various times: (a) $t = 0$, (b) $t = 0.025$, (c) $t = 0.05$, (d) $t = 0.075$.

6.5.4 The case $f(x,y) = \sin(\pi x)\sin(2\pi y)$ with $\nu = \kappa = \beta = 0$, $T[U] = \triangle^2 U$

Now consider the case of viscous dissipation when the period in x is double the period in y. Let us take $\Omega[U] = \Omega_1[U]$ with initial condition

$$f(x,y) = \sin(\pi x)\sin(2\pi y). \tag{6.50}$$

Then the first two terms are

$$u_0(x,y,t;h,\alpha) = \sin(\pi x)\sin(2\pi y)e^{-\alpha t}, \tag{6.51}$$

$$u_1(x,y,t;h,\alpha) = h(25\pi^4 - 5\pi^2\alpha - \alpha)\sin(\pi x)\sin(2\pi y)e^{-\alpha t}, \tag{6.52}$$

and $u_2(x,y,t;h,\alpha)$ is given similarly. With $\hat{u}(x,y,t;h,\alpha)$ being the sum of the first three terms of our approximation, the squared residual error is

$$E(h,\alpha) = \int_0^\infty \int_0^1 \int_0^1 \Omega_1[\hat{u}(x,y,t;h,\alpha)]^2 dxdydt. \tag{6.53}$$

The minimum of $E(h,\alpha)$ is 1.4029×10^{-17}, occurring at $h = 1.985 \times 10^{-2}, \alpha = 48.368$. The plot of $E(h,\alpha)$ is given in Figure 6.7, and the plots of the approximation for four values of t are Figure 6.8.

Again, the method performs very well. It appears as though the decay rate increases proportionally tot he complexity of the initial condition. The condition used here has two extreme points, and the decay rate is faster than that of the case where the initial condition had one extreme point, yet slower than the cases where the initial condition had four extreme points. This suggests that the more complicated the initial condition, the less stable the

solutions are, with more complicated initial conditions decaying much more rapidly to zero as time increases.

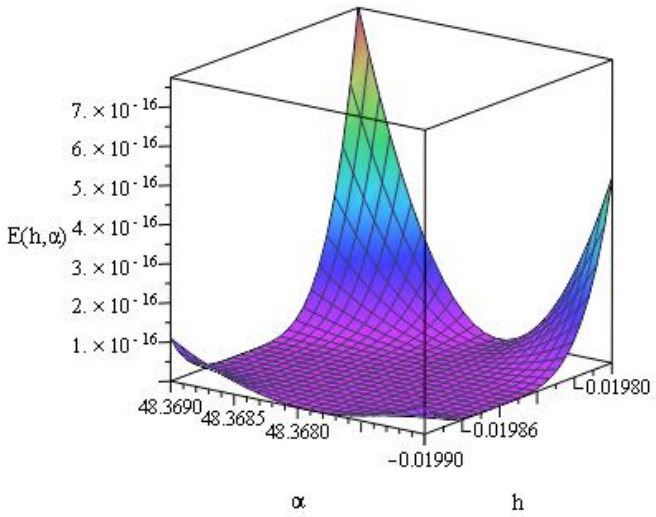

Figure 6.7: Plot of $E(h, \alpha)$, the squared residual error as a function of h and α, the convergence control parameter and the exponential coefficient. The error function has minimum $E(h, \alpha) = 1.4029 \times 10^{-17}$ obtained at $h = 1.985 \times 10^{-2}, \alpha = 48.368$.

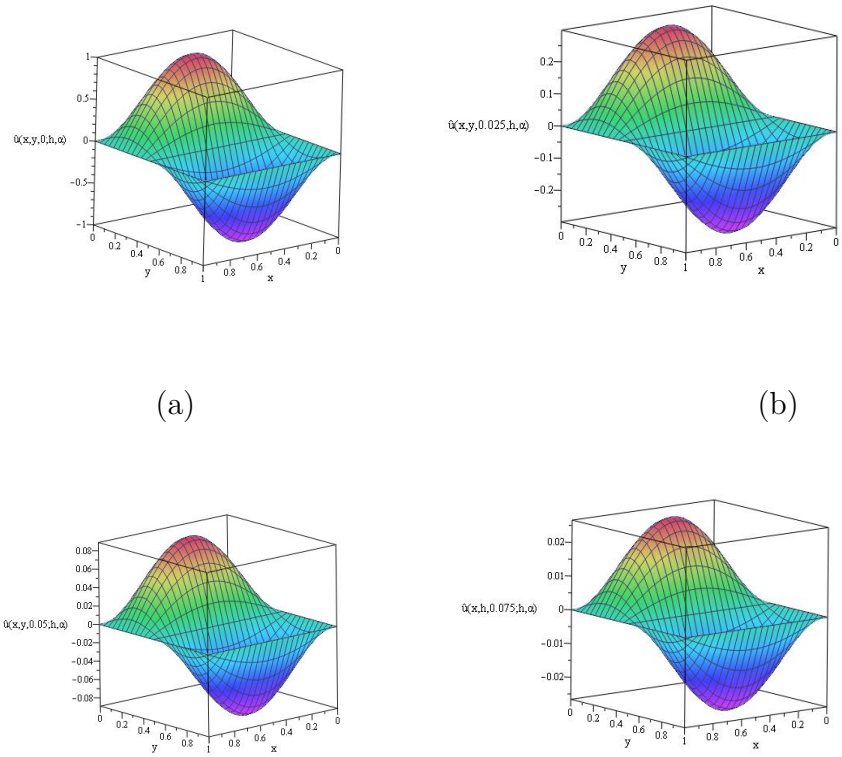

(a) (b)

(c) (d)

Figure 6.8: Plot of the approximate solution $\hat{u}(x, y, t, h, \alpha)$, the three-term approximation to $\Omega_1[u] = 0$ with initial condition $f(x, y) = \sin(\pi x)\sin(2\pi y)$. The minimizing values of $h = 1.985 \times 10^{-2}$ and $\alpha = 48.368$ have been plugged in. We have taken the solution at various times: (a) $t = 0$, (b) $t = 0.025$, (c) $t = 0.05$, (d) $t = 0.075$.

6.5.5 The case $f(x,y) = \sin(\pi x)\sin(\pi y)$ $\nu = \kappa = \beta = 1$, $T[U] = \triangle^2 U$

Finally, we consider the case where the model is as nonlinear as possible ($\nu = \kappa = \beta = 1$) with viscous dissipation so that

$$\Omega[U] = \Omega_3[U] = (1 - \triangle)_t U - [U, \triangle U] + U_y + U_{yy} - [U, U_y] + \triangle^2 U. \tag{6.54}$$

We take the initial condition given in (6.35). If we take the first three terms of the approximation, call their sum $\hat{u}(x, y, t; h, \alpha)$. The residual error is given by $\Omega_3[\hat{u}(x, y, t; h, \alpha)]$. Squaring this and integrating is challenging, so instead we will evaluate the absolute value of this function at 125 points in its domain. Consider the sum of absolute residual error

$$\hat{E}(h, \alpha) = \frac{1}{125} \sum_{p=0}^{4} \sum_{k=0}^{4} \sum_{j=0}^{4} \left| \Omega_3 \left[\hat{u} \left(\frac{j}{4}, \frac{k}{4}, p; h, \alpha \right) \right] \right|. \tag{6.55}$$

We obtain a minimum of 4.08359×10^{-2} at $h = -2.8 \times 10^{-2}$ and $\alpha = 18.3115$. The plot of $\hat{E}(h, \alpha)$ is given in Figure 6.9, and the plots of the approximation for four values of t is given in Figures 6.10.

Note that the error in this case is still relatively small (it is residual error, not absolute error), and is good up to plotting accuracy. For more accuracy, one would want to use more terms. We keep three terms so that the error in this case may be compared to error in the previous cases. We see that, due to added nonlinear effects, the rate of convergence of the homotopy solutions is slower. If one does not wish to compute more terms, then one would likely need to look fro a different auxiliary linear operator $\mathcal{L}$. It is possible that for such solutions, the manner to time evolution is not a general exponential decay. A different

class of auxiliary linear operators which promote such time evolution would then have to be found, which is not always easy.

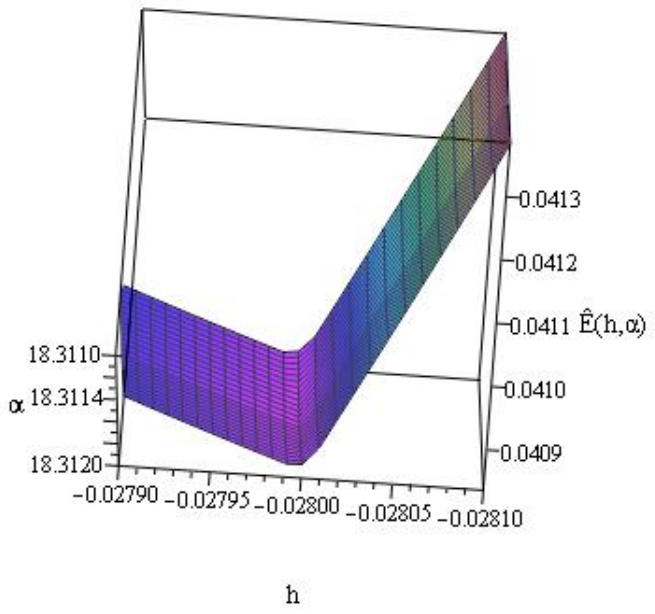

Figure 6.9: Plot of $\hat{E}(h, \alpha)$, the absolute residual error over 125 points as a function of h and α, the convergence control parameter and the exponential coefficient. The error function has minimum $\hat{E}(h, \alpha) = 4.08359 \times 10^{-2}$ where $h = -2.8 \times 10^{-2}$ and $\alpha = 18.3115$.

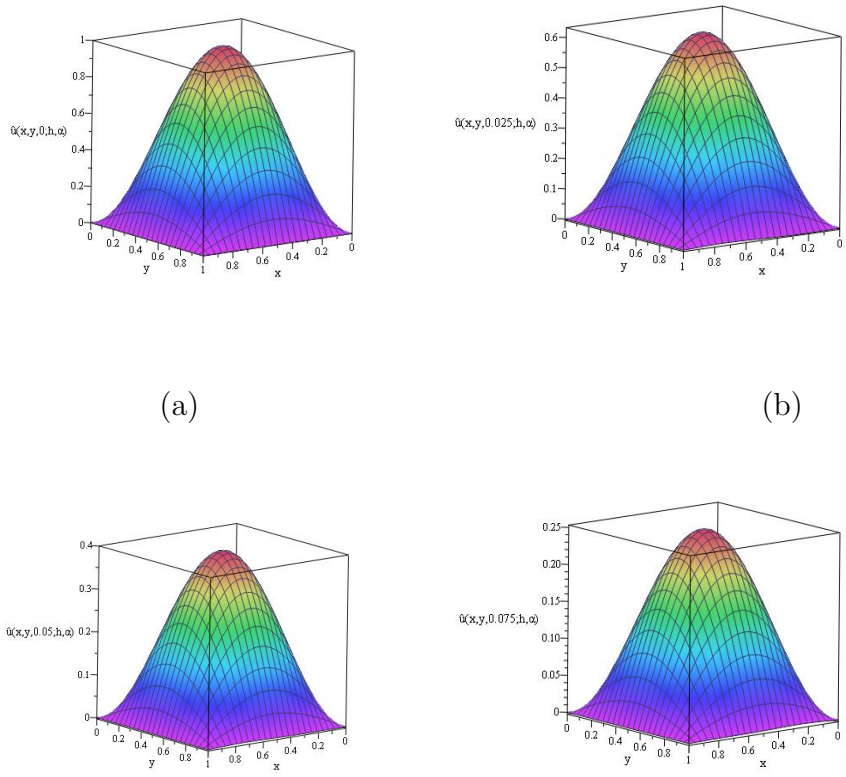

(a) (b)

(c) (d)

Figure 6.10: Plot of the approximate solution $\hat{u}(x, y, t, h, \alpha)$, the three-term approximation to $\Omega_3[u] = 0$ with initial condition $f(x, y) = \sin(\pi x)\sin(\pi y)$. The minimizing values of $h = -2.8 \times 10^{-2}$ and $\alpha = 18.3115$ have been plugged in. We have taken the solution at various times: (a) $t = 0$, (b) $t = 0.025$, (c) $t = 0.05$, (d) $t = 0.075$.

6.6 Discussion

The purpose of this article is to apply the homotopy analysis method to obtain analytical approximation to the Hasegawa-Mima equation (6.1). When using the homotopy analysis method to solve a differential equation, one conjecture about an auxiliary linear operator to use is the one that most resembles the linear portion of said differential equation. However, trying to manufacture convergence of the approximation and being able to calculate integrals or sums of evaluations at several points can lead to lengthy (nearly impossible) computations. A new idea that has surfaced [87] is to use simpler linear operators, but introduce another parameter to the problem in order to control error. This makes the terms of the approximations more manageable, which further reduces the complications in the residual error.

Yet with the Hasegawa-Mima equation, taking even the simple operator $L_\alpha[U] = U_t + \alpha U$ in the method can yield approximations with many terms. The case with initial data $f(x, y) = \sin(\pi x)\sin(\pi y)$ yields very nice results as long as the constants α, β, κ, and δ are small. However, as soon as we allow the extra terms in the computations, we are forced to result to sums to get a look at the residual error. The closer we got to using the original $\Omega[U]$ given in (6.10), the more complicated the terms in our approximation get. Moreover, taking a sum of two terms like $f(x, y) = \sin(\pi x)\sin(\pi y) + \sin(2\pi x)\sin(\pi y)$ in the initial condition leads to much longer computations.

This is not to say that the operator $L[U] = U_t + \alpha U$ worked well in all cases, either. Considering initial $f(x, y) = \sin(2\pi x)\sin(3\pi y)$ gave undesirable error. Using the initial condition $f(x, y) = x(1 - x)y(1 - y)$ we found the squared residual error by integrating and obtained 0.29, which is rather high. The conclusion, then, is that when applicable, the operator $\mathcal{L} = L_\alpha = U_t + \alpha U$ gives very good residual error (less than 10^{-15}), while in other cases it is not so useful.

In a way, this makes sense. We mentioned in Section 3 that due to the rule of solution expression, α is essentially a decay rate of the solutions. So, for cases where this operator is useful, the parameter α actually does realistically act in such a way. Clearly, this is useful when the manner of decay is exponential in nature, like $e^{-\alpha t}$. On the other hand, when the manner of decay is not exponential, $\mathcal{L} = L_\alpha = U_t + \alpha U$ should not give solutions which converge quickly. For such cases, perhaps solutions decay in another manner, perhaps like $e^{-\alpha t^2}$. For such cases, more complicated techniques may be required; see [49].

In terms of the physics of the model (6.1), we find that the analytical approximations decay in time, as shown in Figures 2, 4, 6, 8, and 10. This tells us that the solutions we obtain for the Hasegawa-Mima equation (6.1) are highly locallized in time. The solutions decay rapidly, but note that here time is non-dimensional. Generally, the solutions maintain much of the shape of the initial profile, yet decay as they evolve in time. In other words, for the solutions considered here, the initial structure of a perturbation to the electric potential due to a drift wave is maintained even though the perturbation collapses in time.

We should note that there are other methods to determine the best value of the convergence control parameter, h. Turkyilmazoglu [88] uses new method to give an upper bound on the error of a homotopy series solution (see equation (5.13) in [88]). Similarly, given a homotopy solution

$$U(x,y,t;h) = U_0(x,y,t) + U_1(x,y,t;h) + \cdots U_k(x,y,t;h) + U_{k+1}(x,y,t;h) + \cdots ,$$

if one can show that there exists $0 < r < 1$ with $|U_{k+1}(x,y,t;h)| < r|U_k(x,y,t;h)|$ for all (x,y,t) in the domain and sufficiently large k (given a restricted range of h) for an appropriate norm $|u| = \int_{(x,y,t)\in \text{Domain}} |u| dxdydt$, then then quantity

$$\beta_k(h) = \frac{|U_{k+1}(x,y,t;h)|}{|U_k(x,y,t;h)|}$$

should be bounded above by r. The quantity $\beta_k(h)$ determines the rate of geometric convergence of the homotopy series. One can then pick h so as to minimize the function $\beta_k(h)$ (given that k is fixed). Not that this value of h will not, in general, correspond to the error-minimizing value h^* [46]. However, for some examples, the values can be close. For several examples of ODEs and some PDEs for which the method of minimizing $\beta_k(h)$ was used in order to find h, see [46].

For very complicated PDEs, like the Hasegawa-Mima equation, computing very many terms in the homotopy expansion becomes too computationally demanding, so the method of minimizing $\beta_k(h)$ in [46] is not particularly efficient. Additionally, it is not a simple matter to show that $|U_{k+1}(x,y,t;h)| < |U_k(x,y,t;h)|$; actually, it is not in general true for PDEs. Furthermore, since from the error plots we see that the residual errors are rather

sensitive to the specific choice of h, the approximation from instead minimizing $\beta_k(h)$ may result in larger residual errors. That said, while the method is not suited for the present problem, it is likely to work well for a number of other problems, namely those for which many terms in the homotopy series can be computed, and cases for which one can show $|U_{k+1}(x, y, t; h)| < |U_k(x, y, t; h)|$ for all (x, y, t). Therefore, the method presents a rather promising possible direction in terms of future work. Several studies have considered this manner of convergence of homotopy solutions [89, 90, 91].

CHAPTER 7

OPTIMAL SELECTION OF THE AUXILIARY LINEAR OPERATOR IN THE HOMOTOPY ANALYSIS OF THE HUNTER-SAXTON BOUNDARY VALUE PROBLEM

The following chapter is original research.

7.1 Background

The orientation of molecules in liquid crystals is described by a field of unit vectors $\mathbf{n}(x,t) \in S^2$. If this field is nematic, it means the crystals are invariant under an inversion: $\mathbf{n} \to -\mathbf{n}$. In this case, $\mathbf{n}$ is called a director field [92]. The Hunter-Saxton equation

$$(u_t + uu_x)_x = \frac{1}{2}u_x^2, \tag{7.1}$$

or

$$u_{xt} + uu_{xx} + \frac{1}{2}u_x^2 = 0, \tag{7.2}$$

is a nonlinear wave equation that is used to study a nonlinear instability in the director field of a nematic liquid crystal [92]. The equation is the asymptotic model of waves moving in

one direction that satisfy the variational principle

$$\delta \int_{t_1}^{t_2} \int_{-\infty}^{\infty} \left\{ \psi_t^2 - c^2(\psi)\psi_x^2 \right\} dxdt = 0, \tag{7.3}$$

where c is the wave speed. The Euler-Lagrange equation derived from (7.3) is

$$\psi_{tt} = c(\psi) \left\{ c(\psi)\psi_x \right\}_x . \tag{7.4}$$

If there is a perturbation in ψ about some constant $\psi = \psi_0$ and x is a space variable corresponding to a reference frame that moves with the linear velocity, then the Euler-Lagrange equation for the variational principle

$$\delta \int_{t_1}^{t_2} \int_{-\infty}^{\infty} \left(u_t u_x + u u_x^2 \right) dxdt = 0$$

is simply (7.1).

The Hunter-Saxton equation was shown to have solutions that break down in finite time, but are, however, smooth [92]. The initial value problem

$$u(x, 0) = f(x) \tag{7.5}$$

with boundary condition

$$\lim_{x \to \infty} u(x, t) = 0 \tag{7.6}$$

is considered physically relevant in [92]. In [93], the inverse scattering solutions to the Hunter-Saxton equation are studied. The Hunter-Saxton equation models the geodesic flow on a spherical manifold, and the properties of this manifold are studied in [94].

In the present paper, we consider the method of homotopy analysis to provide analytic approximations to the solution to (7.1) with various initial data, including some considered

in the literature. This is an improvement since presently only numerical solutions exist in the literature. The method of homotopy analysis [14]-[22] has been applied to the study of a number of non-trivial and traditionally hard to solve nonlinear differential equations, with applications arising in heat transfer [23]-[26], fluid mechanics [27]-[34], solitons and integrable models [35]-[39], nanofluids [40]-[41] and the Lane-Emden equation which appears in stellar astrophysics [42]-[45].

Using the homotopy analysis method, we shall be able to do two things to find the "best" approximation at a fixed order. First, we shall use the so-called optimal homotopy analysis method, where one chooses the convergence control parameter in order to minimize residual errors [48]-[50]. We shall dive a detailed error analysis in order to demonstrate this approach. Secondly, we shall optimally select the auxiliary linear operator from a family of operators indexed by a free parameter. By selecting both the free parameter and the convergence control parameter, we shall be able to obtain accurate approximate solutions after very few iterations of the method.

7.2 Optimal auxiliary operator selection

First we consider the nonlinear operator

$$N[u] = u_{xt} + uu_{xx} + \frac{1}{2}u_x^2. \tag{7.7}$$

We can write the homotopy as

$$0 \equiv \mathcal{H}(u, q) = (1 - q)L[u] - qhN[u]. \tag{7.8}$$

Here $q \in [0, 1]$ is the homotopy parameter, h is the convergence control parameter, and L is some linear operator that can be chosen. Note that when $q = 0$ in (7.8) we have $L[u] = 0$, and when $q = 1$ we have $N[u] = 0$, which is (7.2). The homotopy is continuously deforming the linear operator L into the nonlinear operator N as q moves from 0 to 1. We assume an expansion of $u(x, t)$ around q:

$$u(x, t) = \sum_{j=0}^{\infty} u_j(x, t)q^j. \tag{7.9}$$

We use our expansion (7.9) in (7.8) and we have

$$(1 - q)\sum_{j=0}^{\infty} L[u_j]q^j = qhN\left[\sum_{j=0}^{\infty} u_j q^j\right]. \tag{7.10}$$

The nonlinear operator we will choose to use is the ODE operator

$$L[u] = u_t + \alpha u. \tag{7.11}$$

This operator has shown to provide not only ease in finding solutions to the corresponding linear equations, but also with decent accuracy when $\alpha = 1$ [87]. In this paper, what we will do is use α as an extra parameter to decrease residual error, resulting in a higher accuracy of our analytical approximation.

Using our auxiliary linear operator (7.11) in the homotopy (7.10), we equate powers of q on both sides of the equation. This turns the nonlinear problem (7.1) into infinitely

many linear problems. Then, up to $O(q^2)$, we have the so-called deformation equations

$$L[u_0] = 0, \qquad u_0(x,0) = f(x), \tag{7.12}$$

$$L[u_1] = h\left\{u_{0xt} + u_0 u_{0xx} + \frac{1}{2}u_{0x}^2\right\}, \quad u_1(x,0) = 0, \tag{7.13}$$

and

$$L[u_2] = L[u_1] + h\left\{u_{1xt} + u_1 u_{0xx} + u_{0x}u_{1x} + u_0 u_{1xx}\right\}, \quad u_2(x,0) = 0. \tag{7.14}$$

Note that each new equation in u_j is a linear problem in the functions $u_0, ..., u_{j-1}$ that came before it. So these equations can be solved sequentially until a desired number of terms are found, or it is too computationally difficult to manage.

The solution to the zeroth order deformation equation (7.12) is

$$u_0(x,t;\alpha) = f(x)e^{-\alpha t}. \tag{7.15}$$

The solution of higher-order deformation equations

$$u_{nt} + \alpha u_n = g_n(x,t), \quad u_n(x,0) = 0, \tag{7.16}$$

is

$$u_n(x,t) = e^{-\alpha t}\int_0^t e^{\alpha y} g_n(x,y)dy. \tag{7.17}$$

If we write the first term out, we obtain

$$u_1(x,t;h,\alpha) = A(x,h,\alpha)e^{-2\alpha t} + B(x,h,\alpha)te^{-\alpha t} - A(x,h,\alpha)e^{-\alpha t}, \tag{7.18}$$

where

$$\begin{aligned} A(x,h,\alpha) &= -\frac{h}{\alpha}\left(f(x)\cdot f''(x) + \frac{1}{2}f'(x)^2\right) \\ B(x,h,\alpha) &= -h\alpha f'(x). \end{aligned} \tag{7.19}$$

For the second-order term, we have

$$\begin{aligned} u_2(x,t;h,\alpha) &= E(x,h,\alpha)e^{-3\alpha t} + F(x,h,\alpha)te^{-2\alpha t} + G(x,h,\alpha)e^{-2\alpha t} \\ &\quad + H(x,h,\alpha)t^2e^{-\alpha t} + I(x,h,\alpha)te^{-\alpha t} + J(x,h,\alpha)e^{-\alpha t}, \end{aligned} \tag{7.20}$$

where

$$\begin{aligned} E(x,h,\alpha) &= \frac{h^2}{\alpha^2}\left(\frac{1}{2}f^2f^{(4)} + 2f'''f'f + \frac{3}{2}f''^2f + \frac{5}{4}f''f'^2\right), \\ F(x,h,\alpha) &= h^2f\cdot f''' + 2h^2f''f', \\ G(x,h,\alpha) &= -\frac{h}{2\alpha}f'^2 - \frac{2h^2}{\alpha}f''f' - \frac{h^2}{\alpha^2}f^2f^{(4)} - \frac{5h^2}{2\alpha^2}f''f'^2 - \frac{h^2}{\alpha}f'''f \\ &\quad - \frac{3h^2}{\alpha^2}f''^2f - \frac{4h^2}{\alpha^2}f'''f' - \frac{h}{\alpha}f''f, \\ H(x,h,\alpha) &= \frac{h^2\alpha^2}{2}f'', \\ I(x,h,\alpha) &= -2h^2f''f' - h^2f'''f - h\alpha f' - h^2\alpha f'', \\ J(x,h,\alpha) &= \frac{h}{2\alpha}f'^2 + \frac{h}{\alpha}f''f + \frac{h^2}{\alpha}f'''f + \frac{h^2}{2\alpha^2}f^2f^{(4)} + \frac{3h^2}{2\alpha^2}f''^2f \\ &\quad \frac{5h^2}{4\alpha^2}f''f'^2 + \frac{2h^2}{\alpha^2}f'''f'f + \frac{2h^2}{\alpha}f''f'. \end{aligned} \tag{7.21}$$

We have the general three-term approximation when $q = 1$ in (7.9):

$$\hat{u}(x,t;h,\alpha) = u_0(x,t;\alpha) + u_1(x,t;h,\alpha) + u_2(x,t;h,\alpha). \tag{7.22}$$

7.2.1 Note on error analysis - optimal selection of the convergence control parameter

Using the initial condition

$$u(x,0) = f(x) \tag{7.23}$$

we can find the first three terms of our expansion (7.9) when $q = 1$. So we call it

$$\hat{u}(x,t;h) = u_0(x,t) + u_1(x,t) + u_2(x,t). \tag{7.24}$$

To get a sense of how good this approximation is, we need to calculate some function of error. We do not have the exact solution to compare to. One way of obtaining error is calculating the residual error $N[\hat{u}(x,t;h)]$. If we get a residual error of 0 for all x and t, then the solution is exact. To see how close to zero the residual error is we can take a sum of values of the residual error at different values of x and t. We take the absolute value of each of the evaluations, or square the residual error depending on the ease of calculation. So we will have sums of the form

$$E(h) = \frac{1}{mn}\sum_{k=0}^{m}\sum_{j=0}^{n}(N[\hat{u}(j,k;h)])^2, \quad \hat{E}(h) = \frac{1}{mn}\sum_{k=0}^{m}\sum_{j=0}^{n}|N[\hat{u}(j,k;h)]| \tag{7.25}$$

We have divided the sum by the number of points to weight each point evenly. Note that (7.25) is a function of h. In fact, it is a sum of nonnegative polynomials in h. Since the function (7.25) is positive, it will necessarily have a global minimum at some h^*. We then have our approximation $\hat{u}(x,t;h^*)$.

7.2.2 Hyperbolic Tangent

In [92], one initial condition studied is

$$u(x,0) = f(x) = 1 - \tanh\left(10x - \frac{20}{3}\right) \tag{7.26}$$

We can take the three-term approximation (7.22) and call it $\hat{u}(x,t;h,\alpha)$. To test the residual error, we define the function

$$\hat{E}(h,\alpha) = \frac{1}{25}\sum_{k=0}^{4}\sum_{j=0}^{4}\left|N\left[\hat{u}\left(\frac{j}{4},k;h,\alpha\right)\right]\right|. \tag{7.27}$$

Now we have a function of two variables, which we can minimize. Graphing $\hat{E}(h,\alpha)$ as in Figure 7.1, we have a minimum of 0.015 reached at $h = 0.037484, \alpha = 30.5655$. The resulting three-term approximation $\hat{u}(x,t;h,\alpha)$ is graphed in Figure 7.2.

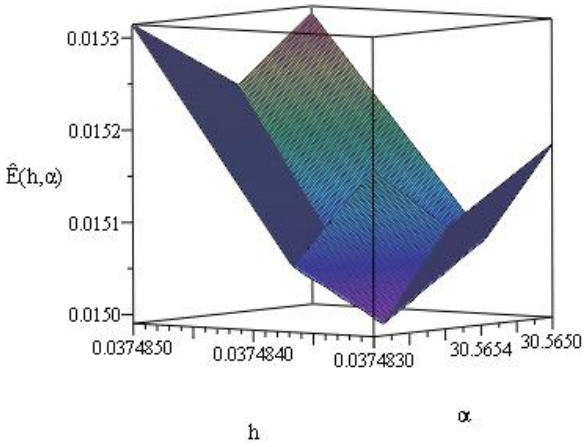

Figure 7.1: Plot of $\hat{E}(h, \alpha)$, the sum of absolute residual error over 25 points in the square $x \in [0, 1]$, $t \in [0, 4]$ as a function of h and α, the convergence control parameter and the exponential coefficient. The error function has minimum $\hat{E}(h, \alpha) = 0.015$ where $h = 0.037484, \alpha = 30.5655$.

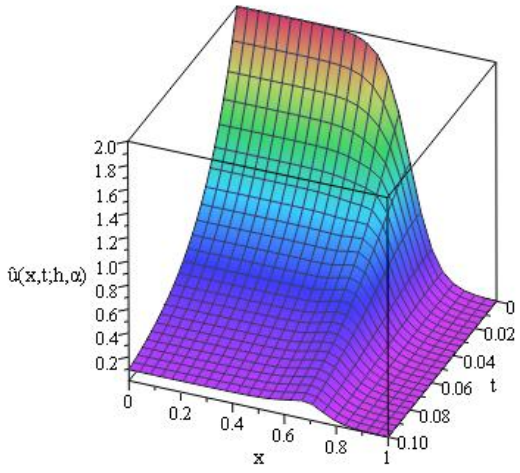

Figure 7.2: Plot of $\hat{u}(x,t;h,\alpha)$, the three-term approximation to the solution of (7.1) under initial condition (7.26) with minimizing h- and α-value plugged in, where $h = 0.037484, \alpha = 30.5655$.

7.2.3 Gaussian

Let $\hat{u}(x,t;h,\alpha)$ be the three-term approximation using the initial condition

$$u(x,0) = e^{-x^2}. \tag{7.28}$$

Then the function

$$\hat{E}(h,\alpha) = \frac{1}{25}\sum_{k=0}^{4}\sum_{j=-2}^{2}\left|N\left[\hat{u}\left(\frac{j}{2},k;h,\alpha\right)\right]\right| \tag{7.29}$$

has minimum 0.022559 obtained at $h = -0.075, \alpha = 20$. The plot of the error $\hat{E}(h,\alpha)$ is Figure 7.3 and the plot of $\hat{u}(x,t;h,\alpha)$ is Figure 7.4.

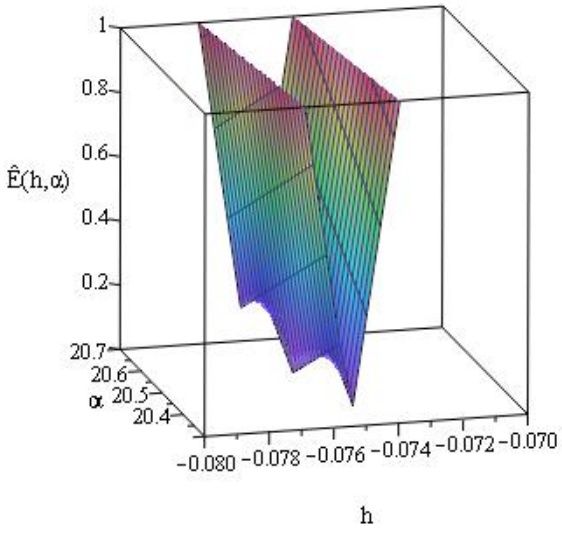

Figure 7.3: Plot of $\hat{E}(h, \alpha)$, the sum of absolute residual error over 25 points in the square $x \in [-1, 1]$, $t \in [0, 4]$ as a function of h and α, the convergence control parameter and the exponential coefficient. The error function has minimum has minimum $\hat{E}(h, \alpha) = 0.022559$ obtained at $h = -0.075, \alpha = 20$.

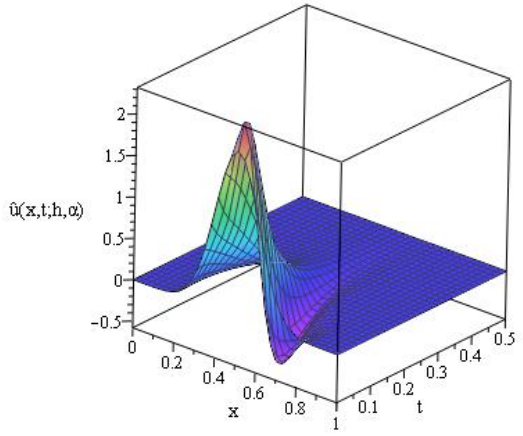

Figure 7.4: Plot of $\hat{u}(x,t;h,\alpha)$, the three-term approximation to the solution of (7.1) under initial condition (7.28) with minimizing h- and α-value plugged in, where $h = -0.075, \alpha = 20$.

7.2.4 Decaying exponential

If we use the initial condition

$$u(x,0) = e^{-x}, \tag{7.30}$$

then call the three-term approximation (7.22) by $\hat{u}(x,t;h,\alpha)$. Then the function

$$E(h,\alpha) = \frac{1}{625}\sum_{k=0}^{24}\sum_{j=0}^{24}\left(N\left[\hat{u}\left(\frac{j}{24},k;h,\alpha\right)\right]\right)^2. \tag{7.31}$$

has minimum 8.27×10^{-3} at $h=0.772$, $\alpha=5.959$. The graph of the error $E(h,\alpha)$ is given in Figure 7.5 and the plot of the three-term approximation $\hat{u}(x,t;h_m,\alpha_m)$ is given in Figure 7.6.

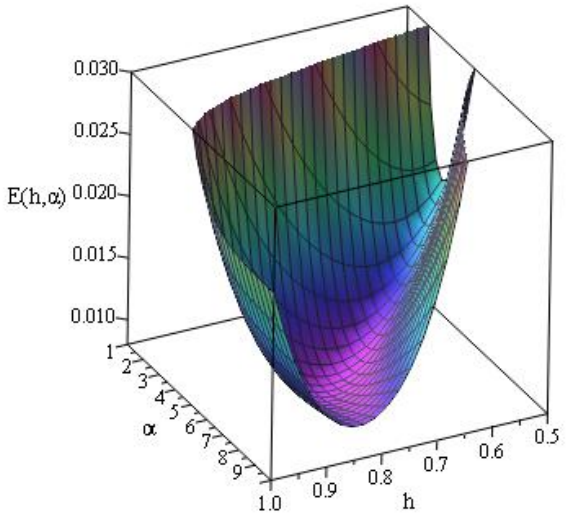

Figure 7.5: Plot of $E(h, \alpha)$, the sum of absolute residual error over 625 points in the square $x \in [0, 1]$, $t \in [0, 24]$ as a function of h and α, the convergence control parameter and the exponential coefficient. The error function has minimum has minimum $E(h, \alpha) = 8.2725 \times 10^{-3}$ obtained at $h = 0.772, \alpha = 5.959$.

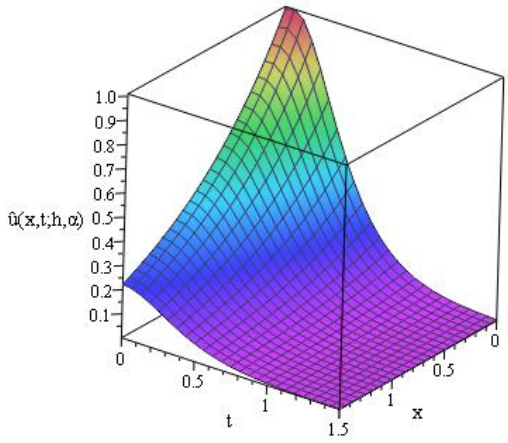

Figure 7.6: Plot of $\hat{u}(x,t;h,\alpha)$, the three-term approximation to the solution of (7.1) under initial condition (7.30) with minimizing h- and α-value plugged in, where $h = 0.772, \alpha = 5.959$.

7.2.5 Constant initial condition and trivial exact solutions

If the initial condition is a constant $u(x,0) = c$, then the homotopy expansion of infinite terms converges immediately to $u_0(x,t) = ce^{-\alpha t}$. And the residual error for this function is zero. So the homotopy analysis method has detected an exact solution. In point of fact, any function of just the temporal variable is an exact solution to the Hunter-Saxton equation.

Meanwhile, if we wanted a function of just the spatial variable, assume $u(x,t) = f(x)$. Then the PDE (7.2) becomes

$$f(x)f''(x) + \frac{1}{2}f'(x)^2 = 0. \tag{7.32}$$

If we add and subtract a factor of $\frac{1}{2}f'(x)^2$, then our equation (7.32) becomes $f(x)f''(x) + f'(x)^2 - \frac{1}{2}f'(x)^2 = 0$, or better yet,

$$(f(x)^2)' - (f'(x))^2 = 0. \tag{7.33}$$

This equation has a solution in $f(x) = ce^{2x}$, where c is a constant. Thus $u(x,t) = ce^{2x}$ is a function of just the spatial variable and an exact solution of the Hunter-Saxton equation.

7.2.6 Identity function

Let's take the initial condition $u(x,0) = x$. Then the zeroth order term is $u_0(x,t;\alpha) = xe^{-\alpha t}$. Note that every term in the nonlinear operator (7.7) having an x derivative will eliminate

the spatial variable in the equation for $u_1(x,t;h,\alpha)$. And so

$$u_1(x,t;h,\alpha) = -\frac{h}{2\alpha}e^{-2\alpha t} - h\alpha t e^{-\alpha t} + \frac{h}{2\alpha}e^{-\alpha t}. \tag{7.34}$$

Furthermore, since every term of (7.7) has a partial with respect to x in it, every term of the expansion of $N\left[\sum_{j=0}^{\infty} u_j q^j\right]$ will make every deformation equation have spatial derivatives in it. So the right-hand side of every equation will be $L[u_j] = L[u_{j-1}] = L[u_1] = -\alpha h e^{-\alpha t} + \frac{h}{2}e^{-2\alpha t}$ for $j \geq 2$. So every term of our expansion will be the same as $u_1(x,t)$ (7.34). This is an example where the infinite series (7.9) will diverge when $q = 1$ unless $h = 0$; but, then our approximation is just $u_0(x,t;\alpha)$, and upon minimizing this with respect to α, we get $\alpha = 0$ and a trivial solution. That being said, since the terms are redundant after the $O(q)$ term, let us only take the two-term approximation $\hat{u}(x,t,h,\alpha) = u_0(x,t;\alpha) + u_1(x,t;h,\alpha)$.

Even with the h in the u_1 term, we still lose h when we find the residual error because u_1 is just a function of t and α. In fact, we have

$$R(x,t;h,\alpha) = (N[\hat{u}(x,t;h,\alpha)])^2 = \alpha^2 e^{-2\alpha t} - \alpha e^{-3\alpha t} + \frac{1}{4}e^{-4\alpha t}. \tag{7.35}$$

We can integrate this on $[0,\infty)$, and take a sum of points for the x coordinates to get

$$E_1(\alpha) = \frac{1}{M}\sum_{j=0}^{M}\int_0^{\infty} R(j,t;h,\alpha)dt = \frac{1}{2}\alpha + \frac{1}{16\alpha} - \frac{1}{3}. \tag{7.36}$$

The minimum value of $E_1(\alpha)$ is 0.02022 and occurs at $\alpha = 0.353553$.

Now, if we find the residual error using a double sum (instead of integrating) of 100 points for $t \in [0,2]$, we get

$$E_2(\alpha) = \frac{1}{100M}\sum_{k=0}^{99}\sum_{j=0}^{M} R\left(j, \frac{k}{50}; h, \alpha\right). \tag{7.37}$$

This function has a minimum of 2.9557×10^{-3} occurring at $\alpha = 0.380018$.

So we can choose h to be whatever we want, and as long as we take a finite number of terms in our approximation (7.9), we will still get the same global residual error.

Thus, even with the accumulation of infinite integration we still get an error that is good: 0.02. But if we take the discrete sum of 100 points that error goes down further by almost a factor of 10 to 0.0029557.

The plots of the error functions $E_1(\alpha)$ and $E_2(\alpha)$ are given in Figures 7.7 and 7.8, respectively. The plot of the approximation $\hat{u}(x, t; h, \alpha)$ is given in Figure 7.9 with minimizing $\alpha = 0.380018$ and arbitrary $h = 1$ plugged in.

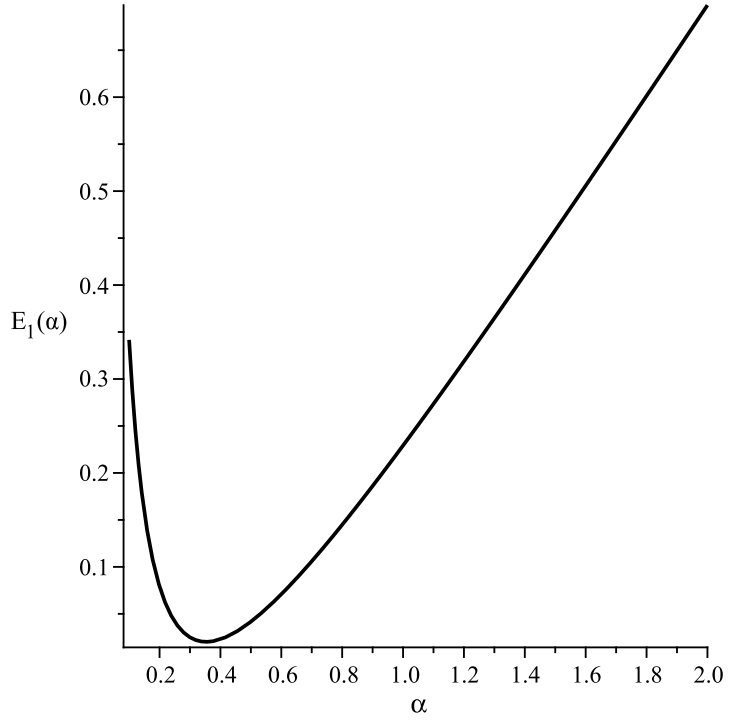

Figure 7.7: The plot of $E_1(\alpha)$, the function of the integral of the squared residual error on $t \in [0, \infty)$ for the initial condition $u(x, 0) = x$. The function has a minimum value of 0.02022 when $\alpha = 0.353553$.

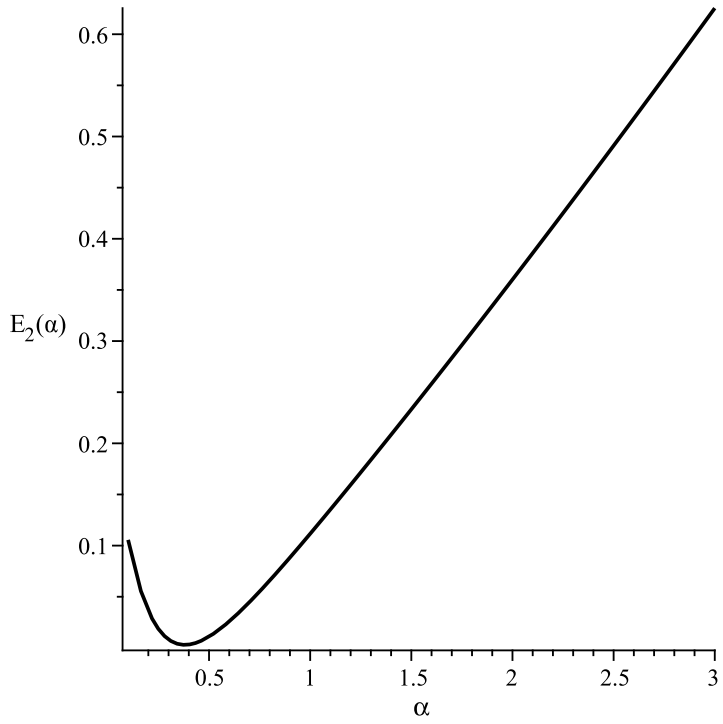

Figure 7.8: The plot of $E_{@}(\alpha)$, the sum of 100 points for t in the interval $[0, 2]$ for the initial condition $u(x, 0) = x$. The function has a minimum value of 2.9557×10^{-3} when $\alpha = 0.380018$.

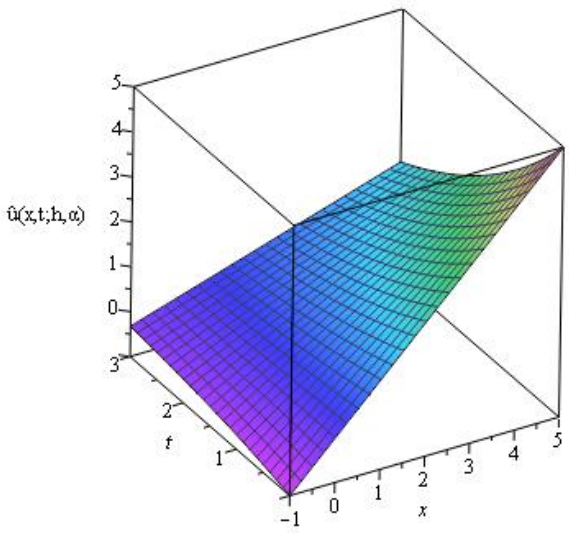

Figure 7.9: The plot of $\hat{u}(x,t;h,\alpha)$, the three term approximation to (7.2) under the initial condition u(x,0) = x. The minimizing value $\alpha = 0.380018$ is used along with an arbitrary $h = 1$.

7.2.7 Sine function

Now we will take the initial condition

$$u(x,0) = \sin x. \tag{7.38}$$

With the three term approximation $\hat{u}(x,t;h,\alpha)$, we have the sum of squared residual error function

$$E(h,\alpha) = \frac{1}{100}\sum_{k=0}^{9}\sum_{j=0}^{9} N\left[\hat{u}\left(\frac{j}{9},\frac{k}{5},h,\alpha\right)\right]^2. \tag{7.39}$$

The minimum value of $E(h,\alpha)$ is 0.0275, occurring at $h = -0.1772538, \alpha = 0.423$. The graph of $E(h,\alpha)$ is Figure 7.10, and the graph of the approximation $\hat{u}(x,t;-0.1772538,0.423)$ is Figure 7.11.

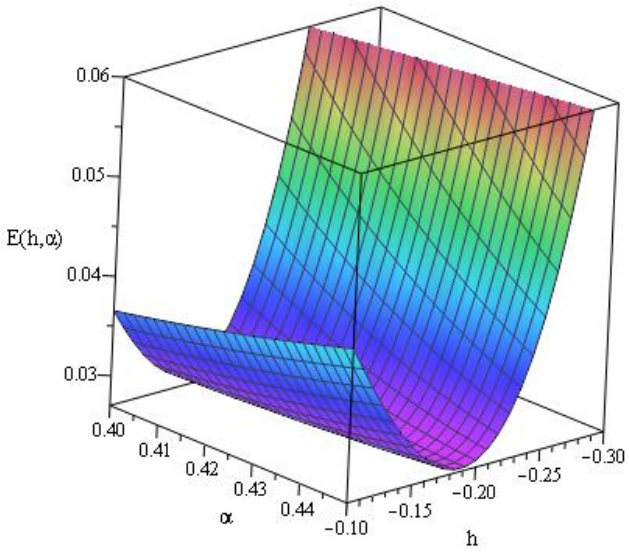

Figure 7.10: The plot of $E(h, \alpha)$, the sum of 100 points in the rectangle $[0, 1] \times [0, 2]$ as a function of the convergence control parameter h and operator parameter α. The minimum value is 0.0275 when $h = -0.1772538, \alpha = 0.423$.

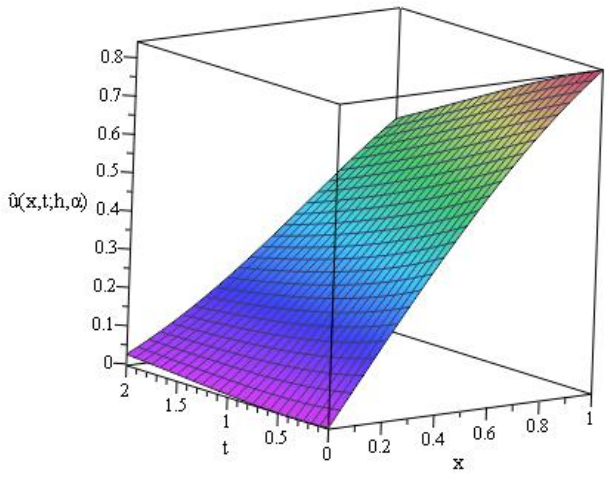

Figure 7.11: The plot of the three-term approximation $\hat{u}(x,t;h,\alpha)$to the solution of (7.2) with initial condition $u(x,0) = \sin x$, where minimizing values $h = -0.1772538$ and $\alpha = 0.423$ are used.

7.3 Discussion

We have applied the optimal homotopy analysis method to the Hunter-Saxton PDE under relevant boundary conditions. Interestingly, we have kept the equation as a PDE, as opposed to transforming it into an ODE, since the boundary conditions are relevant for a PDE formulation. In addition to presenting the general method for the approximate analytical solution of this equation, we have considered several specific examples of relevant boundary data. Some of these conditions were studied numerically studied in the original paper by Hunter and Saxton [92].

Nonlinear partial differential equations, in particular, are difficult to apply the homotopy method to. Much work has been done on ordinary differential equations, but not nearly as much has been done with PDEs. For example, picking the linear operator is a difficult choice. The linear deformation equations may become too unwieldy if the operator is too complicated. But if it is too trivial (just $\frac{\partial}{\partial t}$) then the outcome can be unsatisfactory due to a lack of accuracy in the approximations.

The operator $\frac{\partial}{\partial t} + 1$ has been used before in some degree of success [87]. However, some cases, like the hyperbolic tangent as initial data (7.26), lead to much higher error when this operator is selected. To get around this, we consider adding an additional parameter in the auxiliary linear operator. We consider operators of the form $\frac{\partial}{\partial t} + \alpha$, and we were able to pick $\alpha > 0$ so that the residual error inherent in the solutions was minimal. For all examples

considered, this approach reduced the residual error (compared with the standard optimal homotopy analysis method).

The method employed allowed us to construct approximate analytical solutions after few terms were calculated. As had been discussed elsewhere, for nonlinear PDEs calculating the additional higher-order terms becomes very complicated. So, it is advantageous to be able to obtain accurate approximations with few terms. The error results obtained here are impressive, if one notes that they measure global error (that is, the error accumulated over the domain) as opposed to simple error at a point.

The results obtained here suggest the method of optimally selecting the auxiliary linear operator in the homotopy analysis method is a viable way to obtain approximate analytical solutions to nonlinear partial differential equations and related nonlinear boundary value problems. In the future, we shall apply this method to other complicated integrable and non-intergrable nonlinear wave equations.

CHAPTER 8

SEVERAL TYPES OF SIMILARITY SOLUTIONS FOR THE HUNTER-SAXTON EQUATION

The following results are from the article [115].

8.1 Background

The orientation of molecules in liquid crystals is described by a field of unit vectors $\mathbf{n}(x,t) \in S^2$. If this field is nematic, it means the crystals are invariant under an inversion: $\mathbf{n} \to -\mathbf{n}$. In this case, $\mathbf{n}$ is called a director field [92]. The Hunter-Saxton equation

$$(u_t + uu_x)_x = \frac{1}{2}u_x^2, \tag{8.1}$$

or, equivalently,

$$u_{xt} + uu_{xx} + \frac{1}{2}u_x^2 = 0, \tag{8.2}$$

is a nonlinear wave equation that has been used to study a nonlinear instability in the director field of a nematic liquid crystal [92]. The equation is an asymptotic model of waves

moving in one direction that satisfy the variational principle

$$\delta \int_{t_1}^{t_2} \int_{-\infty}^{\infty} \left\{ \psi_t^2 - c^2(\psi) \psi_x^2 \right\} dxdt = 0. \tag{8.3}$$

Here c is the constant wave speed. The Euler-Lagrange equation derived from (8.3) is

$$\psi_{tt} = c(\psi) \left\{ c(\psi) \psi_x \right\}_x . \tag{8.4}$$

If there is a perturbation in ψ about some constant $\psi = \psi_0$ and x is a space variable corresponding to a reference frame that moves with the linear velocity, then the Euler-Lagrange equation of the variational principle

$$\delta \int_{t_1}^{t_2} \int_{-\infty}^{\infty} \left(u_t u_x + u u_x^2 \right) dxdt = 0$$

is exactly (8.1).

The Hunter-Saxton equation was shown to have a class of solutions that break down in finite time, but are, however, smooth [92]. The initial value problem is typically [92]

$$u(x, 0) = f(x) \tag{8.5}$$

with boundary condition

$$\lim_{x \to \infty} u(x, t) = 0 . \tag{8.6}$$

For other situations, it may be more reasonable to enforce a boundary condition

$$\lim_{t \to \infty} u(x, t) = 0 , \tag{8.7}$$

which yields a solution that decays for large time. Mathematically, the Hunter-Saxton equation is interesting, in that it is a rather simple nonlinear partial differential equation that

admits a variety of solutions. In [93], the inverse scattering solutions to the Hunter-Saxton equation were studied. In addition to the application mentioned above, the Hunter-Saxton equation models the geodesic flow on a spherical manifold [94]. Therefore, solutions of (8.1) are interesting and useful for a variety of reasons. A Lie group symmetry analysis of the Hunter-Saxton equation (8.1) was recently carried out[95], and some exact solutions were obtained. Therefore, it makes sense that self-similar solutions should exist for a rather general variety of physical scenarios. We discuss similarity solutions in two contexts. First, we consider some exact solutions. While interesting, the applicability of such solutions can be narrow. Secondly, we consider approximate analytical solutions to the nonlinear ordinary differential equation governing the self-similar solutions of the Hunter-Saxton equation.

To be specific, the present paper is devoted to describing two classes of solutions to the Hunter-Saxton equation (8.1). We first consider solutions under a separability condition on the temporal and spatial variables. Such solutions can be found which satisfy boundary conditions of the form (8.7). A family of exact separable solutions are found. The second class of solutions are self-similar solutions. These solutions are parameterized by a constant which gives an indication of the strength of a zero (or a pole) at some finite value of time. In the case where there is a pole, we obtain solutions which would blow-up at finite time. Both exact and analytical solutions are found within this class of solutions: the exact solutions correspond to specific narrow cases, hence an analytical technique is required in order to study most of the solutions. We use a method known as homotopy analysis, which has been applied to a number of nonlinear partial differential equations. In particular, the

method gives a simple way for one to minimize the residual error inherent in the analytical approximations. By doing so, we obtain rather accurate approximations to the self-similar solutions after considering relatively few terms. As it turns out, the separable solutions are really a type of special case reduction of the self-similar solutions, corresponding to the case where there is a pole in the time variable of order unity.

In this paper we present several elegant exact solutions, of the self-similar variety, to a nonlinear partial differential equation. Of course, it is true that such exact solutions to complicated nonlinear partial differential equations are of course interesting in their own right. However, such solutions have other practical uses, as well. For instance, these types of solutions can be useful in verifying numerical solution techniques for such nonlinear partial differential equations. This give a good check to numerical methods which can then be used to solve for solutions in more complicated regimes where exact solutions are not possible (or are not feasible). Additionally, these exact solutions obtained here demonstrate that the Hunter-Saxton equation (8.1) admits a variety of solutions, even when we restrict our attention to solutions satisfying certain symmetry properties (i.e., self-similarity). For instance, if solutions tend to zero as $t \to \infty$, then the solutions are localized in time, meaning that such similarity solutions gradually dissipate as time becomes large. On the other hand, if solutions decay as $|x| \to \infty$, this means that the solutions are localized in space. Examples of such solutions would be solitary waves.

To obtain the approximate analytical solutions, we shall apply the homotopy analysis method [14]-[22], since it gives one the ability to adjust and control the convergence of the

solutions. Through an appropriate choice of the convergence control parameter, we are able to obtain residual error minimizing approximations to the solutions. This method is often referred to as the optimal homotopy analysis method, since it allows one to "optimally" select the convergence control parameter in order to minimize errors. We discuss the behavior of solutions obtained using this approach. This technique allows one to obtain many solutions which can not be written in explicit exact form.

8.2 Separable solutions

Suppose $u(x,t)$ splits into functions $l(t)$ and $k(x)$ as

$$u(x,t) = l(t)k(x). \tag{8.8}$$

Then plugging this into (8.2), we obtain $l'(t)k'(x) + l(t)^2k''(x)k(x) + \frac{1}{2}l(t)^2k'(x)^2 = 0$, which can be written as

$$\frac{k''(x)k(x) + \frac{1}{2}k'(x)^2}{k'(x)} = -\frac{l'(x)}{l(x)^2} = \lambda. \tag{8.9}$$

This yields the system of equations

$$\begin{cases} l'(t) + \lambda l(t)^2 = 0, \\ \\ k''(x)k(x) + \frac{1}{2}k'(x)^2 - \lambda k'(x) = 0. \end{cases} \tag{8.10}$$

Then we will take

$$l(t) = \frac{1}{\lambda t + c_0}, \tag{8.11}$$

where $\lambda, c_0 > 0$. Without loss of generality, set $c_0 = 1$. At $t = 0$, we recover $u(x, 0) = k(x)$. Meanwhile, note that as $t \to \infty$, we should have $u \to 0$ (provided that $k(x)$ is sufficiently bounded). Therefore,

$$u(x,t) = \frac{k(x)}{1+\lambda t} \tag{8.12}$$

is an exact solution to the boundary value problem

$$\begin{cases} u_{xt} + uu_{xx} + \frac{1}{2}u_x^2 = 0, \\ \\ u(x,0) = k(x), \quad \lim\limits_{t\to\infty} u(x,t) = 0\,. \end{cases} \tag{8.13}$$

There is a consistency condition, namely that any initial data $k(x)$ must satisfy (8.10). Therefore, while a variety of solutions are possible, one is not free to select any function $k(x)$ as initial data.

8.2.1 Exact separable solutions

Let us assume that a solution $k(x)$ takes the form $k(x) = \mu x + \nu$ for constants $\mu > 0$ and ν. Then, (8.10) implies $\frac{1}{2}\mu^2 - \lambda\mu = 0$, hence $\mu = 2\lambda$. Therefore, for each $\lambda > 0$, the function $k(x) = 2\lambda x + \nu$ is always an exact solution to (8.10). For any $t \geq 0$, we therefore have the family of exact solutions

$$u(x,t) = \frac{2\lambda x + \nu}{1+\lambda t} \tag{8.14}$$

which are parameterized by the constants $\lambda > 0$ and $\nu \in \mathbb{R}$. The parameter ν can be taken to zero, since it does not effect the qualitative structure of the solution. Let us define a

function

$$\overline{u}(x,t) = \frac{x}{1+t}\,. \tag{8.15}$$

Then, we may represent a separable solution u in terms of the fundamental solution $\overline{u}$ by $u(x,t) = \overline{u}(2\lambda x, \lambda t)$. This gives an infinite family of solutions, all of which are really just scalings of the fundamental solution $\overline{u}(x,t)$.

In the narrow case when $\lambda = 0$, the solutions become static solutions, and $u(x,t) = k(x)$ where $k''(x)k(x) + \frac{1}{2}k'(x)^2 = 0$. The general solution is found to be $u(x,t) = (c_1 x + c_0)^{2/3}$. Interestingly, the spatial derivatives of $u(x,t)$ become singular at $x = 0$, although the function itself is always continuous. Therefore, the solution $u(x,t) = (c_1 x + c_0)^{2/3}$ is an example of a *weak* solution.

Other exact solutions may be possible, but the method of finding them would be adhoc. One could prescribe desired initial or boundary conditions on $k(x)$ in order to seek such solutions numerically. The solution family we found corresponds to the initial conditions $k(0) = \nu$, $k'(0) = 2\lambda$.

8.3 Self-similar solutions

The separable solution discussed in the previous section is essentially a specific case of a more general type of solution, namely a self-similar solution. While the Hunter-Saxton equation has received attention on the literature, self-similar solutions of the equation have not been

fully explored. Note that from the Lie group symmetry analysis of [95], it makes sense that self-similar solutions should exist for a rather general variety of physical scenarios. Some special exact solutions were found in [95] in this regard. As we shall see, it is often the case that such solutions cannot be expressed in any exact closed-form. For this reason, we later consider an analytical approximation method in order to study such solutions.

We begin with the Hunter-Saxton equation (8.2), and assume a self-similar solution

$$u(x,t) = (1+t)^a U(\eta)\,, \quad \text{where} \quad \eta = x(1+t)^b \tag{8.16}$$

is a similarity variable for constant parameters a and b (which are to be determined). This puts the PDE (8.2) into the form

$$\left\{b\eta t^{a+b-1} + t^{2a+2b}U\right\}\frac{d^2U}{d\eta^2} + \frac{1}{2}t^{2a+2b}\left(\frac{dU}{d\eta}\right)^2 + (a+b)t^{a+b-1}\frac{dU}{d\eta} = 0\,. \tag{8.17}$$

Then, if we require $a+b-1 = 2a+2b$, or $a+b=-1$, a similarity solution exists. We have selected the factor $1+t$ to avoid a singularity for $t \geq 0$. However, the methods applied here will work for any factor of the form $t_0 + t$, where t_0 is an arbitrary constant. Let us write $a = -1-b$ so that our solutions will be written in terms of one parameter. Note that the separable case of the previous section corresponds to $a=-1$ and $b=0$. We find, setting $a=-1-b$, that the unknown function U satisfies the equation

$$(U+b\eta)\frac{d^2U}{d\eta^2} + \frac{1}{2}\left(\frac{dU}{d\eta}\right)^2 - \frac{dU}{d\eta} = 0. \tag{8.18}$$

In general, a self-similar solution will correspond to

$$u(x,t) = \frac{U(x(1+t)^b)}{(1+t)^{1+b}}\,. \tag{8.19}$$

Next we apply the boundary conditions. At $t = 0$, we have $u(x, 0) = U(x)$.

Instead of a condition corresponding to $t \to \infty$, some applications call for a condition when $x \to \infty$. As $x \to \infty$ for (8.6), we consider

$$0 = \lim_{x\to\infty} u(x,t) = \lim_{x\to\infty} \frac{U(x(1+t)^b)}{(1+t)^{1+b}}, \tag{8.20}$$

so we require $\lim_{x\to\infty} U(x(1+t)^b) = 0$. That is, we require

$$\lim_{\eta\to\infty} U(\eta) = 0. \tag{8.21}$$

Therefore, any solution $U(\eta)$ to the boundary value problem

$$\begin{cases} (U + b\eta)\dfrac{d^2U}{d\eta^2} + \dfrac{1}{2}\left(\dfrac{dU}{d\eta}\right)^2 - \dfrac{dU}{d\eta} = 0 \\ \lim\limits_{\eta\to\infty} U(\eta) = 0, \end{cases} \tag{8.22}$$

yields a solution to the boundary value problem

$$\begin{cases} u_{xt} + uu_{xx} + \frac{1}{2}u_x^2 = 0, \\ u(x,0) = U(x), \quad \lim\limits_{x\to\infty} u(x,t) = 0, \end{cases} \tag{8.23}$$

of the form

$$u(x,t) = \frac{U(x(1+t)^b)}{(1+t)^{1+b}}. \tag{8.24}$$

Once again, there will be one free parameter to choose for (8.22). We will take a condition at $\eta = 0$, $U(0) = \alpha$ for some constant α.

8.3.1 Exact self-similar solutions

Let us ignore the condition (8.20) for the moment. Then, some exact solutions are possible. If we assume $U(\eta) = \eta^r$ in the ODE (8.22), we obtain

$$(\eta^r + b\eta)r(r-1)\eta^{r-2} + \frac{1}{2}r^2\eta^{2r-2} - r\eta^{r-1} = 0. \tag{8.25}$$

After simplification, we can write this as

$$\eta^{2r-2}\left(\frac{3}{2}r^2 - r\right) = \eta^{r-1}\left(-br^2 + br + r\right). \tag{8.26}$$

Note the case when $r = 0$ implies $U(\eta)$ is constant, so our solution $u(x,t)$ is only a function of the temporal variable. Any function of t is a trivial solution to (8.2). On the other hand, if $r = \frac{2}{3}$, this implies that $b = -3$ and we obtain a solution that is only a function of the spatial variable:

$$u(x,t) = x^{\frac{2}{3}}. \tag{8.27}$$

It is interesting to note that this is exactly the type of solution obtained in Section 2, which we called a stationary solution (the solution does not change in time).

If we assume $b = 0$, observe that we recover the exact solutions of Section 2.1.

Another interesting note is that the Homotopy Analysis Method can be used to discover an exact solution. First we find the three-term approximation $\hat{u}(\eta; h, b)$. Next, we take the squared residual error

$$\hat{E}(h,\beta) = \frac{1}{500}\sum_{j=1}^{500}\left(N\left[\hat{u}(j;h,b)\right]\right)^2. \tag{8.28}$$

The plot of this function is given in Figure 8.1. Note the residual error along $\beta = 3$ is zero, indicating an exact solution. Also, at $\beta = 3$, the squared residual error is $E(h, 3) = 2.5 \times 10^{-5} h^4$, giving a minimum when $h = 0$.

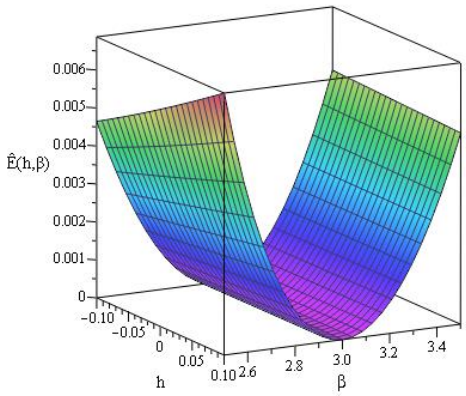

Figure 8.1: Plot of $\hat{E}(h, b)$, the sum of squared residual error over 500 points in the interval $\eta \in [1, 500]$ as a function of h and b, the convergence control parameter and the scale of t in the self-similarity. The error is zero along $b = 3$.

8.4 Analytical-numerical computation of self-similar solutions

While some exact self-similar solutions can be obtained for rather narrow restrictions of initial data, most of the time no exact solutions can be found. Therefore, we shall have to resort to approximate methods. In the present section, we shall apply an analytical-numerical method in order to obtain self-similar solutions. In particular, we will obtain an analytical approximation to the solution of the ODE (8.22) using the homotopy analysis method, and then we shall numerically optimize the convergence control parameter which ensures that residual errors are minimized.

We take the condition at zero to be of the form $U(0) = \alpha$. An example of a homotopy in topology is a continuous deformation of one curve into another, and the homotopy analysis method proceeds similarly. In the method, one constructs a homotopy between the original differential operator and an auxiliary operator that is easier to solve. For details of the method, see [14]-[22]. The nonlinear differential operator is

$$N[U] = (U + b\eta)\,\frac{d^2U}{d\eta^2} + \frac{1}{2}\left(\frac{dU}{d\eta}\right)^2 - \frac{dU}{d\eta}, \tag{8.29}$$

where we will note that $N[U] = 0$ is equivalent to (8.22). With an auxiliary linear operator $L[U]$, we can write a homotopy between L and N as

$$0 \equiv \mathcal{H}(U, q) = (1 - q)L[U] - qhN[U]. \tag{8.30}$$

Here, $q \in [0, 1]$ is the homotopy parameter, $\mathcal{H}$ is the homotopy function, and h is the convergence control parameter that allows us to customize a function of error later. The

homotopy gives us a differential equation of the same degree as the original equation (8.22). A solution to this differential equation is of the form $U = U(\eta; q)$, where we highlight the dependence on the embedding parameter, q. If $u(\eta; 1)$ exists and converges, then it is a solution of (8.22); see Liao [15]. We will use the auxiliary linear operator

$$L[U] = \frac{d^2U}{d\eta^2} + \frac{dU}{d\eta}. \tag{8.31}$$

Next, we will expand $U(\eta; q)$ as a Taylor series in q. We propose that

$$U(\eta; q) = \sum_{j=0}^{\infty} u_j(\eta) q^j. \tag{8.32}$$

We circumvent the question of the convergence of this series representation for $U(\eta; q)$ when $q = 1$ by showing that only taking a few terms of this sum is a good way to approximate the solution to (8.22). This will yield an approximate solution to the problem. However, note that the homotopy (8.30) includes a parameter $h \neq 0$. This parameter can be used to control and modify the convergence of the homotopy solution. In a more modern approach, referred to as the *optimal homotopy analysis method*, one chooses the parameter h so that the residual errors due to such an approximation are minimized. This technique has been used to obtain solutions for a number of nonlinear ordinary and partial differential equations, see the references [96, 97, 98, 99, 100, 101] for several successful examples.

Placing the solution form (8.32) into the homotopy (8.30) yields

$$(1 - q)L\left[\sum_{j=0}^{\infty} u_j q^j\right] = qhN\left[\sum_{j=0}^{\infty} u_j q^j\right]. \tag{8.33}$$

By the linearity of L, this yields

$$\sum_{j=0}^{\infty} L[u_j]q^j = \sum_{j=0}^{\infty} L[u_j]q^{j+1} + qhN\left[\sum_{j=0}^{\infty} u_j q^j\right]. \tag{8.34}$$

Similarly, the initial data become

$$\sum_{j=0}^{\infty} u_j(0)q^j = \alpha, \qquad \lim_{\eta\to\infty}\sum_{j=0}^{\infty} u_j(\eta)q^j = 0. \tag{8.35}$$

Now, expanding the right-hand side of (8.34) around q, and equating powers of q on each side, we can write the order zero equation

$$L[u_0] = 0. \tag{8.36}$$

Expanding the conditions out and matching powers of q, we see (8.36) is subject to

$$u_0(0) = \alpha, \qquad \lim_{\eta\to\infty} u_0(\eta) = 0. \tag{8.37}$$

The $O(q^m)$ equation is, for $m \geq 1$,

$$L[u_m] = L[u_{m-1}] + \frac{h}{(m-1)!}\left(\frac{\partial^{m-1}}{\partial q^{m-1}} N\left[\sum_{j=0}^{\infty} u_j q^j\right]\right)\Big|_{q=0}, \tag{8.38}$$

subject to

$$u_m(0) = 0, \qquad \lim_{\eta\to\infty} u_m(\eta) = 0. \tag{8.39}$$

Note that (8.38) is recursive in that the solution of $u_m(\eta)$ depends upon the functions $u_0(\eta), ..., u_{m-1}(\eta)$. So we can compute up to the order of term that gives a tolerable error, and then obtain our approximation. We will show in what follows that very few terms are needed to obtain a decent approximation. Below, we take the first three terms in the

homotopy expansion,

$$u^*(\eta; h, b, \alpha) = u_0(\eta; \alpha) + u_1(\eta; h, b, \alpha) + u_2(\eta; h, b, \alpha) \tag{8.40}$$

and compute the corresponding squared residual error

$$E(h, b, \alpha) = \frac{1}{500} \sum_{j=0}^{499} \left(N \left[u^* \left(\frac{j}{50}; h, b, \alpha \right) \right] \right)^2. \tag{8.41}$$

We take the discrete approximation to the residual error, since this formulation speeds up computation. The alternative is to integrate over the squared residuals, but such an approach is far more computationally demanding. We include the argument h to highlight the functional dependence, where relevant. We may minimize $E(h, b)$ for fixed values of the initial condition, $U(0) = \alpha$, and the similarity parameter, b. That is, for fixed α and v, we seek

$$h^*(\alpha, b) = \text{argmin}_{h \neq 0} E(h, b, \alpha) = \frac{1}{500} \sum_{j=0}^{499} \left(N \left[u^* \left(\frac{j}{50}; h, b, \alpha \right) \right] \right)^2. \tag{8.42}$$

To demonstrate the method, let us consider two cases. First, we assume $U(0) = 1$ in (8.37). Then the solution to the order-zero equation (8.36) subject to (8.37) is $u_0(\eta) = e^{-\eta}$. The solution to the $O(q)$ equation is found to be

$$u_1(\eta; h, b) = \left(\frac{1}{2} bh\eta^2 + bh\eta - h\eta + \frac{1}{4} h \right) e^{-\eta} - \frac{1}{4} h e^{-2\eta}. \tag{8.43}$$

We find $u_2(\eta; h, b)$ in a similar way using (8.38). As a sample, $E(h, b)$ is plotted for $b = 0.28$ in Figure 8.2. The minimum error is 2.098×10^{-4} and this occurs when $h = -2.3089$. Of course, one can improve upon this error by adding more terms to the homotopy approximation. However, we find that a three-term approximation is more than sufficient for plotting

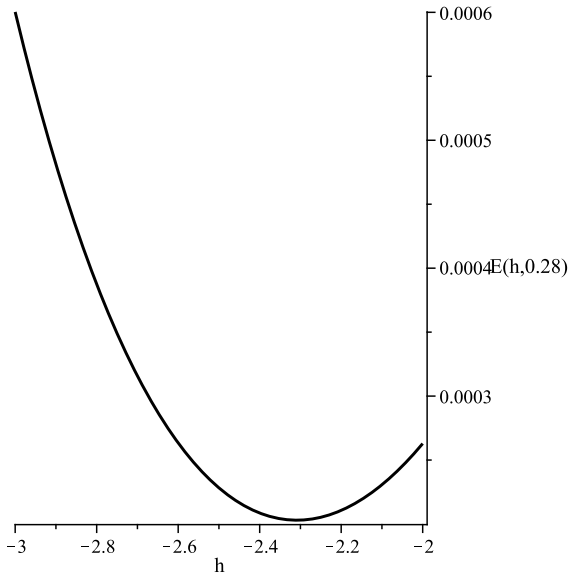

Figure 8.2: Plot of $E(h, 0.28)$, the sum of squared residual error over 500 points for $\eta \in [0, 10]$ as a function of h, the convergence control parameter. The error function has minimum 2.0298×10^{-4} obtained at $h = -2.3089$. We consider the initial condition $U(0) = 1$.

accuracy. The corresponding three-term approximations $u^*(\eta; h, b)$ for $b = -0.5, 0.1, 0.28$ and 1, evaluated at the minimizing convergence control parameter values, h, are all plotted in Figure 8.3.

Next, consider the case $\alpha = \frac{1}{2}$ in (8.37). The solution to the order-zero equation (8.36) subject to (8.37) is $u_0(\eta) = \frac{1}{2}e^{-\eta}$, while the solution to the first order equation is

$$u_1(\eta; h, b) = \left(\frac{1}{4}bh\eta^2 - \frac{1}{2}h\eta + \frac{1}{2}bh\eta + \frac{1}{16}h\right)e^{-\eta} - \frac{1}{16}he^{-2\eta}. \tag{8.44}$$

The third term in the approximation is found similarly. The plot of $E(h, b)$ for $b = 0.28$ is given in Figure 8.4. The minimum error is 2.915×10^{-4}, occurring at $h = -3.497$.

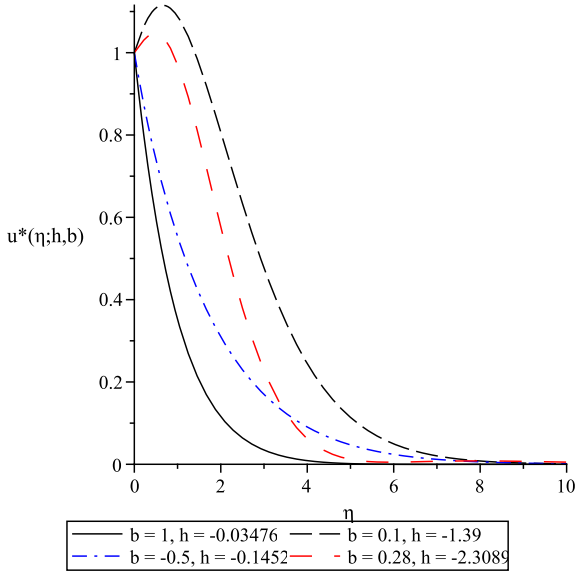

Figure 8.3: Plot of $u^*(\eta; h, b)$, the three-term approximation to the solution of (8.22) assuming $U(0) = 1$, for four values of b with solutions evaluated at the residual error minimizing value of the convergence control parameter, h.

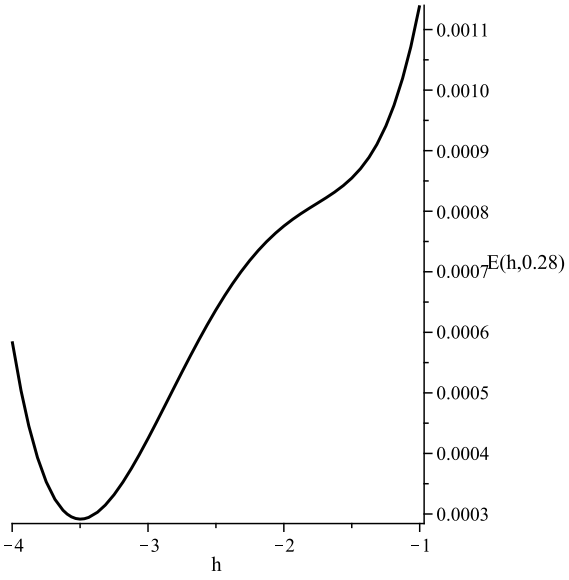

Figure 8.4: Plot of $E(h, 0.28)$, the sum of squared residual error over 500 points for $\eta \in [0, 10]$ as a function of h, the convergence control parameter. The error function has minimum 2.915×10^{-4} obtained at $h = -3.497$. We consider the initial condition $U(0) = \frac{1}{2}$.

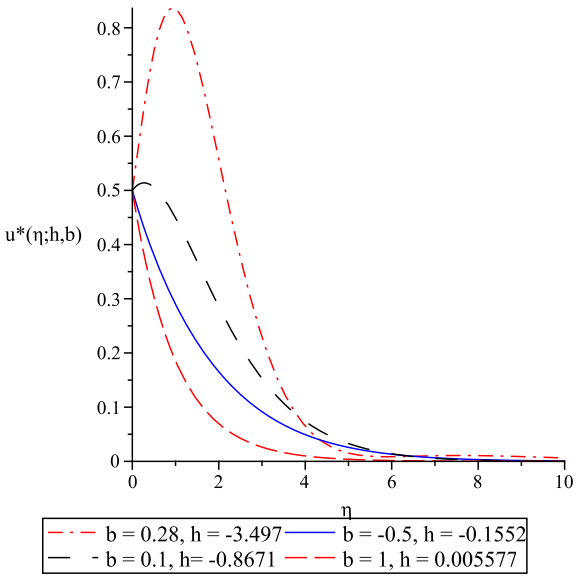

Figure 8.5: Plot of $u^*(\eta; h, b)$, the three-term approximation to the solution of (8.22) assuming $U(0) = \frac{1}{2}$, for four values of b with solutions evaluated at the residual error minimizing value of the convergence control parameter, h.

The corresponding three-term approximations $u^*(\eta; h, b)$ for $b = -0.5, 0.1, 0.28$, and 1, with minimizing h-values plugged in, are all plotted in Figure 8.5.

From the solution plots, it is clear that while all solutions satisfy the far-field condition $U \to 0$ as $\eta \to \infty$, and therefore the solutions $u(x,t)$ satisfy the condition (8.6), the value of b (the similarity parameter) strongly influences the behavior of the solution profiles for small enough η. Interestingly, the influence of b does not result in a steady trend in the solution curves, highlighting the importance of considering specific cases for the similarity parameter separately. To see why this might be, let us consider the function $V(\eta)$, where we set $U(\eta) = V(\eta) - b\eta$. The (8.22) is put into the form

$$V\frac{d^2V}{d\eta} + \frac{1}{2}\left(\frac{dV}{d\eta}\right)^2 - (1+b)\frac{dV}{d\eta} + b + \frac{1}{2}b^2 = 0\,. \tag{8.45}$$

The $1+b$ factor of $\frac{dV}{d\eta}$ is a simple scaling, but the inhomogeneous term $b + \frac{1}{2}b^2$ tells us that solutions should depend on the parameter function $\chi(b) = b + \frac{1}{2}b^2$. Since this is a nonlinear combination of the similarity parameter, it is natural that solutions should themselves depend nonlinearly on b.

There is sometimes a linear solution to (8.45). Let us assume that $V(\eta) = \mu\eta + \nu$, where μ and ν are real-valued constants. Then, a necessary and sufficient condition for the existence of such a solution is found (by substitution) to be

$$\frac{1}{2}\mu^2 - (1+b)\mu + b + \frac{1}{2}b^2 = 0\,. \tag{8.46}$$

This gives solutions $\mu = b$ and $\mu = 2 + b$. Therefore, $V(\eta) = b\eta + \nu$ and $V(\eta) = (b+2)\eta + \nu$ are two distinct linear solutions. In the first case, we find $U(\eta) = \nu$, a constant. In the

second case, we find $U(\eta) = 2\eta + \nu$. We therefore have two distinct solutions, which implies that multiple solutions are possible in some parameter regimes. Putting these solutions back into natural variables, we have the exact solutions

$$u(x,t) = \frac{\nu}{(1+t)^{1+b}} \tag{8.47}$$

and

$$u(x,t) = \frac{2x}{1+t} + \frac{\nu}{(1+t)^{1+b}}\,, \tag{8.48}$$

respectively.

8.5 Discussion

We have studied separable and self-similar solutions of the Hunter-Saxton wave equation. We were able to obtain exact solutions for both cases in closed form, under some relevant assumptions. In the case where $u(x,t) \to 0$ as $t \to \infty$, the separable solutions give us a solution with algebraic decay,

$$u(x,t) = \frac{k(x)}{1+\lambda t}\,, \tag{8.49}$$

where $k(x)$ satisfies a suitable ordinary differential equation. We show that such separable solutions are essentially special cases of self-similar solutions. The self-similar solutions allow us to consider other boundary conditions, such as $u(x,t) \to 0$ as $x \to \pm\infty$. The type of self-similarity inherent in the Hunter-Saxton equation is

$$u(x,t) = \frac{U(x(1+t)^b)}{(1+t)^{1+b}}\,. \tag{8.50}$$

Note that the separable solutions correspond to $b = 0$. For other values of b, solutions correspond to differing initial conditions. This is interesting, as for a number of other partial differential equations, the form of the similarity variable $\eta = x(1+t)^b$ is fixed. For instance, in the case of many nonlinear wave equations, one often obtains the unique similarity variable $\eta = x/\sqrt{t}$ [102]. So, we have obtained a general family of such solutions, all parameterized by the similarity parameter b.

While exact solutions are possible in some narrow cases, for the physically interesting case of $u(x,t) \to 0$ as $x \to \pm\infty$, we should have $U(\eta) \to 0$ as $\eta \to \infty$. To study such solutions, we applied an analytical-numerical method, the so-called optimal homotopy analysis. The primary benefit of this method is that it permits one to obtain accurate analytical approximations to solutions of nonlinear differential equations after relatively few terms are computed. We obtain error on the order of 10^{-4} after only three terms are considered. The existence of such self-similar solutions is completely consistent with what one would expect from the Lie group analysis presented in [95]. From the present results, it is clear that the value of the similarity parameter, b, strongly influences the behavior of the solutions.

We have obtained a number of solutions for the Hunter-Saxton equation, which illustrates the rich variety of solutions possible for this equation. For other initial-boundary value conditions, perhaps other more exotic solution forms can be constructed.

CHAPTER 9

EXACT SIMILARITY SOLUTIONS OF THE KHOKHLOV-ZABOLOTSKAYA EQUATION

The following results are from the paper [116].

9.1 Background

The Khokhlov-Zaboloskaya (KZ) equation is used to describe the propagation of a sound beam in a nonlinear medium [103]. The Khokhlov-Zabolotskaya equation is give by

$$u_{xt} - (uu_x)_x - u_{yy} = 0, \tag{9.1}$$

or, equivalently,

$$u_{xt} - uu_{xx} - u_x^2 - u_{yy} = 0. \tag{9.2}$$

The Lie Symmetries and conservation laws of the KZ equation are discussed in a paper by Chowdhury and Naskar [104]. The conservation laws are used in the analysis of the dispersion of the sound beam throughout its propagation [104]. All the similarity reductions of the Lie Point Symmetries of the KZ equation are derived by Zhang, Zhu, and Lin [105].

These symmetries reduce the KZ equation to a lower dimensional PDE [105]. Non-classical symmetries of the KZ equation, as well as exact solutions in transformed coordinate systems are given in [106]. The paper by Sanchez [107] studies the existence of solutions to the KZ equation. Morozov [108] studied multi-valued solutions of the KZ equation using the Maurer-Cartan forms of its symmetry group. Dispersionless Lax equations, of which the KZ equation is one, are studied by Krichever in [109].

An in-depth study of the history of the KZ equation is given by Rudenko in [110]. This paper also talks about an equation similar to the KZ equation, the Khokhlov-Zabolotskaya-Kuznetsov (KZK) equation. The KZK equation is the KZ equation with a dissipative term [110]. In [111], Rozanova derives the KZK equation from the Navier-Stokes system and studies the existence, uniqueness, and stability of the solution.

In this paper, many self-similar solutions to the KZ equation are studied and some exact solutions are found. In section 2, we consider a self-similar transformation which reduces the PDE (9.2) to an ODE. Exact solutions are found for this ODE. In section 3, we transform the self-similar ODE obtained in Section 2 into an integral equation. This allows us to ascertain certain interesting properties of self-similar solutions of the KZ equation. Following this, we discuss a second distinct type of self-similar solution to the KZ equation in Section 4. An exact solution is recovered, and this solution has the interesting property that it is stationary in time. Based on the solutions obtained in Sections 2-4, we are led to consider a method of reducing the KZ equation into a new, lower-dimensional PDE in Section 5. As we shall demonstrate, certain additively separable solutions of this new PDE result in

exact solutions of the type obtained in the earlier sections. This therefore gives one a nice framework in which to study the possible exact self-similar solutions to the KZ equation. Finally, in Section 6 we consider a type of hybrid self-similar traveling wave solution.

While exact solutions to complicated nonlinear partial differential equations are of course interesting in their own right, there are other practical uses for such exact solutions. One may use such exact solutions in order to calibrate numerical solution techniques for the KZ equation. Secondly, such exact solutions demonstrate the variety of behaviors possible when we are studying the KZ equation. Indeed, we find that the various exact solutions will have different asymptotic properties. For instance, we see that some of the solutions remain bounded as $t \to \infty$, while other solutions exhibit unbounded growth in this limit. Additionally, some solutions may be well-behaved for all finite time, yet other solutions will exhibit finite time blow-up. The rich variety of structures possible in our exact solutions demonstrates the diverse collection of possible solutions of the KZ equation.

9.2 First self-similar solutions to the Khokhlov-Zabolotskaya equation

In this section, we will group the x and t together to get a self-similar transform, and then we will group t and y to get an ODE. This way it is easy to keep track of the similarity

variables. We begin by assuming $u(x,y,t) = t^a R(\xi, y)$, where $\xi = xt^b$. Then

$$\begin{aligned} u_x &= t^{a+b} R_\xi, \\ u_{xt} &= \Big\{(a+b)R_\xi + b\xi R_{\xi\xi}\Big\} t^{a+b-1}, \\ (uu_x)_x &= t^{2a+2b}(RR_{\xi\xi} + R_\xi^2), \\ u_{yy} &= t^a R_{yy}. \end{aligned} \tag{9.3}$$

Plugging this into our original PDE (9.1) we obtain

$$\Big\{(a+b)R_\xi + b\xi R_{\xi\xi}\Big\} t^{a+b-1} - t^{2a+2b}(RR_{\xi\xi} + R_\xi^2) - t^a R_{yy} = 0. \tag{9.4}$$

The similarity transform exists if $a = -2$ and $b = 1$. So our PDE has become

$$RR_{\xi\xi} + R_\xi^2 + R_{yy} - \xi R_{\xi\xi} + R_\xi = 0. \tag{9.5}$$

Next, we will group together the t and y variables by assuming $R(\xi, y) = y^a U(\eta)$, where $\eta = \xi y^b$. After necessary preparation, the equation (9.5) becomes

$$y^{2a+2b}\Big\{U''U + U'^2\Big\} + a(a-1)y^{a-2}U + (2ab + b^2 - b)y^{a-2}\eta U' + b^2 y^{a-2}\eta^2 U'' - y^{a+b}\eta U'' + y^{a+b}U' = 0. \tag{9.6}$$

We see that if $a = 2$ and $b = -2$, then we can write

$$(4\eta^2 - \eta + U(\eta))\frac{d^2U}{d\eta^2} + \left(\frac{dU}{d\eta}\right)^2 + (1 - 2\eta)\frac{dU}{d\eta} + 2U(\eta) = 0. \tag{9.7}$$

If we write our solutions in standard coordinates, we have

$$u(x,y,t) = \frac{1}{t^2}R(xt, y) = \frac{y^2}{t^2}U\left(\frac{xt}{y^2}\right). \tag{9.8}$$

Since this is a second-degree equation, we assume a quadratic solution

$$U(\eta) = \alpha\eta^2 + \beta\eta + \gamma\eta, \tag{9.9}$$

where α, β, γ are constants.

We find one solution if $\alpha = 0$, and get

$$U(\eta) = \beta\eta - \frac{1}{2}(\beta + \beta^2). \tag{9.10}$$

In standard coordinates, this is

$$u(x, y, t) = \beta\frac{x}{t} - \frac{1}{2}(\beta + \beta^2)\frac{y^2}{t^2}. \tag{9.11}$$

We also find another solution using the assumption above (9.9) if $\alpha = -1$, in which case $U(\eta) = \gamma - \eta^2$. In standard coordinates this becomes

$$u(x, y, t) = \gamma\frac{y^2}{t^2} - \frac{x^2}{y^2}. \tag{9.12}$$

9.3 A transform of the similarity ODE to an integral equation

Consider our self-similar ODE (9.7). Let us define a function $V(\eta)$ such that

$$U(\eta) = V(\eta) - 4\eta^2 + \eta. \tag{9.13}$$

Then, we can put the ODE (9.7) into the form

$$VV'' + V'^2 + 3(1 - 6\eta)V' - 6V + 2(1 - 6\eta)^2 = 0. \tag{9.14}$$

Let us write

$$V(\eta) = \frac{1}{24} w(\tau), \qquad \text{where } \tau = \sqrt{2}(1 - 6\eta). \tag{9.15}$$

Then by the Chain Rule,

$$\begin{aligned} \frac{dV}{d\eta} &= \frac{dV}{d\tau}\frac{d\tau}{d\eta} = -\frac{\sqrt{2}}{4} w'(\tau), \\ \frac{d^2V}{d\eta^2} &= -\frac{\sqrt{2}}{4} w''(\tau)(-6\sqrt{2}) = 3w''(\tau). \end{aligned} \tag{9.16}$$

From here our ODE becomes

$$\frac{1}{24} w(\tau)\left(3w''(\tau)\right) + \frac{1}{8} w'(\tau)^2 + \frac{3}{\sqrt{2}} \tau \left(-\frac{\sqrt{2}}{4}\right) w'(\tau) - \frac{1}{4} w + \tau^2 = 0, \tag{9.17}$$

which simplifies to

$$ww'' + w'^2 - 6\tau w - 2w + 8\tau^2 = 0. \tag{9.18}$$

We can write this as

$$(w^2)'' - 12\tau w' - 4w + 16\tau^2 = 0. \tag{9.19}$$

If we can solve this equation, then we have a solution

$$U(\eta) = \frac{1}{24} w(\tau) - 4\eta^2 + \eta = \frac{1}{24} w\big(\sqrt{2}(1 - 6\eta)\big) - 4\eta^2 + \eta. \tag{9.20}$$

Integrating our transformed ODE (9.19) from 0 to τ gives

$$(w^2)' - 12\tau w(\tau) + 8\int_0^\tau w(s)ds + \frac{16}{3}\tau^3 = 2w(0)w'(0). \tag{9.21}$$

Integrating again, we obtain

$$w(\tau)^2 - 12\int_0^\tau s w(s)ds + 8\int_0^\tau \int_0^s w(\sigma)d\sigma ds + \frac{4}{3}\tau^4 = 2w(0)w'(0). \tag{9.22}$$

Here we use the fact that

$$\int_0^\tau \int_0^\sigma w(s)dsd\sigma = \int_0^\tau (\tau - s)w(s)ds \tag{9.23}$$

to simplify this to

$$w(\tau)^2 + \int_0^\tau (8\tau - 20s)w(s)ds + \frac{4}{3}\tau^3 = 2w(0)w'(0)\tau + w(0)^2. \tag{9.24}$$

Therefore, the nonlinear ODE for $w(\tau)$ can be put into the form of a nonlinear integral equation.

We may use the ODE to find the local curvature of $w(\tau)$ near $\tau = 0$. Considering the ODE (9.19) at $\tau = 0$, this gives

$$w(0)w''(0) + w'(0)^2 - 2w(0) = 0, \tag{9.25}$$

hence

$$w''(0) = 2 - \frac{w'(0)^2}{w(0)}. \tag{9.26}$$

The signed curvature of the graph of $w(\tau)$ is then

$$\kappa(t) = \frac{w''(\tau)}{(1 + w'(\tau)^2)^{3/2}}, \tag{9.27}$$

so

$$\kappa(\tau) = \left(2 - \frac{w'(0)^2}{w(0)}\right)\left(1 + w'(0)^2\right)^{-3/2}, \tag{9.28}$$

for $\tau \approx 0$. The minimum of the curvature is when $w''(0) = 0$, and it is zero there. And using (9.26) this happens when $w'(0) = \pm\sqrt{2w(0)}$, provided $w(0) > 0$. If $w(0) < 0$, then

curvature is not zero at $\tau = 0$, because $w''(0) \geq 2$ in that case. Note that $w(0) \neq 0$ is required throughout the above discussion.

If we construct a series solution, we can see the need for the restriction $w(0) \neq 0$. To demonstrate this, let us consider the case where $w'(0) = 1$. We find (treating $w(0)$ as a parameter)

$$\begin{aligned} w(\tau) = w(0) + \tau + \frac{1}{2}\left(\frac{2w(0)-1}{w(0)}\right)\tau^2 + \frac{1}{6}\left(\frac{2w(0)+3}{w(0)^2}\right)\tau^3 - \frac{5}{24}\left(\frac{2w(0)+3}{w(0)^3}\right)\tau^4 \\ + \frac{7}{24}\left(\frac{2w(0)+3}{w(0)^4}\right)\tau^5 - \frac{7}{16}\left(\frac{2w(0)+3}{w(0)^5}\right)\tau^6 + \frac{11}{16}\left(\frac{2w(0)+3}{w(0)^6}\right)\tau^7 \cdots . \end{aligned} \tag{9.29}$$

Note we pick up our exact solution if we assume $w(0) = -\frac{3}{2}$. Then the series expansion (9.29) becomes

$$\begin{aligned} U(\eta) &= \frac{1}{24}\left(\frac{8}{3}(1-6\eta)^2 + \sqrt{2}(1-6\eta) - \frac{3}{2}\right) - 4\eta^2 + \eta \\ &= -\left(\frac{1}{3} + \frac{\sqrt{2}}{4}\right)\eta + \frac{7}{144} - \frac{\sqrt{2}}{24}. \end{aligned} \tag{9.30}$$

Observe that this is just (9.10) with $\beta = -\left(\frac{1}{3} + \frac{\sqrt{2}}{24}\right)$.

So for very small $|w(0)|$, the series terms (9.29) become arbitrarily large, while when $|w(0)|$ is very large, the terms in the series become arbitrarily small. Consider the case when $|w(0)|$ is very large, so that $w(\tau) \approx w(0) + \tau + \tau^2$. Then

$$\begin{aligned} U(\eta) &\approx \frac{1}{24}\left(w(0) + \sqrt{2}(1-6\eta) + 2(1-6\eta)^2\right) - 4\eta^2 + \eta \\ &= -\eta^2 - \frac{\sqrt{2}}{4}\eta + \frac{1}{24}(w(0) + \sqrt{2} + 2), \end{aligned} \tag{9.31}$$

for small enough τ (i.e., for small enough $|1 - 6\eta|$).

9.4 A second self-similar solution to the Khokhlov-Zabolotskaya equation

In this section we will try a more general self-similar solution

$$u(x,y,t) = x^a y^b U(\eta), \tag{9.32}$$

where

$$\eta = x^c y^d t. \tag{9.33}$$

Plugging our assumption (9.32) into the original PDE (9.2) and simplifying, we obtain

$$\begin{aligned}
&\Big\{cx^{c+a-1}y^{b+d}\eta - c^2x^{2a-2}y^{2b}\eta^2 U(\eta) - d^2x^a y^{b-2}\eta^2\Big\}U''(\eta) + \Big\{ax^{a+c-1}y^{b+d} + cx^{a+c-1}y^{b+d} \\
&\quad - acx^{2a-2}y^{2b}\eta U(\eta) - c(a+c-1)x^{2a-2}y^{2b}\eta U(\eta) - c^2x^{2a-2}y^{2b}\eta^2 U'(\eta) \\
&\quad - 2acx^{2a-2}y^{2b}\eta U(\eta) - bdx^a y^{b-2}\eta - d(b+d-1)x^a y^{b-2}\eta\Big\}U'(\eta) \\
&\quad - \Big\{a(a-1)x^{2a-2}y^{2b}U(\eta) + a^2x^{2a-2}y^{2b}U(\eta) + b(b-1)x^a y^{b-2}\Big\}U(\eta) = 0.
\end{aligned} \tag{9.34}$$

It follows that there is a self-similarity when $a = 2, b = -2, c = 1$, and $d = -2$. Using these values, our ODE becomes

$$\Big\{\eta - \eta^2 U(\eta) - 4\eta^2\Big\}U''(\eta) + \Big\{3 - \eta^2 U'(\eta) - 8\eta U(\eta) - 14\eta\Big\}U'(\eta) - \Big\{6U(\eta) + 6\Big\}U(\eta) = 0. \tag{9.35}$$

Although highly nonlinear, this is still a second-order equation. If we assume a quadratic solution $U(\eta) = \alpha\eta^2 + \beta\eta + \gamma$, then plugging this into the equation (9.35) we get a trivial solution $U(\eta) = 0$ or the constant solution $U(\eta) = -1$. In the standard coordinates this

solution becomes

$$u(x, y, t) = -\frac{x^2}{y^2}. \tag{9.36}$$

Unlike other solutions discussed above, this solution has the property that it is time-independent, or stationary. Therefore, the solution exhibits no blow-up for either $t \to \infty$ or $t \to 0$.

9.5 A PDE method for an exact solution to the KZ equation

Let us begin with the original PDE (9.2). Based on solutions we found earlier, as in (9.11), (9.12), and (9.36), we decide to try an assumption that $u(x, y, t) = V(\alpha, \beta)$, where

$$\alpha = \frac{y^2}{t^2}, \quad \beta = \frac{x^2}{y^2}. \tag{9.37}$$

Then

$$\begin{aligned}
\frac{\partial V}{\partial x} &= V_\alpha \alpha_x + V_\beta \beta_x = \frac{2x}{y^2} V_\beta, \\
\frac{\partial^2 V}{\partial x \partial t} &= \frac{2x}{y^2} \left(V_{\beta\alpha} \alpha_t + V_{\beta\beta} \beta_t \right) \\
&= \frac{2x}{y^2} \left(-\frac{2y^2}{t^3} V_{\alpha\beta} \right) = -\frac{4x}{t^3} V_{\alpha\beta}, \\
\frac{\partial^2 V}{\partial x^2} &= \frac{2}{y^2} V_\beta + \frac{2x}{y^2} \left(V_{\beta\alpha} \alpha_x + V_{\beta\beta} \beta_x \right) = \frac{2}{y^2} V_\beta + \frac{2x}{y^2} \left(\frac{2x}{y^2} V_{\beta\beta} \right) = \frac{2}{y^2} V_\beta + \frac{4x^2}{y^4} V_{\beta\beta}, \\
\frac{\partial V}{\partial y} &= V_\alpha \alpha_y + V_\beta \beta_y = \frac{2y}{t^2} V_\alpha - \frac{2x^2}{y^3} V_\beta, \\
\frac{\partial^2 V}{\partial y^2} &= \frac{2}{t^2} V_\alpha + \frac{2y}{t^2} \left(V_{\alpha\alpha} \alpha_y + V_{\beta\alpha} \beta_y \right) + \frac{6x^2}{y^4} V_\beta - \frac{2x^2}{y^3} \left(V_{\beta\alpha} \alpha_y + V_{\beta\beta} \beta_y \right) \\
&= \frac{2}{t^2} V_\alpha + \frac{2y}{t^2} \left(\frac{2y}{t^2} V_{\alpha\alpha} - \frac{2x^2}{y^3} V_{\alpha\beta} \right) + \frac{6x^2}{y^4} V_\beta - \frac{2x^2}{y^3} \left(\frac{2y}{t^2} V_{\alpha\beta} - \frac{2x^2}{y^3} V_{\beta\beta} \right) \\
&= \frac{2}{t^2} V_\alpha + \frac{6x^2}{y^4} V_\beta + \frac{4y^2}{t^4} V_{\alpha\alpha} + \frac{4x^4}{y^6} V_{\beta\beta} - \frac{8x^2}{y^2 t^2} V_{\alpha\beta}.
\end{aligned} \tag{9.38}$$

Now plugging $V(\alpha, \beta)$ into (9.2) we have

$$-\frac{4x}{t^3} V_{\alpha\beta} - \frac{2}{y^2} V_\beta V - \frac{4x^2}{y^4} V_{\beta\beta} V - \frac{4x^2}{y^4} (V_\beta)^2 - \frac{2}{t^2} V_\alpha - \frac{6x^2}{y^4} V_\beta - \frac{4y^2}{t^4} V_{\alpha\alpha} - \frac{4x^4}{y^6} V_{\beta\beta} + \frac{8x^2}{y^2 t^2} V_{\alpha\beta} = 0. \tag{9.39}$$

Multiplication by y^2 gives

$$\left(\frac{8x^2}{t^2} - \frac{4xy^2}{t^3} \right) V_{\alpha\beta} - 2V_\beta V - \frac{4x^2}{y^2} V_{\beta\beta} V - \frac{4x^2}{y^2} (V_\beta)^2 - \frac{2y^2}{t^2} V_\alpha - \frac{6x^2}{y^2} V_\beta - \frac{4y^4}{t^4} V_{\alpha\alpha} - \frac{4x^4}{y^4} V_{\beta\beta} = 0. \tag{9.40}$$

Let us now use (9.37) along with the fact that $\alpha\beta = \dfrac{x^2}{t^2}$ to get

$$(8\alpha\beta - 4\alpha\sqrt{\alpha\beta}) V_{\alpha\beta} - 2V_\beta V - 4\beta V_{\beta\beta} V - 4\beta (V_\beta)^2 - 2\alpha V_\alpha - 6\beta V_\beta - 4\alpha^2 V_{\alpha\alpha} - 4\beta^2 V_{\beta\beta} = 0. \tag{9.41}$$

The exact solution was a sum of α and β, so we suppose that V has the form

$$V(\alpha, \beta) = F(\alpha) + G(\beta). \tag{9.42}$$

Then $V_\alpha = F'(\alpha), V_\beta = G'(\beta)$, etc., and we have

$$-2G'(F+G) - 4\beta G''(F+G) - 4\beta(G')^2 - 2\alpha F' - 6\beta G' - 4\alpha^2 F'' - 4\beta^2 G'' = 0. \quad (9.43)$$

After dividing by -2, we can simplify this as

$$F(G' + 2\beta G'') + G'G + 2\beta G''G + 2\beta(G')^2 + \alpha F' + 3\beta G' + 2\alpha^2 F'' + 2\beta^2 G'' = 0. \quad (9.44)$$

If the terms including both F and G in the above equation (9.44) would vanish, we might be able to split this equation. So if we further assume that $G'(\beta) + 2\beta G''(\beta) = 0$, the solution is $G(\beta) = c_1\sqrt{\beta} + c_2$. Plugging this function back into (9.44) yields

$$\alpha F' + 2\alpha^2 F'' + \frac{1}{2}c_1^2 + c_1\sqrt{\beta} = 0. \quad (9.45)$$

At this point, there are two cases. Case 1 is if $c_1 = 0$. This means that $G(\beta)$ is constant, and the equation (9.45) becomes $\alpha F' + 2\alpha^2 F'' = 0$, which has solution $F(\alpha) = c_1\sqrt{\alpha}$. Then in standard coordinates, our solution becomes

$$u(x, y, t) = c_1\frac{y}{t} + c_2. \quad (9.46)$$

The second case is if $c_1 \neq 0$. Here, (9.45) will have no solution since F is a function of only α. But now we are free to assume

$$G'(\beta) + 2\beta G''(\beta) \neq 0, \quad (9.47)$$

so we may divide by it to solve for F in (9.44). Doing so, we obtain

$$F(\alpha) = \frac{-G'G - 2\beta G''G - 2\beta(G')^2 - \alpha F' - 3\beta G' - 2\alpha^2 F'' - 2\beta^2 G''}{G' + 2\beta G''}. \quad (9.48)$$

To try and get an equation that will split, let us take the derivative of both sides of (9.48) to get

$$F'(\alpha) = \frac{(-F' - \alpha F'' - 4\alpha F'' - 2\alpha^2 F''')\,(G' + 2\beta G'')}{(G' + 2\beta G'')^2} = \frac{-F' - 5\alpha F'' - 2\alpha^2 F'''}{G' + 2\beta G''}. \tag{9.49}$$

If we assume $F'(\alpha) \neq 0$, we have

$$G' + 2\beta G'' = \frac{-F' - 5\alpha F'' - 2\alpha^2 F'''}{F'}. \tag{9.50}$$

This equation is split, and now we can assume both sides are equal to λ, where $\lambda \neq 0$. So we have a system

$$\begin{cases} G'(\beta) + 2\beta G''(\beta) = \lambda, \\ \\ 2\alpha^2 F'''(\alpha) + 5\alpha F''(\alpha) + (1+\lambda)F'(\alpha) = 0. \end{cases} \tag{9.51}$$

These two equations have solutions

$$F(\alpha) = c_1 \alpha^{\frac{1}{4} + \frac{1}{4}\sqrt{1-8\lambda}} + c_2 \alpha^{\frac{1}{4} - \frac{1}{4}\sqrt{1-8\lambda}} + c_6, \tag{9.52}$$

and

$$G(\beta) = \lambda\beta + c_3\sqrt{\beta} + c_4. \tag{9.53}$$

By definition, α is nonnegative. So if we allow non-real exponents for α, there is no restriction on λ. However, plugging the solutions (9.52) and (9.53) back into $V(\alpha, \beta) = F(\alpha) + G(\beta)$ and then back into the original PDE (9.2), what is left is

$$\frac{-(2\lambda c_4 + c_3^2)y^2 - 6c_3(\lambda + \frac{1}{3})xy - 6\lambda(1+\lambda)x^2}{y^4}. \tag{9.54}$$

In order to get this to be zero, we must have either $\lambda = 0$ or $\lambda = -1$. If $\lambda = 0$, then we must also have $c_3 = 0$ and our solution in standard coordinates is

$$u(x, y, t) = c_1 \frac{y}{t} + c_5. \tag{9.55}$$

If, however, $\lambda = -1$, then $c_3 = c_4 = 0$ and our solution is

$$V(\alpha, \beta) = F(\alpha) + G(\beta) = c_1 \alpha + \frac{c_2}{\sqrt{\alpha}} - \beta. \tag{9.56}$$

In standard coordinates, our solution is

$$u(x, y, t) = c_1 \frac{y^2}{t^2} + c_2 \frac{t}{y} - \frac{x^2}{y^2}. \tag{9.57}$$

Note that our solution (9.11) had a factor of $\dfrac{x}{t}$ that was not picked up in the above exact solution (9.57), hence by using different methods we are able to find additional solutions. However, the specific solution (9.12) is equivalent to our solution (9.57) (upon setting $c_2 = \gamma$). Our exact solution (9.36) corresponds to (9.57) in the case where $c_1 = c_2 = 0$. Therefore, the exact solution obtained here through a PDE approach allows us to recover some, but not all, of the solutions obtained through some ODE approaches. The PDE approach is this section is perhaps a more unified way to view these solutions.

Note that, depending on the choice of c_1 and c_2, the family of solutions (9.57) can be calibrated to satisfy various asymptotic conditions. For instance, if we seek solutions which remain bounded as $t \to \infty$, we can select $c_2 = 0$. Meanwhile, if we wish to avoid blow-up of solutions in finite time, we select $c_1 = 0$ so that solutions remain finite when $t \to 0$.

9.6 Wave similarity

All of the previous solutions and solution methods discussed in this paper have involved the search for various self-similar forms of solutions. Of course, other solution forms are possible. Standard traveling wave solutions of the equation (9.1) are relatively simple to obtain. What is perhaps more interesting would be the case where solutions are simultaneously wave-like in a pair of variables while self-similar in a grouping of the resulting wave variable with the remaining space variable. Therefore, instead of a self-similarity, we now investigate the possibility of a translational similarity in x and t, and a self-similarity in t and y. Suppose $z = x - ct$, where c is a constant. Then the equation (9.1) becomes

$$cQ_{zz} + Q_z^2 + QQ_{zz} + Q_{yy} = 0. \tag{9.58}$$

Now we will impose the self-similarity of $Q(z,t) = y^a q(\psi)$, where $\psi = zy^b$. Then

$$Q_{zz} = y^{a+2b} q''(\psi) \tag{9.59}$$

and

$$Q_{yy} = a(a-1)y^{a-2}q(\psi) + y^{2a+2b}q(\psi)q''(\psi) + \{ab + b(a+b-1)\}\, y^{a-2}q'(\psi). \tag{9.60}$$

So now our PDE becomes

$$\begin{aligned} cy^{a+2b}q''(\psi) + y^{2a+2b}q'(\psi)^2 + y^2 a + 2bq(\psi)q''(\psi) + a(a-1)y^{a-2}q(\psi) \\ + \{ab + b(a+b-1)\}\, y^{a-2}\psi q'(\psi) + b^2 y^{a-2}\psi^2 q''(\psi) = 0. \end{aligned} \tag{9.61}$$

The similarity occurs when $a - 2 = a + 2b = 2a + 2b$, or when $a = 0$ and $b = -1$. So the ODE above (9.61) becomes

$$\left\{\psi^2 + c + q(\psi)\right\} q''(\psi) + q'(\psi)^2 + 2\psi q'(\psi) = 0. \tag{9.62}$$

Once ψ is known, we have

$$u(x, y, t) = q\left(\frac{z}{y}\right) = q\left(\frac{x - ct}{y}\right). \tag{9.63}$$

For a first solution, we can assume

$$q(\psi) = A_0 + A_1\psi + A_2\psi^2. \tag{9.64}$$

If we use this in the above equation (9.62), then we find that $A_0 = -c$, $A_1 = 0$, and $A_2 = -1$. Thus the solution is $q(\psi) = -\psi^2 - c$. In the original coordinates, we find

$$u(x, y, t) = -\frac{(x - ct)^2}{y^2} - c \tag{9.65}$$

to be another exact solution to the Khokhlov-Zabolotskaya equation. This is another solution with the presence of the $-\dfrac{x^2}{y^2}$ term. Therefore, in the case where the wave reduces to a standing wave ($c = 0$), we recover the exact solution of Section 4.

For any fixed value of y, say $y = y_0$, this solution has a global maximal value at $x = ct$. This maximal value is equal to $-c$ and is invariant of the choice of y_0. We have

$$u(x, y, t) \leq u(ct, y, t) = -c\,, \tag{9.66}$$

thus the maximal value of u does not depend on time. The peak of the wave moves along the x-axis, with the value of y contributing only to the shape of the wave (but not to the position or the maximal value of the wave).

9.7 Discussion

We have found several exact solutions to the Khokhlov-Zabolotskaya equation through the use of self-similar transforms. Our first self-similarity transform helped us find two unique solutions (9.11) and (9.12) in Section 2. These solutions constitute rate exact solutions to a nonlinear PDE. We also found an integral equation (9.24) in Section 3 that we derived from our self-similar ODE (9.7) obtained in Section 2, and we demonstrated various properties of a family of self-similar solutions.

In Section 4, we tried a more general self-similar transform, and wound up with a more difficult equation to solve, (9.35). However, despite the complications in this equation, under appropriate assumptions we were able to recover the solution (9.36) which is equivalent (after scaling) to one of the exact solutions that had been found earlier in Section 2, (9.12).

Noticing the variety of solutions found thus far, we performed a change of variables on the original PDE in section 5, which reduced the original PDE in three variables into a new PDE in two variables, $\alpha = y^2/t^2$ and $\beta = x^2/y^2$. The resulting PDE, while more complicated than the original PDE, permits a nice separation of variables. While multiple forms of solutions are possible, we decided to assume a solution that was additively separable in each of the transformed variables α and β. This lead to the new exact solutions (9.55) and (9.57), which hold some of the previously investigated solutions as special cases.

Finally, we assumed a similarity-wave type of solution in Section 6. We supposed that x and t were related through a traveling wave, and that y and t were related through a

self-similarity. Using this ODE, we then found another exact solution (9.65). This family of solutions would model one specific type of traveling sound beam in a nonlinear medium. In the limit where the wave speed tends to zero, the solution gives a standing wave which takes the form of the solution found in Section 4. Therefore, one can view the stationary solution of Section 4 as a type of standing wave.

With this, we have described a number of exact similarity solutions to the Khokhlov-Zabolotskaya equation, and we have highlighted a number of techniques for finding such solutions. The results show that the Khokhlov-Zabolotskaya equation admits a variety of self-similar structures. The particular structure of physical relevance would be dictated by any asymptotic or initial conditions. For instance, solutions which tend toward zero or finite values as $t \to \infty$ are useful for studying waves or perturbations in the Khokhlov-Zabolotskaya equation. On the other hand, solutions giving blow-up at finite time (say, $t = 0$) help us better understand when singularities may arise in such mathematical models.

CHAPTER 10

CONCLUSIONS

In this dissertation, the Homotopy Analysis Method is used to find approximate analytical solutions to nonlinear differential equations.

The choice of the linear operator has been the main focus of the author's work. The method begins with a nonlinear operator $N[u]$ and asks the user to find a suitable linear operator $L[u]$. An obvious first choice is to use the linear part of the nonlinear operator. This is done successfully in Chapters 2 and 3 with the reduced Ernst Equation (2.21) and the simplified optical vortex equation (3.10). In using the method on the reduced Ernst equation (2.21), the solution form of the ODE was given in (2.33). Note the convergence of the terms to zero as the independent variable increases without bound. This structure is key to being able to perform error analysis on the resulting approximation. In Chapter 3, the linear part of the nonlinear operator (3.14) was again a good choice for L. The type of nonlinearity depended on which model was used.

However, this method of linearizing the nonlinear operator does not always yield tractable results. Consider the nonlinear sigma model in Chapter 4, where we were solving the ODE (4.22). The linear part of the nonlinear operator is $L = \dfrac{d^2}{dz^2}$. The solutions to

$L[g] = 0$ are linear functions that would yield undesirable error on an infinite domain. This is where we decided to try two different linear operators: one that yielded solutions like the error function, and one that yielded solutions that decay exponentially.

After this, we studied the Cahn-Hilliard equation in Chapter 5. This is a partial differential equation. Prior to this, the Homotopy Analysis Method had been mostly used to solve ODEs. On a PDE, especially an evolution equation, linearizing the nonlinear operator is usually a bad choice due to the presence of only one partial derivative with respect to the temporal variable. So, a large undertaking of three different linear operators and many varying initial data were used.

In Chapter 6, the Hasegawa-Mima equation is studied. Here, again, the linear part of the problem is not a good choice for L. What becomes clear here is the choice of linear operator is a delicate one. A linear operator that gave complicated expressions for the first three terms of the expansion was used next, and these terms proved impossible to test in error analysis under any (non-trivializing) simplifying assumption. Finally, we settled on the linear operator that itself gives another parameter to the problem: $L[U] = U_t + \alpha U$. This parameter α provides another way to tailor the approximation to our needs. For instance, if just using the linear operator $L[U] = U_t + U$, we get solutions that decay on the order of e^{-t}. All of the data found in this Chapter had α being approximately 18, 77, or 390 (see Figures 6.1, 6.3, 6.5)! Structurally the exponential decay is there, but think of the differences in the residual error for $t \in [0, 1]$ for e^{-t} versus e^{-370t}: $e^{-0.1} \approx 0.9$, but $e^{-370 \cdot 0.1} \approx 8.5 \times 10^{-17}$.

The Hunter-Saxton equation, in Chapter 7, was vexing. The equation, while much simpler to write out than previous equations (like the Hasegawa-Mima equation), yielded only lukewarm results when tested using the linear operators we have previously used. The residuals found were on the order of 10^{-2}, which is not ideal. We would like to see something more along the lines of 10^{-3} or better. What this shows is that no single choice of linear operator is good enough for all partial differential equations.

In Chapter 8, we found separable and exact solutions to the Hunter-Saxton equation. By turning the PDE to an ODE using a self-similar transform, we were then able to use the Homotopy Analysis Method to get error on the order of 10^{-4} (see Figure 8.2). Note that we used an exponential decay producing linear operator, which was not just the linear portion of the nonlinear operator.

In Chapter 9, we did not need the Homotopy Analysis Method to find approximate solutions, because all of the solutions we found were exact.

The question remains: is there a linear operator that works best? Based on the results obtained, specifically in Chapters 6 and 7, we did not find one particular operator (or family of operators) that works best. This is still an interesting topic for future work, discussed below.

Next, we would highlight the usefulness of the Homotopy Analysis Method. Most importantly, we are able to get functions as solutions– not just data. Having the plot of the approximate solution can give information about how certain properties of the solution can be retained using different initial data. Also, consider the nonlinear σ model with a slowly

converging exact solution (4.13). This is a Maclaurin series, so taking a finite number of terms would not give good residual error for large values in the domain. Through homotopy analysis, we are able to find an approximate solution that is good an a semi-infinite interval. The method sometimes finds exact solutions. For example, in the Cahn-Hilliard equation the method detects an exact solution that is constant (5.78). Also, in the self-similar case of the Hunter-Saxton equation, the method finds an exact solution. See Figure 8.1.

Future work includes applying the method to more problems. This has been one of the main goals of this report. But still, more successful cases should be documented so that general results can be synthesized. Also, the problem of finding the best linear operator for a class of nonlinear operators should be addressed. This is a problem that requires working in generalities. Simply taking a even a simple nonlinear ODE operator and trying a general linear operator leads to unwieldy algebra. And then trying to perform error analysis on an approximation (with how many terms?) is near impossible. The author is inclined to think that perhaps some functional analysis is in order, where we can study operators that depend on a parameter. Also, more information could certainly be gained by delving deeper into the topology of the problem. Finally, computer algebra systems are also a limiting factor in the work. More efficient coding can be implemented to do the evaluations of the squared residual error more efficiently.

APPENDIX - PAPERS PUBLISHED

1. M. Baxter and R. A. Van Gorder, Exact and analytic solutions of the Ernst equation governing axially symmetric stationary vacuum gravitational fields, Physica Scripta 87 (2013) 035005.

2. M. Baxter and R. A. Van Gorder, Exact and analytical solutions for a nonlinear sigma model, Mathematical Methods in the Applied Sciences, doi: 10.1002/mma.2926, August 2013.

3. M. Baxter, R. A. Van Gorder, and K. Vajravelu, On the choice of auxiliary linear operator in the optimal homotopy analysis of the Cahn-Hilliard initial value problem, Numerical Algorithms, dx.doi.org/10.1007/s11075-013-9733-8, July 2013.

4. M. Baxter, R. A. Van Gorder, and K. Vajravelu, Optimal analytic method for the nonlinear Hasegawa-Mima equation, European Physical Journal Plus 129 98, 2014.

Submitted for publication

5. M. Baxter, R. A. Van Gorder, and K. Vajravelu, Peaked solutions for the nonlinear evolution of a vector potential of an electromagnetic pulse propagating in an arbitrary pair plasma with temperature asymmetry, Quaestiones Mathematicae, presently under review.

6. M. Baxter, R. A. Van Gorder, and K. Vajravelu, Several types of exact similarity solutions for the Hunter-Saxton equation, Communications in Theoretical Physics, presently under review.

7. M. Baxter, R. A. Van Gorder, and K. Vajravelu, Exact similarity solutions of the Khokhlov-Zabolotskaya equation, Communications in Nonlinear Science and Numerical Simulation, presently under review.

LIST OF REFERENCES

[1] Ed. S.-J. Liao, Advances in the Homotopy Analysis Method, World Scientific, 2014.

[2] F. J. Ernst, New Formulation of the Axially Symmetric Gravitational Field Problem, Phys. Rev. 167 (1968) 1175.

[3] A. Tomimatsu and H. Sato, New Exact Solution for the Gravitational Field of a Spinning Mass, Phys. Rev. Lett. 29, 1344 (1972).

[4] A. Tomimatsu and H. Sato, New Series of Exact Solutions for Gravitational Fields of Spinning Masses, Prog. Theor. Phys. 50, 95 (1973).

[5] F. J. Ernst, A new family of solutions of the Einstein eld equations, J. Math. Phys. 18, 233 (1977).

[6] C. Reina and A. Treves, Axisymmetric gravitational elds, J. Gen. Rel. Gravity 7, 817 (1976).

[7] B.K. Harrison, Backlund Transformation for the Ernst Equation of General Relativity, Phys. Rev. Lett. 41, 1197 (1978).

[8] D. Korotkin and H. Nicolai, Separation of Variables and Hamiltonian Formulation for the Ernst Equation, Phys. Rev. Lett. 74, 1272 (1995).

[9] Bo-Yu Hou and Wei Lee, Virasoro algebra in the solution space of the Ernst equation, Lett. in Math. Phys. 13, 1 (1987).

[10] G. Neugebauer and R. Meinel, Astrophys. Journal, Part 2 - Letters 414, 97 (1993).

[11] G. Helms, H. Dathe, and P. Dechent, Quantitative FLASH MRI at 3T using a rational approximation of the Ernst equation, Magnetic Resonance in Medicine 59, 667 (2008).

[12] M. Omote and M. Wadati, The Backlund Transformations and the Inverse Scattering Method of the Ernst Equation, Prog. Theor. Phys. Vol. 65, 1621 (1981).

[13] D. A. Korotkin and V. B. Matveev, Functional Analysis and its Applications Vol. 34, 252 (2000).

[14] S.J. Liao, On the proposed homotopy analysis techniques for nonlinear problems and its application, Ph.D. dissertation, Shanghai Jiao Tong University, 1992.

[15] S.J. Liao, Beyond Perturbation: Introduction to the Homotopy Analysis Method, Chapman & Hall/CRC Press, Boca Raton, 2003.

[16] S.J. Liao, An explicit, totally analytic approximation of Blasius viscous flow problems, International Journal of Non-Linear Mechanics 34 (1999) 759-778.

[17] S.J. Liao, On the homotopy analysis method for nonlinear problems, Applied Mathematics and Computation 147 (2004) 499-513.

[18] S.J. Liao and Y. Tan, A general approach to obtain series solutions of nonlinear differential equations, Studies in Applied Mathematics 119 (2007) 297-354.

[19] S.J. Liao, Notes on the homotopy analysis method: some definitions and theorems, Communications in Nonlinear Science and Numerical Simulation 14 (2009) 983-997.

[20] S.J. Liao, Homotopy Analysis Method in Nonlinear Differential Equations. Springer & Higher Education Press, Heidelberg, 2012.

[21] R.A. Van Gorder and K. Vajravelu, On the selection of auxiliary functions, operators, and convergence control parameters in the application of the Homotopy Analysis Method to nonlinear differential equations: A general approach, Communications in Nonlinear Science and Numerical Simulation 14 (2009) 4078-4089.

[22] S. Liao, An optimal homotopy-analysis approach for strongly nonlinear differential equations, Communications in Nonlinear Science and Numerical Simulation 15 (2010) 2315-2332.

[23] S. Abbasbandy, The application of homotopy analysis method to nonlinear equations arising in heat transfer, Physics Letters A 360 (2006) 109-113.

[24] S. Abbasbandy, Homotopy analysis method for heat radiation equations, International communications in heat and mass transfer 34 (2007) 380-387.

[25] S. J. Liao, J. Su and A.T. Chwang, Series solutions for a nonlinear model of combined convective and radiative cooling of a spherical body, Int. J. Heat and Mass Transfer 49 (2006) 2437-2445.

[26] S. J. Liao and A. Campo, Analytic solutions of the temperature distribution in Blasius viscous flow problems, Journal of Fluid Mechanics 453 (2002) 411-425.

[27] S. J. Liao, An explicit, totally analytic approximation of Blasius viscous flow problems, International Journal of Non-Linear Mechanics 34 (1999) 759-778.

[28] S. J. Liao, A uniformly valid analytic solution of 2D viscous flow past a semi-infinite flat plate, Journal of Fluid Mechanics 385 (1999) 101-128.

[29] S. J. Liao, On the analytic solution of magnetohydrodynamic flows of non-Newtonian fluids over a stretching sheet, Journal of Fluid Mechanics 488 (2003) 189-212.

[30] F. T. Akyildiz, K. Vajravelu, R. N. Mohapatra, E. Sweet, and R. A. Van Gorder, Implicit Differential Equation Arising in the Steady Flow of a Sisko Fluid, Applied Mathematics and Computation 210 (2009) 189-196.

[31] X. Hang, Z.L. Lin, S.J. Liao, J.Z. Wu and J. Majdalani, Homotopy based solutions of the Navier-Stokes equations for a porous channel with orthogonally moving walls, Physics of Fluids 22 (2010) 053601.

[32] M. Sajid, T. Hayat, and S. Asghar, Comparison between the HAM and HPM solutions of thin film flows of non-Newtonian fluids on a moving belt, Nonlinear Dynamics 50 (2007) 27-35.

[33] T. Hayat and M. Sajid, On analytic solution for thin film flow of a fourth grade fluid down a vertical cylinder, Physics Letters A 361 (2007) 316-322.

[34] M. Turkyilmazoglu, Purely analytic solutions of the compressible boundary layer flow due to a porous rotating disk with heat transfer, Physics of Fluids 21 (2009) 106104.

[35] S. Abbasbandy and F.S. Zakaria, Soliton solutions for the fifth-order KdV equation with the homotopy analysis method, Nonlinear Dynamics 51 (2008) 83-87.

[36] W. Wu and S.J. Liao, Solving solitary waves with discontinuity by means of the homotopy analysis method, Chaos, Solitons & Fractals 26 (2005) 177-185.

[37] E. Sweet and R. A. Van Gorder, Analytical solutions to a generalized Drinfel'd - Sokolov equation related to DSSH and KdV6, Applied Mathematics and Computation 216 (2010) 2783-2791.

[38] E. Sweet and R. A. Van Gorder, Exponential type solutions to a generalized Drinfel'd - Sokolov equation, Physica Scripta 82 (2010) 035006.

[39] Y. Wu, C. Wang and S.J. Liao, Solving the one-loop soliton solution of the Vakhnenko equation by means of the homotopy analysis method, Chaos, Solitons & Fractals 23 (2005) 1733-1740.

[40] J. Cheng, S.J. Liao, R.N. Mohapatra and K. Vajravelu, Series solutions of Nano-boundary-layer flows by means of the homotopy analysis method, Journal of Mathematical Analysis and Applications 343 (2008) 233-245.

[41] R. A. Van Gorder, E. Sweet and K. Vajravelu, Nano boundary layers over stretching surfaces, Communications in Nonlinear Science and Numerical Simulation 15 (2010) 1494-1500.

[42] A.S. Bataineh, M.S.M. Noorani and I. Hashim, Solutions of time-dependent Emden-Fowler type equations by homotopy analysis method, Physics Letters A 371 (2007) 72-82.

[43] A.S. Bataineh, M.S.M. Noorani and I. Hashim, Homotopy analysis method for singular IVPs of Emden-Fowler type, Communications in Nonlinear Science and Numerical Simulation 14 (2009) 1121-1131.

[44] R. A. Van Gorder and K. Vajravelu, Analytic and numerical solutions to the Lane-Emden equation, Physics Letters A 372 (2008) 6060-6065.

[45] S. Liao, A new analytic algorithm of Lane-Emden type equations, Applied Mathematics and Computation 142 (2003) 1-16.

[46] M. Turkyilmazoglu, The Airy equation and its alternative analytic solution, Phys. Scr. 86 (2012) 055004.

[47] M. Turkyilmazoglu, An effective approach for approximate analytical solutions of the damped Duffing equation, Phys. Scr. 86 (2012) 015301

[48] R. A. Van Gorder, Analytical method for the construction of solutions to the Föppl - von Kármán equations governing deflections of a thin flat plate, International Journal of Non-Linear Mechanics **47** (2012) 1-6.

[49] R. A. Van Gorder, Gaussian waves in the Fitzhugh-Nagumo equation demonstrate one role of the auxiliary function $H(x)$ in the homotopy analysis method, Communications in Nonlinear Science and Numerical Simulation 17 (2012) 1233-1240.

[50] R. A. Van Gorder, Control of error in the homotopy analysis of semi-linear elliptic boundary value problems, Numerical Algorithms, in press (2012) DOI: 10.1007/s11075-012-9554-1.

[51] A.-M. Wazwaz, Solitary waves solutions for extended forms of quantum Zakharov-Kuznetsov equations, Phys. Scr. 85 (2012) 025006.

[52] V.I. Berezhiani, S.M. Mahajan and N.L. Shatashvili, Stable optical vortex solitons in pair plasmas, Physical Review A 81 (2010) 053812.

[53] V. Sharka, V.I. Berezhiani and R. Miklaszewski, Spatiotemporal soliton propagation in saturating nonlinear optical media, Physical Review E 56 (1997) 1080-1087.

[54] H. A. Haus and W. S. Wong, Solitons in optical communications, Rev. Mod. Phys. 68, (1996) 423.

[55] S. M. Mahajan, N. L. Shatashvili, and V. I. Berezhiani, Asymmetry driven structure formation in pair plasmas, Physical Review E 80 (2009) 066404.

[56] J. Haussermann and R. A. Van Gorder, Asymptotic solutions for singularly perturbed Boussinesq equations, Applied Mathematics and Computation 218 (2012) 10238-10243.

[57] A. Constantin and W. A. Strauss, Stability of peakons, Communications on Pure and Applied Mathematics 53 (2000) 603-610.

[58] H. Lundmark and J. Szmigielski, Multi-peakon solutions of the Degasperis-Procesi equation, Inverse Problems 19 (2003) 1241.

[59] M. Ghoreishi, A.I.B. Ismail, A.K. Alomari, A. Sami Bataineh, The comparison between Homotopy Analysis Method and Optimal Homotopy Asymptotic Method for nonlinear age structured population models, Communications in Nonlinear Science and Numerical Simulation 17 (2012) 1163-1177.

[60] S. Abbasbandy, E. Shivanian, K. Vajravelu, Mathematical properties of h-curve in the frame work of the homotopy analysis method, Communications in Nonlinear Science and Numerical Simulation 16 (2011) 4268-4275.

[61] S. Liao, An optimal homotopy-analysis approach for strongly nonlinear differential equations, Communications in Nonlinear Science and Numerical Simulation 15 (2010) 2315-2332.

[62] K. Mallory and R. A. Van Gorder, Control of error in the homotopy analysis of solutions to the Zakharov system with dissipation, Numerical Algorithms, in press (2013) DOI: 10.1007/s11075-012-9683-6.

[63] M. Baxter and R. A. Van Gorder, Exact and analytic solutions of the Ernst equation governing axially symmetric stationary vacuum gravitational fields, Physica Scripta 87 (2013) 035005.

[64] S. Liebling, Singularity threshold of the nonlinear sigma model using 3D adaptive mesh refinement, Phys. Rev. D 66 (2002) 041703.

[65] Sierra, Germán, The nonlinear sigma model and spin ladders, J. Phys. A: Math. Gen. 29 (1966) 3299.

[66] Johnston D C, Johnson J W, Goshorn D P and Jacobsen A J, Magnetic susceptibility of $(VO)_2P_2O_7$: A one-dimensional spin-1/2 Heisenberg antiferromagnet with a ladder spin configuration and a singlet ground state, 1987 Phys. Rev. B 35 219.

[67] K. S. Jhung, R. S. Wiley, Nonlinear -model Padé calculation of $\pi\pi$ phase shifts, Phys. Rev. D 9 (1974) 3132.

[68] K. Borejsza, N. Dupuis, Antiferromagnetism and single-particle properties in the twodimensional half-filled Hubbard model: A nonlinear sigma model approach, Phys. Rev. B 69 (2004) 085119.

[69] H. O. Girotti, M. Gomes, V. O. Rivelles, A. J. da Silva, The Noncommutative Supersymmetric Nonlinear Sigma Model, arXiv:hep-th/0102101v2 (website is http://arxiv.org/abs/hepth/0102101) 2001.

[70] S. Hikami, Localization, Nonlinear Model and String Theory, Prog. Theor. Phys. Supplement 107 (1992) 213.

[71] F. D. M. Haldane, Continuum dynamics of the 1-D Heisenberg antiferromagnet: Identification with the O(3) nonlinear sigma model, Phys. Lett. A 93 (1983) 464.

[72] C.G. Callan, I.R. Klebanov, M.J. Perry, String theory effective actions, Nuclear Phys. B 278 (1986) 78.

[73] Sumit R. Das, B. Sathiapalan, New Infinities in Two-Dimensional Nonlinear Sigma Models and Consistent String Propagation, Phys. Rev. Lett. 57 (1986) 1511.

[74] J. Cahn and J. Hilliard, Free Energy of a Nonuniform System. I. Interfacial Free Energy, J. Chem. Phys. 28, 258, (1958).

[75] J. Carr, M. Gurtin, M. Slemrod, Structured Phase Transitions on a Finite Interval, Archive for Rational Mechanics and Analysis. 7, 317, (1984).

[76] C. Elliott and Z. Songmu, The Cahn-Hilliard Equation, Archive for Rotational Mechanics and Analysis. 28, 339, (1986).

[77] C. Elliott and D. French, Numerical Studies of the Cahn-Hilliard Equation for Phase Separation, IMA Journal of Applied Mathematics. 38, 97 (1987).

[78] R Toral, A Chakrabarti, JD Gunton, Numerical Study of the Cahn-Hilliard Equation in Three Dimensions, Phys. Rev. Lett. 60, 2311, (1988).

[79] M. I. M. Copetti, C. M. Elliott, Numerical analysis of the Cahn-Hilliard equation with a logarithmic free energy, Numerische Mathematik. 63, 39, (1992).

[80] E.V.L. de Melloa, O. Teixeira da Silveira Filho, Numerical study of the Cahn-Hilliard equation in one, two and three dimensions, Physica A, 429, 347 (2005).

[81] K. Vajravel and R. A. Van Gorder, *Nonlinear Flow Phenomena and Homotopy Analysis: Fluid Flow and Heat Transfer*. (Springer & Higher Education Press, Heidelberg, 2013).

[82] A. Hasegawa and K. Mima, Pseudo-three-dimensional turbulence in magnetized nonuniform plasma, Phys. Fluids 21 (1978) 87-92.

[83] A. Hasegawa and K. Mima, Stationary spectrum of strong turbulence in magnetized nonuniform plasma, Phys. Rev. Lett. 39 (1977) 205.

[84] K. Mallory and R.A. Van Gorder, Control of error in the homotopy analysis of solutions to the Zakharov system with dissipation, Numerical Algorithms, in press (2013); DOI 10.1007/s11075-012-9683-6.

[85] K. Mallory and R.A. Van Gorder, Optimal homotopy analysis and control of error for solutions to the non-local Whitham equation, Numerical Algorithms, in press (2013); DOI 10.1007/s11075-013-9765-0.

[86] K. Mallory and R. A. Van Gorder, Method for constructing analytical solutions to the Dym initial value problem, Applied Mathematics and Computation 226 (2014) 67-82.

[87] M. Baxter, R. A. Van Gorder, and K. Vajravelu, On the choice of auxiliary linear operator in the optimal homotopy analysis of the Cahn-Hilliard initial value problem, Numerical Algorithms, in press (2013) DOI 10.1007/s11075-013-9733-8.

[88] M. Turkyilmazoglu, A convergence condition of the Homotopy Analysis Method, in Advances in the Homotopy Analysis Method. Ed. S.-J. Liao. World Scientific, 2014. pp. 181-257.

[89] M. Turkyilmazoglu, Numerical and analytical solutions for the flow and heat transfer near the equator of an mhd boundary layer over a porous rotating sphere, International Journal of Thermal Sciences 50 (2011) 831-842.

[90] M. Turkyilmazoglu, An effective approach for approximate analytical solutions of the damped duffing equation, Physica Scripta 86 (2012) 015301.

[91] M. Turkyilmazoglu, Some issues on hpm and ham methods: A convergence scheme, Mathematical and Computer Modelling 53 (2011) 1929-1936.

[92] J. Hunter and R. Saxton, Dynamics of director fields, SIAM J. Appl. Math. 51 (6) (1991) 1498.

[93] R. Beals, D. Sattinger, J. Szmigielski, Inverse scattering solutions of the Hunter-Saxton equation, Applicable Analysis 78 (2000) 255.

[94] J. Lenells, The Hunter-Saxton equation describes the geodesic flow on a sphere, J. of Geo. and Phys., 57 (10) (2007) 2049.

[95] M. Nadjafikhah and F. Ahangari, Symmetry Analysis and Conservation Laws for the Hunter-Saxton Equation, Communications in Theoretical Physics 59 (2013) 335-348.

[96] S. Liao, An optimal homotopy-analysis approach for strongly nonlinear differential equations, Communications in Nonlinear Science and Numerical Simulation 15 (2010) 2315-2332.

[97] S.J. Liao, Homotopy Analysis Method in Nonlinear Differential Equations. Springer & Higher Education Press, Heidelberg, 2012.

[98] K. Vajravelu and R.A. Van Gorder, Nonlinear Flow Phenomena and Homotopy Analysis: Fluid Flow and Heat Transfer. Springer, Heidelberg. 2013.

[99] M. Ghoreishi, A.I.B. Ismail, A.K. Alomari, A. Sami Bataineh, The comparison between Homotopy Analysis Method and Optimal Homotopy Asymptotic Method for nonlinear age-structured population models, Communications in Nonlinear Science and Numerical Simulation 17 (2012) 1163–1177.

[100] K. Mallory and R. A. Van Gorder, Method for constructing analytical solutions to the Dym initial value problem, Applied Mathematics and Computation 226 (2014) 67-82.

[101] M. Baxter, R. A. Van Gorder, and K. Vajravelu, On the choice of auxiliary linear operator in the optimal homotopy analysis of the Cahn-Hilliard initial value problem, Numerical Algorithms, in press (2013) DOI 10.1007/s11075-013-9733-8.

[102] R. A. Van Gorder, Self-similar vortex dynamics in superfluid 4He under the Cartesian representation of the Hall-Vinen model including superfluid friction, Physics of Fluids 25(9) (2013) 095105.

[103] E. A. Zabolotskaya, R. V. Khokhlov, Quasi-plane waves in the nonlinear acoustics of confined beams, Sov. Phys. Acoust. 15 (1969) 35-40.

[104] A. R. Chowdhury and M. Nasker, Towards the conservation laws and Lie symmetries for the Khokhlov-Zabolotskaya equation in three dimensions, J. Phys. A: Math. Gen. 19 (1986) 1775-1781.

[105] J.-F. Zhang, Y.-J. Zhu, and J. Lin, Similarity Reductions for the Khokhlov-Zabolotskaya Equation, Commun. Theor. Phys. 24 (1995) 69-74.

[106] P. Clarkson and S. Hood, Nonclassical symmetry reductions and exact solutions of the Zabolotskaya-Khokhlov equation, Eur. J. of Appl. Math. 3 04 (1992) 381-414.

[107] D. Sanchez, Long waves in ferromagnetic media, Khokhlov-Zabolotskaya equation, J. Differential Equations 210 (2005) 263-289.

[108] O. Morozov, Cartan's Structure Theory of Symmetry Pseudo-Groups, Coverings and Multi-Valued Solutions for the Khokhlov-Zabolotskaya Equation, Acta Appl. Math 101 (2008) 231-241.

[109] I. Krichever, The Dispersionless Lax Equations and Topological Minimal Models, Commun. Math. Phys. 143 (1992) 415-429.

[110] O. V Rudenko, The 40th anniversary of the Khokhlov-Zabolotskaya equation, Acoustical Physics 56 4 (2010), 457-466.

[111] A. Rozanova, The Khokhlov-Zabolotskaya-Kuznetsov equation, C. R. Acad. Sci. Paris, Ser. I (2007) 337-342.

[112] M. Baxter, R. A. Van Gorder, and K. Vajravelu, Peaked solutions for the nonlinear evolution of a vector potential of an electromagnetic pulse propagating in an arbitrary pair plasma with temperature asymmetry, Quaestiones Mathematicae, presently under review.

[113] M. Baxter and R. A. Van Gorder, Exact and analytical solutions for a nonlinear sigma model, Mathematical Methods in the Applied Sciences, doi: 10.1002/mma.2926, August 2013.

[114] M. Baxter, R. A. Van Gorder, and K. Vajravelu, Optimal analytic method for the nonlinear Hasegawa-Mima equation, European Physical Journal Plus 129 98, 2014.

[115] M. Baxter, R. A. Van Gorder, and K. Vajravelu, Several types of exact similarity solutions for the Hunter-Saxton equation, Communications in Nonlinear Science and Numerical Simulation, submitted (2014).

[116] M. Baxter, R. A. Van Gorder, and K. Vajravelu, Exact similarity solutions of the Khokhlov-Zabolotskaya equation. Submitted, presently under review.

[117] C. Klein and O. Richter, Physically realistic solutions to the Ernst equation on hyperelliptic Riemann surfaces, Phys. Review D 58, 124018 (1998).